



Faculteit Bio-ingenieurswetenschappen

Academiejaar 2011-2012

Computational study on the formation of
N-spiro bis-aziridinium ions and their
nucleophile-induced ring-opening reactions

Dietmar Hertsen

Promotoren: Prof. dr. ir. N. De Kimpe en Prof. dr. ir. V. Van Speybroeck

Tutoren: Prof. dr. ir. M. D'hooghe en dr. S. Catak

Masterproef voorgedragen tot het behalen van de graad van
Master in de bio-ingenieurswetenschappen: chemie en bioprocestechnologie



Faculteit Bio-ingenieurswetenschappen

Academiejaar 2011-2012

Computational study on the formation of
N-spiro bis-aziridinium ions and their
nucleophile-induced ring-opening reactions

Dietmar Hertsen

Promotoren: Prof. dr. ir. N. De Kimpe en Prof. dr. ir. V. Van Speybroeck

Tutoren: Prof. dr. ir. M. D'hooghe en dr. S. Catak

Masterproef voorgedragen tot het behalen van de graad van
Master in de bio-ingenieurswetenschappen: chemie en bioprocestechnologie

Deze pagina is niet beschikbaar omdat ze persoonsgegevens bevat.
Universiteitsbibliotheek Gent, 2021.

This page is not available because it contains personal information.
Ghent University, Library, 2021.

Acknowledgments

This page will not spill words over my accomplishments and failures at this university, let alone over my treasured memories or the challenges in life. I deeply believe that words are superfluous to describe the transition that I have undergone in the past few years and I simply, yet not less sincerely, thank Ghent University for this opportunity.

I would also like to thank Hannelore Goossens for her tedious revisions of this work. With a deadline in sight, she has helped me by weighing every word and putting new ones in the balance. This work could not have been finished in time without her, thanks. As helpful as Hannelore was in these final moments, as grateful I am to dr. Saron Catak for introducing me to molecular modeling. She showed me the pitfalls and encouraged me to stay focused when too much data blurred the picture. In this respect I also thank Prof. Veronique Van Speybroeck who not only offered me an interesting topic, but created an environment in which thesis students are treated as true researchers. Her late-night revisions have been of great help to finalize this work. Last but not least I thank Prof. D'hooghe for his experimental feedback and Prof. De Kimpe for the opportunity to let me work at the Center for Molecular Modeling. I show courtesy to Ghent University, the Hercules Foundation and the Flemish Government - department EWI for the computational resources (Stevin Supercomputer Infrastructure) and services that were used in this work.

I am indebted to my family and friends, especially my beloved Annelies, for their support. Furthermore, I am grateful to my fellow master thesis students Michaël Sluydts, Francis Caestecker, Sebastien Versaevel and Michaël Pieters for their pleasant company. May each and every one of you have a head start in life.

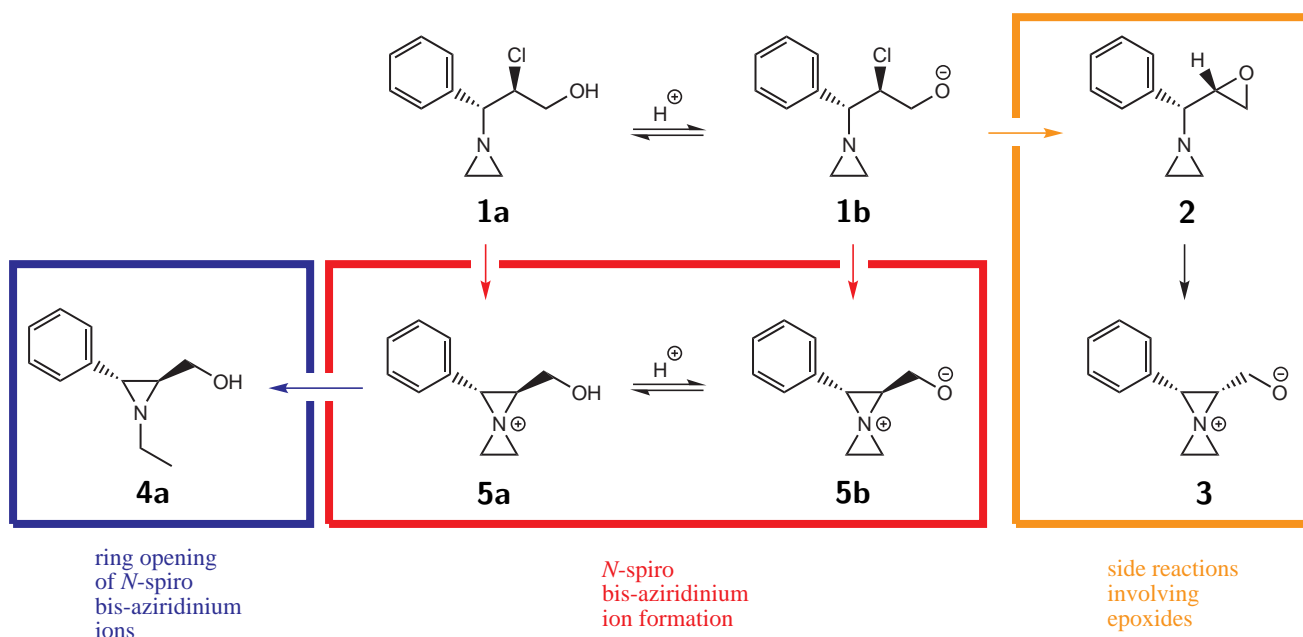
Dietmar Hertsen

Sint-Katelijne-Waver, juni 2012

Samenvatting

De experimenten van Mollet et al. die het bestaan van *N*-spiro bis-aziridinium ionen voorstelden in een reactieschema voor de vorming van aziridine **4a** (Schema 1), dienen als basis voor het computationeel werk dat verricht wordt in deze thesis.¹ Aangezien deze ionen niet werden geïsoleerd en worden beschouwd als onstabiel, is het doel van dit werk deze opmerkelijke intermediaren en de omstandigheden waaronder ze gevormd worden te onderzoeken met computationele methoden. Dit onderzoek fungeerde als het uitgangspunt voor de studie van spiranische en bicyclische aziridinium ionen in het algemeen en werd aangegrepen om de invloed van verschillende solvatatiemethoden op een systematische manier in kaart te brengen.

Scheme 1: Reacties van aziridine **1a**



Het onderzoek naar *N*-spiro bis-aziridinium ionen werd veralgemeend tot gespannen spiranische en bicyclische aziridinium ionen. De structuur van enkele representatieve verbindingen uit deze klassen werd vergeleken met het 'bent bond model'. Bovendien werd de ringspanning van al deze verbindingen bepaald aan de hand van homodesmotische reacties. De buiging van de bindingen en de σ -delokalisatie is aanzienlijk en kan vergeleken worden met andere drieringen. De ringspanning daarentegen is zeer hoog (> 200 kJ/mol) bij spiranische en bicyclische aziridinium ionen die twee drie-

of vierringen bevatten. Bicyclische verbindingen zijn meer gespannen dan hun spiranische isomeren en in het algemeen daalt de ringspanning als de ringgrootte stijgt. De ringspanning van spiranische en bicyclische aziridinium ionen is kleiner dan de som van de spanningen van de ringen waaruit ze bestaan.

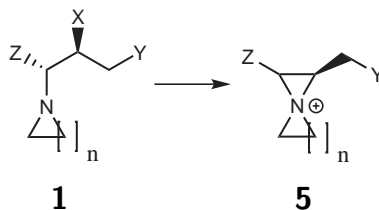
De vorming van spiranische aziridinium ionen **5a** en **5b** uit aziridinen **1a** en **1b** (Schema 1) wordt gemodelleerd met vier solvatatiemodellen: in vacuo, expliciete, impliciete en expliciet/impliciete of gemengde solvatatie tijdens de optimalisatie. De laatste twee methoden zijn state-of-the-art modellen die nog niet getest werden op een systematische manier. Ze resulteerden in andere transitietoestandsgeometrieën en lagere energiebarrières voor de vorming van spiranische aziridinium ionen. Impliciete solvatatie werd als de methode voor verdere berekeningen in tetrahydrofuraan (THF) gekozen. In het geval van methanol (MeOH) is het aangewezen ook een aantal expliciete solventmoleculen in het model op te nemen, aangezien dit solvent in staat is tot expliciete interacties.

De volgende conclusies werden bereikt met de gekozen solventmodellen: de vorming van spiranische intermediairen **5a** en **5b** is meestal endergonisch en heeft activatiebarrières (vrije energie) van de grootteorde van 100 kJ/mol. Hoe hoger de polariteit van het solvent, hoe lager deze barrières worden. De reacties verlopen dus makkelijker in MeOH dan in THF.

Het effect van substitutie op de vorming van intermediairen **5a** en **5b** werd onderzocht in THF met impliciete solvatatie tijdens de optimalisatie. Vier soorten substituenten werden ingevoerd om deze effecten te beschrijven (Schema 2). ΔG_{rxn} en ΔG^\ddagger van de vormingsreactie zijn gecorreleerd met de sterkte van de leaving group X, zoals verwacht. De β -substituent Y bleek zeer belangrijk: zwitterionische stabilisatie door een anionische substituent of een intramoleculaire waterstofbinding tussen de leaving group en de Y-substituent verlagen beide ΔG_{rxn} en ΔG^\ddagger . Het eerste effect is veel groter dan het laatste. Deze reactie wordt dus best uitgevoerd in basisch milieu.

Het effect van de Z-groep kan begrepen worden met het inductief effect: chlooratomen destabiliseren en fenylgroepen bevoordelen de vormingsreactie. Het variëren van de grootte van de heterocyclische ring levert opmerkelijke resultaten: aziridinen zijn minder geneigd om dit type ringsluiting te ondergaan dan azetidinen, pyrrolidinen and piperidinen. Een mogelijke verklaring is de hoekcompressie

Scheme 2: Structurele parameters voor de vorming van spiranisch aziridinium ion **5**



tussen de exocyclische bindingen in aziridinium ionen. Ten slotte werd een Bell-Evans-Polanyirelatie opgesteld voor al deze substituenteffecten.

Aziridine **1b**, in evenwicht met aziridine **1a** in basisch milieu, zal altijd reageren tot epoxide **2**. Dit zal tevens het eindproduct zijn onder kinetische controle, hoewel verdere reacties tot aminen en aziridinen met een *cis*-configuratie zullen optreden onder thermodynamische controle. Deze thermodynamische producten worden gevormd uit intermediaren **5b** en **3** via verscheidene snelle ringopeningsreacties. In de oorspronkelijke experimenten werden geen epoxiden of aziridinen met een *cis*-configuratie aangetroffen. Dit betekent dat epoxide **2** snel werd omgezet tot meer stabiele verbindingen, hoewel *N*-spiro bis-aziridinium ion **3** niet gevormd werd.

Deze thesis bevestigt dat spiranische aziridinium ionen, die gevormd worden door de intramoleculaire nucleofiele substitutie van een leaving group door het stikstofatoom in aziridine, gevormd worden met activatiebarrières (vrije energie) van ongeveer 100 kJ/mol. De grootte van deze barrières hangt af van het specifieke solvent waarin de reactie wordt uitgevoerd. Deze aziridinium ionen zullen snel na hun vorming verder reageren tot meer stabiele verbindingen zoals aziridine **4a**, aangezien deze omzettingen sterk exergonisch zijn. Deze verbindingen zijn dus moeilijk isoleerbaar en computationele methoden zijn uitermate geschikt om de eigenschappen van dit type intermediaren te onderzoeken. De nevenreacties die epoxidevorming omvatten geven aanleiding tot verbindingen met een andere stereochemie, hoewel deze niet werden aangetroffen in de experimenten van Mollet et al. Deze resultaten tonen aan dat de vorming van epoxide **2** zeer snel verloopt en altijd plaats zal vinden in basisch milieu.

Contents

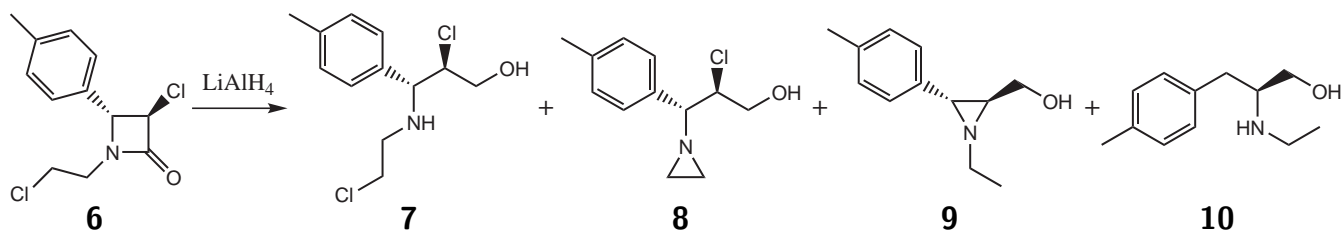
1	Introduction and Goal	1
2	Literature Study	4
2.1	Structure and Stability of Three-Membered Rings	4
2.2	Ring Strain	11
2.3	Aziridines	13
2.3.1	Reactivity	13
2.3.2	Pyramidal Inversion	15
2.4	Strained <i>N</i> -Spiro and <i>N</i> -Bridgehead Aziridinium Ions	16
3	Computational Methods	19
3.1	Ab Initio Methods	19
3.1.1	Hartree-Fock (HF) Method	20
3.1.2	Post-Hartree-Fock (post-HF) Methods	20
3.1.3	Density Functional Theory (DFT)	21
3.2	Topology of the Electron Density	22
3.3	Solvation	23
3.4	Computational Methodology	24
4	Results and Discussion	25
4.1	Structure and Stability of Strained Spiranic and Bicyclic Aziridinium Ions	25
4.1.1	Structure	25
4.1.2	Ring Strain	28
4.2	Formation of Spiranic Aziridinium Ions and Their Nucleophile-Induced Ring-Opening Reactions	33
4.2.1	Introduction	33
4.2.2	Solvation Effects on the Formation of Spiranic Aziridinium Ions	34
4.2.2.1	Reactivity in Vacuo	35

4.2.2.2	Implicit Solvation	38
4.2.2.3	Explicit Solvation	41
4.2.2.4	Explicit/implicit (Mixed) Solvation	42
4.2.2.5	Comparison of Solvation Methods	47
4.2.2.6	Other Solvents	51
4.2.3	Substituent Effects on the Formation of Spiranic Aziridinium Ions	52
4.2.3.1	Leaving Groups (X)	53
4.2.3.2	β -Substituents (Y)	55
4.2.3.3	Z-Substituents	55
4.2.3.4	Heterocyclic Ring Size	58
4.2.3.5	Overview of Substituent Effects	59
4.3	Formation of Spiranic Aziridinium Ions via Side Reactions Involving Epoxides	60
5	Conclusion	67
	References	70

1 Introduction and Goal

In this work the structure, stability, formation and nucleophile-induced ring opening of *N*-spiro or spiranic aziridinium ions will be investigated. Although some of these compounds have been described in the literature, the focus of this work will be on *N*-spiro bis-aziridinium ions, which receive almost no attention in the literature. These ions were reported in the work of Mollet et al.¹ to rationalize the outcome of the reaction in Scheme 3. Since *N*-spiro bis-aziridinium ions are peculiar and possibly elusive intermediates, it was decided to investigate their properties from a computational point of view. With these techniques short-lived species, which cannot be isolated, can be studied in detail.

Scheme 3: Treatment of *trans*-3-chloro-1-(2-chloroethyl)-4-*p*-tolylazetid-2-one **6** with LiAlH₄.¹



As described in the work of Mollet et al., treatment of *trans*-3-chloro-1-(2-chloroethyl)-4-*p*-tolylazetid-2-one **6** with LiAlH₄ yields 2-chloro-3-(2-chloroethylamino)-3-(4-methylphenyl)propan-1-ol **7**, 1-[2-chloro-3-hydroxy-1-(4-methylphenyl)]aziridine **8**, *trans*-1-ethyl-3-hydroxymethyl-2-(4-methylphenyl)aziridine **9** and 2-ethylamino-3-*p*-tolylpropan-1-ol **10**.¹ The possible reaction pathways for this reaction probably involve the deprotonated form of 1-hydroxymethyl-2-*p*-tolyl-3-azoniaspiro[2.2]pentane cation **14** as shown in Scheme 4. The formation of this compound will be studied in detail since highly strained *N*-spiro bis-aziridinium ions are remarkable intermediates.

The reaction product **9** can be formed via two distinct intramolecular nucleophilic substitutions in intermediate **11**, obtained after the hydride-induced ring opening of azetidione **6**. The first pathway (red in Scheme 4) has a *N*-spiro bis-aziridinium ion intermediate and involves the consecutive nucleophilic substitutions of both chlorine atoms by the nitrogen atom. The second pathway (brown in Scheme 4) involves the nucleophilic substitution of one chlorine atom by the nitrogen atom and the reductive removal of the other chlorine atom, but is less likely because it cannot explain the relative

high ratio of **8** formed ($8/9 = 70/30$). The direct attack of the nitrogen atom at the secondary center in **11** leading to **13** is kinetically less favorable than the attack at the primary center leading to compound **12**. If compound **9** is formed via the reductive removal of the chlorine atom in compound **12**, the ratio of compound **8** would be smaller.

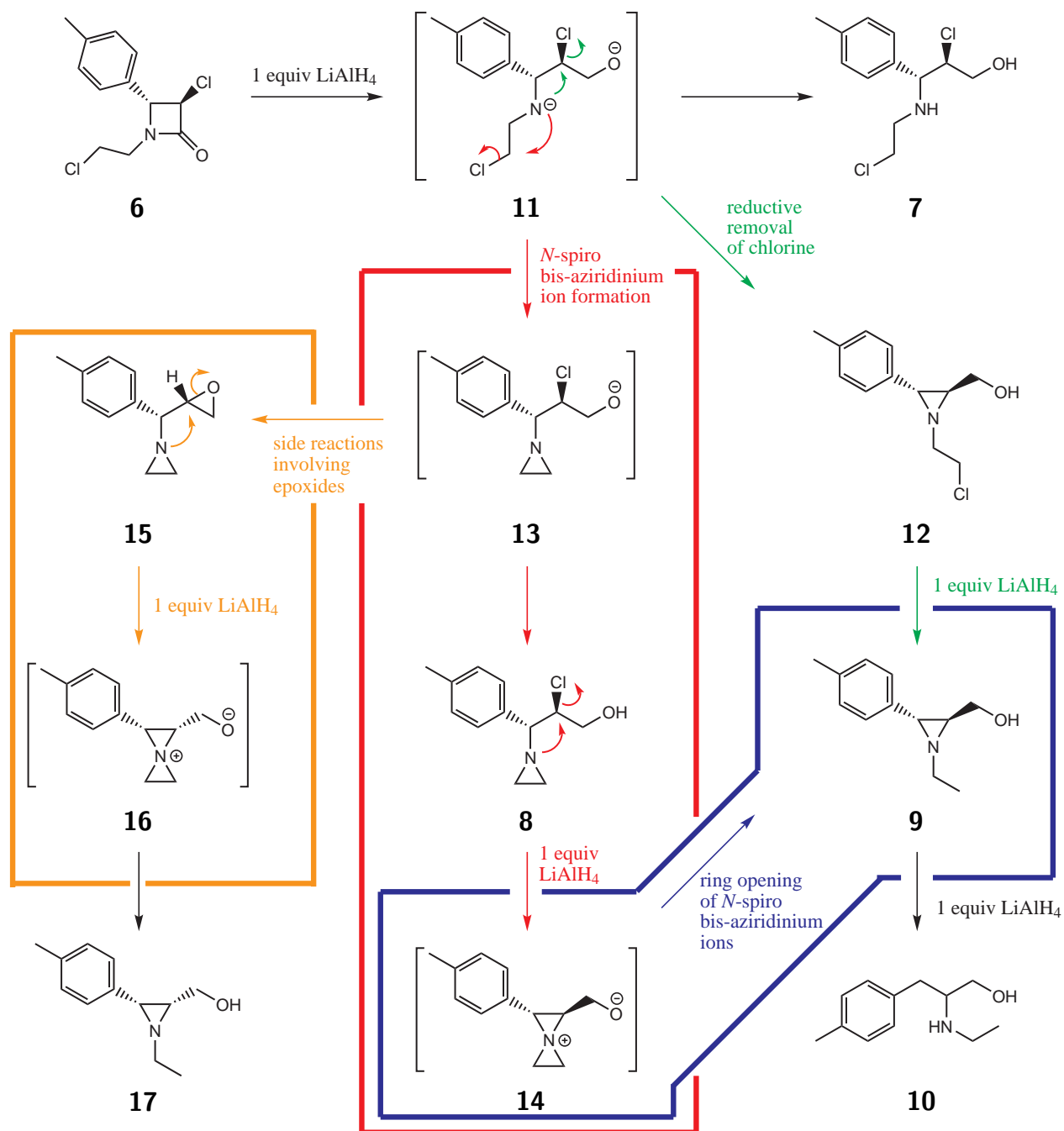
A possible side reaction involves the formation of epoxide **15**, that can be converted into aziridine **17** via *N*-spiro bis-aziridinium ion **16** (brown in Scheme 4). These reactions were not mentioned in the original experiments. Aziridine **17** has a *cis* configuration, in contrast with the *trans* configuration of aziridine **9**. This product was not observed in the experiments, but nonetheless the pathway will briefly be investigated in this work at the suggestion of the experimenters.

The aim of this study is to characterize *N*-spiro bis-aziridinium ion **14** and spiranic aziridinium ions in general in order to support the existence of these unstable intermediates by means of state-of-the-art computational techniques. This work is organized as follows: at first instance a literature study (Chapter 2) and an overview of computational methods (Chapter 3) are given. Before studying the reactions in Scheme 4, a thorough analysis on the structure and strain energy of three-membered rings and spiranic and bicyclic aziridinium ions is given in Section 4.1. Therefore the bent bond model will be applied to these structures and homodesmotic reactions will be used to assess the conventional strain energy.

Computational results on the reactivity of spiranic aziridinium ions are presented in Sections 4.2 and 4.3. The three pathways marked in Scheme 4 are investigated by a range of computational methods, that allow to locate the various transition states involved and to calculate the free energies of the reactions. *N*-spiro bis-aziridinium ion formation and ring opening of *N*-spiro bis-aziridinium ions are discussed in Section 4.2, while side reactions involving epoxides are discussed in Section 4.3. Special emphasis is given on the effect of solvation and substituents on the formation of *N*-spiro bis-aziridinium ions.

Earlier combined experimental and theoretical studies have clearly indicated that the proper inclusion of solvation effects is of utmost importance to assess the reactivity of various organic reactions.²⁻⁵ A scala of solvation models may be used to obtain accurate results. The methods used in this thesis are

Scheme 4: Reaction pathways for the LiAlH_4 -induced transformations of *trans*-3-chloro-1-(2-chloroethyl)-4-*p*-tolylazetid-2-one **6**. Computational results for the pathways in red/blue and brown boxes are presented in Sections 4.2 and 4.3 respectively.



introduced in Chapter 3 and applied for the compounds at hand in Chapter 4. Finally, a summary of the most important conclusions is given in Chapter 5.

2 Literature Study

2.1 Structure and Stability of Three-Membered Rings

Three-membered rings, especially heterocyclic ones, are useful compounds in organic synthesis. Their versatility as intermediates or reagents is largely attributed to ring strain, induced by the equilibrium angles of about 60° instead of 109.5° or 120° in the case of sp^3 or sp^2 hybridization. Although this feature has made some rings inaccessible to the experimental chemist for a long time, even triaziridines⁶ and azirines⁷ have been synthesized today. In this thesis the attention is focused on highly strained three-membered *N*-heterocyclic intermediates, and therefore it is instructive to look at the structure of three-membered rings from a general point of view.

Cyclopropane has attracted a lot of attention as a model for other three-membered rings. Its structure and reactivity cannot be adequately explained by using ring strain alone.⁸⁻¹⁰ The strain energy, which is the difference between the observed heat of formation and its strain-free estimate (proper definitions are given further in this chapter), is remarkably low compared to cyclobutane.¹¹ This indicates that the strain from angle compression is somewhat lifted by another stabilizing effect. Moreover, the bonds are shorter than the ones found in alkanes⁹ and the ring shows in some respect similar behaviour as alkenes.¹²

The failure of the standard valence-bond picture for this system, led to two classical models for the bonding in cyclopropane, developed by Walsh¹³ and Coulson and Moffitt.¹⁴ In Walsh's model each carbon atom is sp^2 hybridized with the p orbital positioned tangential with respect to the ring and one sp^2 orbital pointing to the center of the ring. This gives rise to three representative bonding molecular orbitals (MOs) as illustrated in Figure 1. The lowest-energy MO arises from the overlap of sp^2 orbitals. Two degenerate higher-lying MOs arise from overlap of the p orbitals and make up a π system that explains the chemical behaviour of cyclopropanes. Walsh proposed that bonding in other heterocyclic systems should follow the same pattern and applied the concept to oxirane.

In the model of Coulson and Moffitt, also called the bent bond model, all carbon atoms are sp^3 hybridized. The sp^3 orbitals that participate in ring bonding, have an increased p character. Hence,

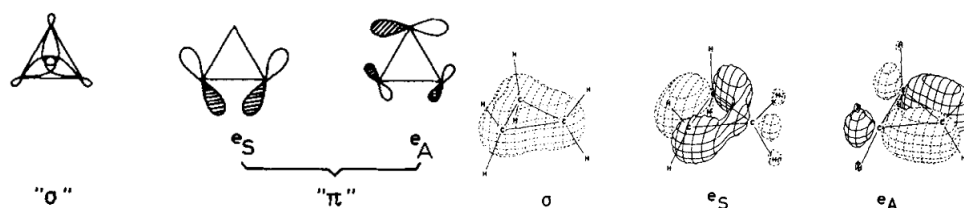


Figure 1: Construction of MOs in Walsh's model for cyclopropane¹⁰

the three bonding MOs that result from the overlap of these orbitals are bent outwards. The sp^3 orbitals that participate in exocyclic bonding have an increased s character, which results in shorter CH bonds. Strictly speaking, the carbon atoms are not sp^3 hybridized since they do not contain four equivalent orbitals.

It is important to acknowledge that both models describe the same system and are mathematically equivalent. In both models the chemical bond, resulting from the electron density, is bent and lies outside of the triangle drawn between the three carbon atoms, hence the term bent bonds is used. The reactivity similar to alkenes can be interpreted in terms of Walsh's model. The low strain energy of cyclopropane can be understood by looking at the energies of the MOs: a stabilization relative to non-cyclic aliphatic bonds is obtained due to σ -delocalization, i.e. the electron density is less concentrated in the bonding region.

Advanced computational methods were used to reproduce the valence orbitals of the bent bond model for cyclopropane, aziridine, oxirane, phosphirane and thiirane.⁸ This resulted in orbitals that can be interpreted as sp^x hybrids, further supporting the proposed bent bond model. The bending of the orbitals, however, is more pronounced for first group than for second group elements. In phosphirane, such deformation is hardly present. All molecules have an outward bent, even oxirane, although an electron density map reveals the opposite trend for even more electronegative ring substituents (see further). For second row elements, these theoretical methods place the heteroatom further away from the $(CH_2)_2$ part.

Another way of looking at saturated three-membered rings stems from the existence of so-called T structures like π complexes of ethene. When an atom or atomic group X approaches a molecule A_2 , several structures can arise (Figure 2). When either A_2 or the approaching group possesses a low-

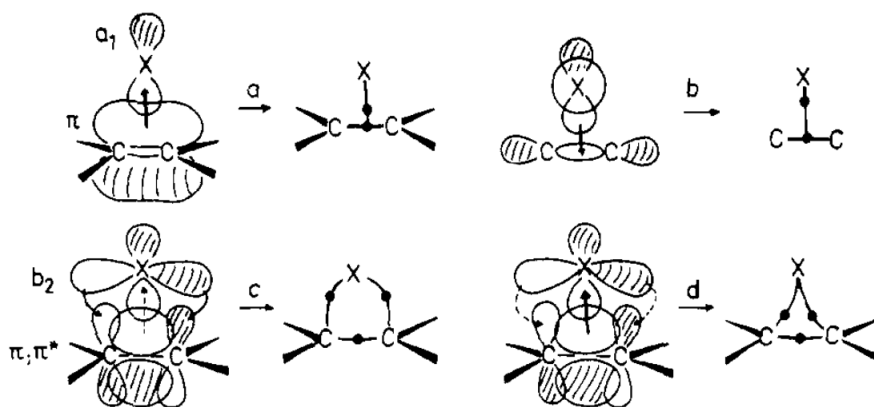


Figure 2: Possible interactions between ethene and an atomic group X: (a) and (b) are T structures, (c) is a convex ring, (d) is a concave ring⁹

energy acceptor orbital which may interact with a corresponding donor orbital of the other reacting species, a T structure arises. In π complexes of ethene, the π molecular orbital is the donor orbital. In T structures the electron density is concentrated along the axis connecting the middle of the AA bond with X. This type of bonding weakens the AA bond, strengthens the AX bond and makes A_2 more accessible to a nucleophilic attack. Aziridine can be envisioned as a complex of ethene and an imidogen radical (NH).

If the acceptor in a T complex also possesses a high-energy donor orbital and the donor group an appropriate acceptor orbital, substantial back-donation can occur. This leads to convex or concave-shaped three-membered rings with a concentration of electron density along the sides. A relatively high electron density can be found in the center. In more convex rings, back-donation is more pronounced, and vice versa.

All these models describe saturated three-membered rings qualitatively as systems in which bent bonds, σ -delocalization and reactivity similar to alkenes occur. A simplified set of parameters to describe these systems was proposed in the literature and a slightly adapted version is presented here⁹ (Figure 3). Bond paths can be interpreted as the true bonds given by the electron density distribution. The given critical points are saddle points of this distribution, either along the paths or in the center of the ring. For a complete discussion see Chapter 3.

While the definition of angles and lengths is straightforward, η and Q need more explanation. Q

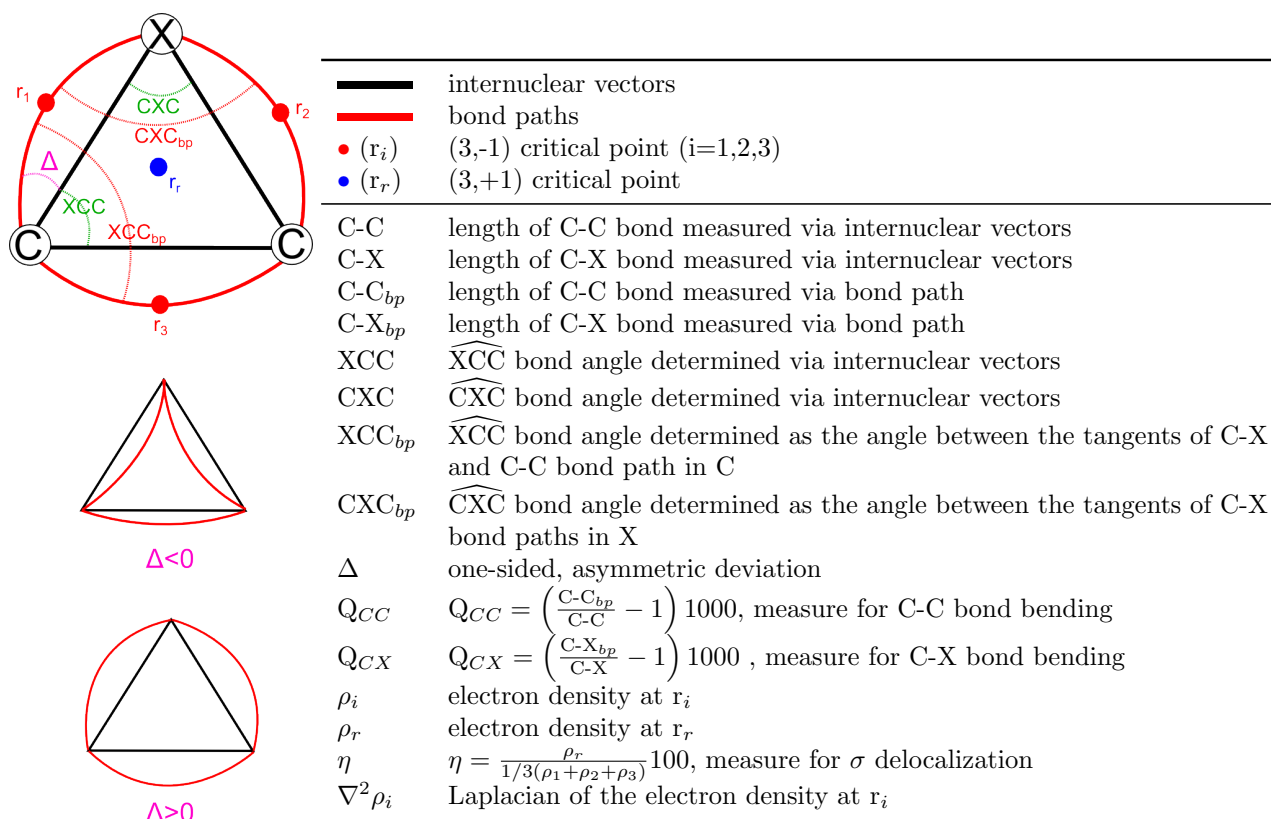


Figure 3: Structural parameters for the description of bent bonds, adapted from the literature⁹

is a measure for bond bending and is a function of the ratio of bond path length and the distance between nuclei. Convex ($\Delta > 0$) and concave ($\Delta < 0$) bending can be distinguished through careful examination of the angles. η is a measure for σ -delocalization and is a function of the ratio of electron densities along the C-X/C-C paths and in the middle of the ring. The bond strength is roughly correlated with $-\nabla^2 \rho_i$ at the critical point along the corresponding bond path for a series of similar bonds.

To clarify the introduced concepts, HF/6-31G(d) calculations were performed in the literature⁹ on a series of C_2X systems and can be found in Table 1. The electronegativity (EN) of the X group can be correlated with some of the parameters described above. Qualitatively EN increases in the series $X = CH^- < CH_2 < NH < O < NH_2^+ < OH_2^+ < F^+$. The relation between structure and EN of X will be discussed next. In Section 4.1 the same methods will be applied to strained bicyclic and spiranic aziridinium ions.

For the least electronegative Xs (cyclopropyl anion (**18**), cyclopropane (**19**) and aziridine (**20**), see Table 1) the ring is convex. Oxirane (**21**) has an intermediate structure, while strongly electronegative Xs (cations **22**, **23** and **24**) show concave structures. For $X=H^+$ a true T form arises (not shown).


The bending of the C-C bond (Q_{CC}) increases with EN in the series **18**, **19**, **20**, and **21**. This is not true for more electronegative Xs; little deformation of the bond is seen in species with a T structure. The bending of the C-X bond (Q_{CX}) increases with $|\Delta|$. In other words, if a three-membered ring becomes more convex or concave, C-X bending occurs. Hence, the bending is minimal for oxirane **21**. This confirms the correspondence between Δ , defined as local bending via a tangent, and Q_{CX} , defined as global bending via a ratio of lengths.

By increasing the EN of X, the C-C bond becomes stronger ($\nabla^2\rho_{CC}$ decreases) and the C-X bond becomes weaker ($\nabla^2\rho_{CX}$ increases, only for X more electronegative than X=O). The interaction between ethene and H^+ in a T structure is obviously weaker than the C-C bond in cyclopropane. Note that the Laplacian of the electron density is only an approximate measure for bond strength. Although the nucleophilic ring opening of aziridine **20** is more difficult than that of oxirane **21**, this conclusion cannot be based on this model alone.

All C-C bonds have a length between 1.445 and 1.505 Å. Acyclic, aliphatic C-C bonds are generally shorter (e.g. 1.523 Å in ethane, taken from calculations in this work at the MP2/6-311+G(2df,2pd) level of theory). C-X bond lengths are between 1.401 and 1.533 Å. Interestingly, the length of C-X bonds increases when the system becomes more convex or concave. It follows that both geometrical and bond path lengths are minimal for oxirane **21** and increase when the EN of X deviates from the EN of O.

Although η does not reveal a clear trend, it is important to note that $\eta \approx 85$ for these three-membered rings, while for cyclobutane $\eta \approx 33$. This difference may explain the relative stability of cyclopropane. For true T structures η cannot be interpreted in the same way since the electron density is concentrated in a single axis with $\rho_1 \approx \rho_2 \approx \rho_r$.

Table 1: Structural parameters of several three-membered rings (C_2X systems)^a

	cyclopropyl anion (18)	cyclopropane (19)	aziridine (20)	oxirane (21)	protonated aziridine (22)	protonated oxirane (23)	halogen-bridged fluorethyl cation (24)
	X=CH ⁻	X=CH ₂	X=NH	X=O	X=NH ₂ ⁺	X=OH ⁺	X=F ⁺
C-C	1.505	1.497	1.470	1.453	1.460	1.446	1.445
C-X	1.526	1.497	1.449	1.401	1.488	1.498	1.533
XCC	60.4	60.0	59.5	58.8	60.6	61.1	61.9
CXC	59.1	60.0	60.9	62.4	58.8	57.7	56.2
XCC _{bp}	80.2	78.8	77.3	72.8	60.9	19.9	0.02
CXC _{bp}	69.6	78.8	76.4	75.8	77.3	56.7	4.3
Δ	11.7	9.4	5.9	0.2	-11.8	-53.4	-73.1
Q _{CC}	4.0	6.7	10.9	15.8	11.6	12.4	10.4
Q _{CX}	6.6	6.7	4.1	2.1	12.8	122.8	350.3
η	83.6	82.0	83.1	85.8	85.0	86.9	85.6
$\nabla^2\rho_{CC}$ ^b	-12.07	-12.86	-14.69	-16.05	-17.83	-20.49	-22.44
$\nabla^2\rho_{CX}$ ^c	-10.37	-12.86	-17.79	-1.88	-6.28	1.52	9.97

^a Taken from previous theoretical calculations found in literature.⁹ Description of all parameters in Figure 3. Geometries optimized at the HF/6-31G(d) level of theory. If multiple values are obtained for the same parameter, the average is taken. All distances in Å, angles in degrees, η and Q relative, Laplacians in eÅ⁻⁵

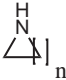
^b $\nabla^2\rho_{CC} = \nabla^2\rho_3$

^c $\nabla^2\rho_{CX} = \frac{1}{2}(\nabla^2\rho_1 + \nabla^2\rho_2)$

The qualitative picture above has been confirmed by both X-ray and gas-phase experiments on saturated and unsaturated C_2X and CXY systems. In saturated C_2X species the C-C bond length indeed decreases with increasing EN of X. Studies with second row substituents point out the same trend within a row. Even in strained systems like bis- and tris(aziridin-1-yl)methane there is little deviation of the parameters.^{15,16} Although they are of little interest in the present study, the C_2X model generally holds for molecules like oxaziridine, 3*H*-diazirine, diaziridine and 1-azirine.⁹ For some systems like 3-amino-2*H*-azirines the preferred tautomer has an endocyclic double bond, again illustrating the stability of three-membered rings.¹⁷

Comparison of the theoretically modeled structure of aziridine with experiment and other saturated *N*-heterocycles can be found in Table 2. The effect of ring conformation (e.g. puckering) on bond lengths and angles is neglected by taking averages. The theoretical methods produce the expected qualitative trends in a satisfactory way. For example, C-C bonds are considerably shorter in aziridine than in its homologues.

Table 2: Overview of structural and thermodynamical characteristics of some saturated *N*-heterocyclic compounds^a

		C-C	C-N	C-H	N-H	CNC	PA	pK _b ^b
aziridine (20 , n=1)	MP2/6-31G(d) ¹¹	1.481	1.474	1.085- 1.087	1.021	60.3	913.4	6.02
	MP2/6-311+G(2df,2pd) ^c	1.478	1.473	1.079	1.014	60.2		
	experimental PA ¹⁸						902	
	experimental ¹⁹	1.484	1.474			60.5		
	experimental ²⁰	1.481	1.475	1.084	1.016			
azetidine (25 , n=2)	MP2/6-31G(d) ^{11,d}	1.553- 2.010	1.534- 2.119	1.095- 2.340	2.180	47.0	965	2.71
	MP2/6-311+G(2df,2pd) ^c	1.540	1.482	1.086- 1.094	1.013	89.5		
	experimental PA ¹⁸						935	
	experimental ²¹	1.553	1.482	1.107	1.022	92.2		
	experimental ²²	1.563	1.473	1.096	1.014	91.2		
pyrrolidine (26 , n=3)	MP2/6-31G(d) ¹¹	1.549- 1.535	1.465	1.105- 1.093	1.020	103.6	958.6	2.73
	experimental PA ¹⁸						942	
piperidine (27 , n=4)	MP2/6-31G(d) ¹¹	1.529- 1.531	1.467	1.096- 1.099	1.017	111.2	962.4	2.80
	experimental PA ¹⁸						947	

^a C-C, C-N, C-H and N-H are bond lengths in Å, CNC is a bond angle in degrees, PA is the proton affinity in kJ/mol, pK_b is relative. The effect of conformers or differences between bonds results in intervals

^b pK_b values are experimental²³

^c Values taken from this work

^d Large errors for N-H and CNC. Reported as such in literature, not confirmed by own MP2 calculations using a different basis set

A property not discussed above is the role of exocyclic substitution. It was already mentioned that the CH bonds of cyclopropane are shorter than non-cyclic aliphatic ones. Moreover, X-ray studies show that for most three-membered rings, including aziridine, the C(endo)-CH₃ bond is longer (1.513 Å for aziridine) than the endocyclic one.¹⁹ Exocyclic substitution at a carbon atom with a π donor lengthens the opposite endocyclic bond and shortens the vicinal bonds, albeit to a smaller extent.

2.2 Ring Strain

In view of previous considerations, any reaction mechanism involving a *N*-spiro bis-aziridinium ion may be regarded as remarkable and deserves special attention. Textbook knowledge dictates that strain energy impedes its formation. In view of the further discussion, however, a more precise definition of strain is necessary. Traditionally, strain has been defined as an ‘excess’ of electronic energy resulting from a deviation of the molecular structure from a low-energy state, keeping all formal bonds in place.²⁴ The most common classification describes four types:²⁵ Baeyer or angle strain, stretching strain, Pitzer strain and Dunitz-Schomaker or steric strain.

Baeyer strain results from bond angle expansion or compression. Small cyclic systems form the most important examples. Stretching strain manifests itself when bonds are elongated or compressed. In tricyclo[2.1.1.0^{1,4}]hexane **28** (Figure 4) for example²⁶ the bond between the two bridgehead carbon atoms is 1.75 Å compared to 1.54 Å for a normal C(sp³)-C(sp³) bond. Pitzer strain is associated with rotation about a single bond and the resulting short-distance repulsions. The torsional barriers of ethane fall into this category. The same interaction between atoms separated by more than two atoms via formal bonds is called the steric effect.

A more precise definition of strain is the difference between the heat of formation (or combustion) and a strain-free estimate of it.²⁷ There are three methods to obtain this estimate. The first method uses the heat of formation of a strain-free structural isomer like an acyclic molecule or a six-membered ring as an estimate. For example, cyclopropane can be seen as half a molecule of cyclohexane. The second method uses additive schemes to extrapolate the energy of a non-isomeric molecule to an appropriate estimate.²⁸ Using the same example, cyclopropane can be seen as one molecule of cyclohexane with three methylene groups subtracted.



28

Figure 4: tricyclo[2.1.1.0^{1,4}]hexane **28**

The third method is a more general one. Here, the difference between the estimate and the heat of formation becomes the enthalpy change of a reaction.^{27,29} The only strained molecule in this reaction is the one for which the strain is calculated. All other reagents and products are chosen in such a way that specific parameters such as bond and hybridization types are conserved during the reaction. If a large number of parameters is conserved, the enthalpy change of the reaction can be fully contributed to strain. The values from the first two methods are more likely to be biased because it is very difficult to find a non-strained system that is chemically equivalent to a strained one.

Extensive classifications with detailed criteria are available for the reactions using the third method.²⁹ In this work, isodesmic and homodesmotic reactions will be considered. Isodesmic reactions conserve (a) the number of atoms with the same atom number and hybridization state and (b) the number of bonds with specific bonding partners (same atom number and hybridization state). Homodesmotic reactions, which form a subset of the isodesmic ones, conserve (a), (b) and (c) the number of atoms with the same atom number, hybridization state and bonding partners (defined by atom number and hybridization state). Condition (c) is a special case of (a). For example, during isodesmic reactions the number of C(sp³) atoms and C(sp³)-C(sp²) bonds has to be conserved. A typical homodesmotic condition is the conservation of the number of C(sp³) atoms bonded to Cl, C(sp²), C(sp³) and H.

All methods above return the conventional strain energy, i.e. the sum of all stabilizing (e.g. σ -delocalization) and destabilizing factors associated with ring strain. It proves hard and often futile to separate these terms. It has, however, been found that the difference of electron-nuclear potential energy is the largest contributing factor.²⁴ Angle strain thus primarily results from decreased electron-nuclear attraction. It should also be noted that the choice of strain-free reference compounds, that is present in all models, is always arbitrary. After the selection of a method, both experimental and theoretical data can be used to calculate the conventional strain energy. In Section 4.1 this will be applied to several strained bicyclic and spiranic aziridinium ions.

2.3 Aziridines

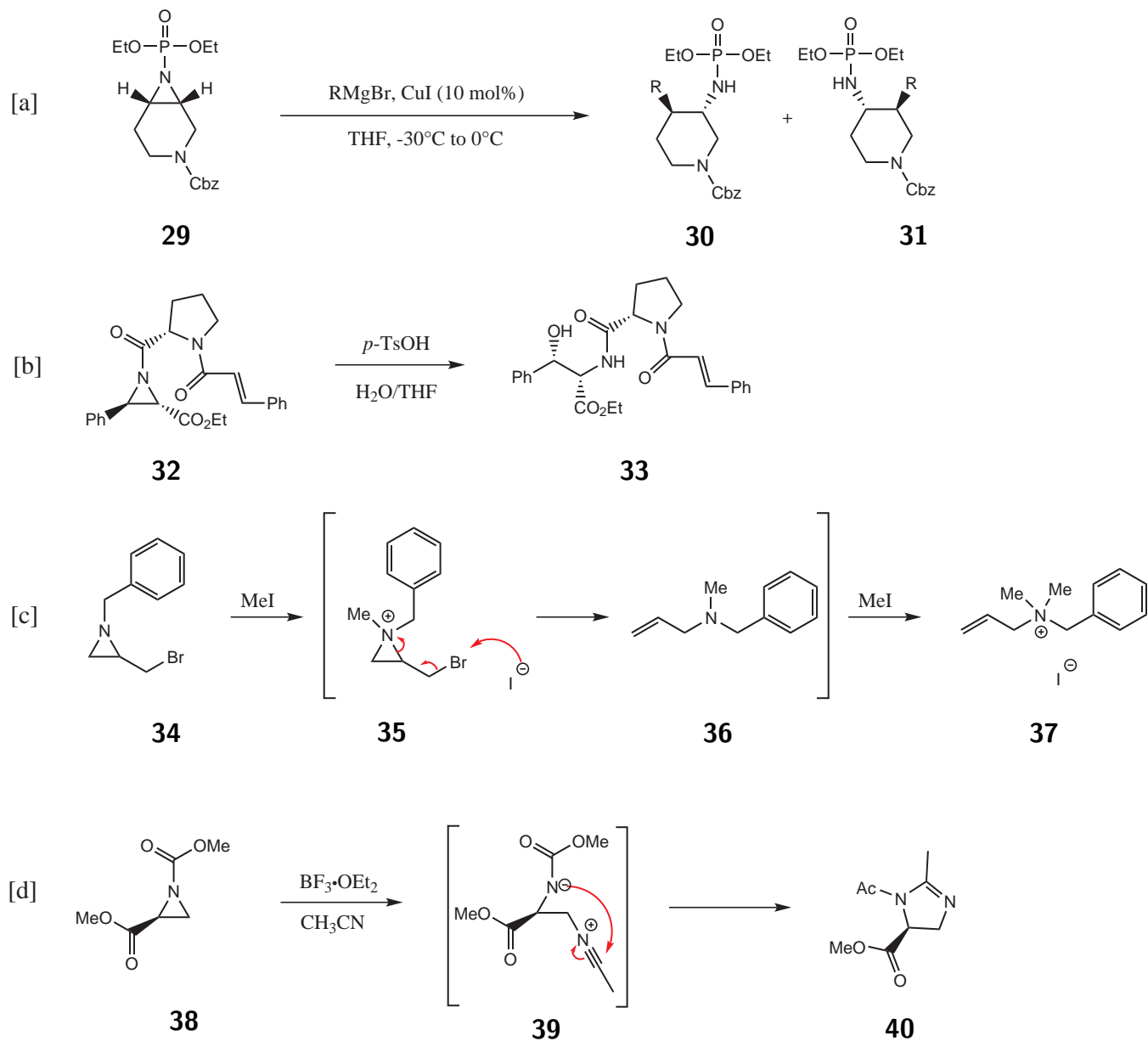
2.3.1 Reactivity

Aziridines have a favorable balance between stability and reactivity which makes them attractive intermediates in organic synthesis. They are prime targets for nucleophilic ring-opening reactions due to the presence of highly polar C-N bonds. They can be classified as activated (bearing an electron-withdrawing group at the nitrogen atom) or nonactivated (bearing an electron-donating group at the nitrogen atom), since they are less reactive toward ring opening than epoxides and often need to be activated to open up, e.g. by complexation of the nitrogen atom with a Lewis acid.

A wide variety of nucleophiles, including carbon, oxygen, sulfur, nitrogen, halogen and hydrogen nucleophiles, have the ability to open the aziridine ring.³⁰ Some examples are given in Scheme 5. Reactions a and b are classical examples in which a nucleophile attacks the 2-position of the aziridine. The C-N bond is broken and the ring strain is relieved. The bicyclic compound **29** is opened with a Grignard reagent to form piperidines **30** and **31**.³¹ An acid-catalyzed hydrolysis of *N*-acylaziridine **32** leads to amide **33**.³² Unlike these examples, the nucleophile does not always attack at the 2-position. In reaction c, 1-benzyl-2-(bromomethyl)aziridine **34** is activated, after which an iodide ion attacks the bromo atom and the C-N bond is broken,³³ resulting in allylic amine **36**, that reacts with an excess of iodomethane to form the quaternary allylammonium salt **37**. The product of a nucleophilic ring opening does not have to be the end product of a reaction sequence however. In reaction d the opening of aziridine **38** leads to intermediate **39**, that reacts further to form 2-imidazoline **40**.³⁴

Furthermore, cycloaddition reactions of aziridines are frequently observed. They proceed either through a 1,3-dipolar species (Scheme 6a) or an azahomoallyl radical species³⁵⁻³⁷ (Scheme 6b). The latter reactions have even been performed sonochemically.³⁶ In addition to reactions at the carbon atoms of the aziridine ring, deprotonation, protonation and Lewis acid complexation at the nitrogen atom can take place. Deprotonation and Lewis acid complexation are less important for the present study. Aziridine has a pK_b value of 6.02 (Table 2) and is therefore less basic than azetidine ($pK_b = 2.71$), pyrrolidine ($pK_b = 2.73$) and piperidine ($pK_b = 2.80$). Theoretical calculations show that the order of aquatic acidity (pK_b) is the same as the order of (gas-phase) proton affinity (PA). This

Scheme 5: Nucleophile-induced ring opening reactions of aziridines



equivalence is not evident: for *p*-X-phenylaziridine (X = NO₂, H, MeO) a reverse relative order is found for PA and pK_b.³⁸

In this thesis the attention is focused on the reactivity of the aziridine nitrogen atom as the nucleophile in a nucleophilic substitution that leads to *N*-spiro bis-aziridinium ions. The ring opening of one of the aziridine rings in these intermediates will be considered only briefly.

Scheme 6: Cycloadditions of aziridines

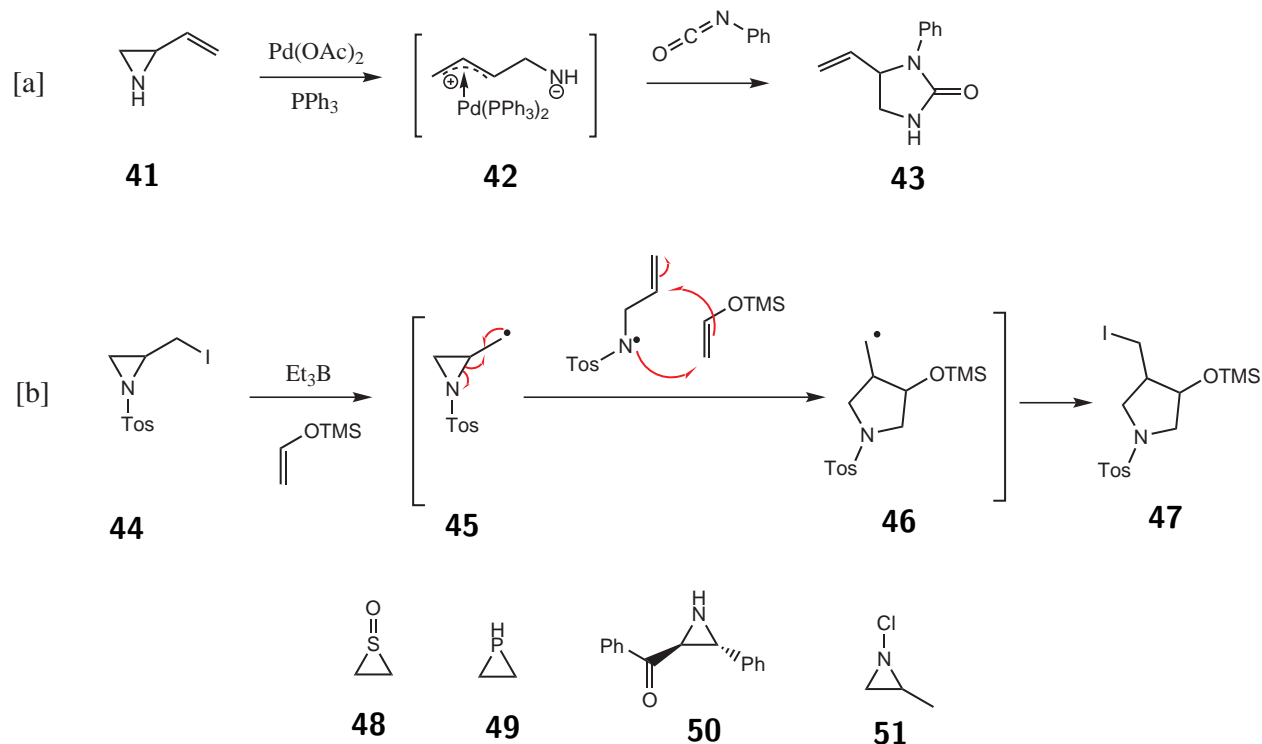


Figure 5: Compounds with pyramidal inversion

2.3.2 Pyramidal Inversion

A molecule that has a tricoordinate atom whose position is not in the plane defined by its bonding partners, can in principle exist as two different conformers or invertomers.³⁹ This is in particular true for three-membered rings such as aziridines, episulfoxides and phosphiranes (Figure 5). The invertomers can interconvert through a planar transition state via pyramidal inversion (Figure 6).

The activation energy barrier for pyramidal inversion is of considerable interest, because a high barrier could allow invertomer isolation. While the Gibbs free energy of activation (ΔG^\ddagger) is only 25-30 kJ/mol for trivalent amines, values of 70-100 kJ/mol are not uncommon for aziridines due to high angle strain.⁴⁰ The invertomers of several aziridines have been isolated,⁴¹⁻⁴⁵ including those of *trans*-phenyl(3-phenylaziridin-2-yl)methanone **50**⁴² and 1-chloro-2-methylaziridine **51**.⁴¹ In most cases ¹H-NMR spectroscopy is used to calculate ΔG^\ddagger by determining the coalescence temperature. Below this temperature certain signals split, because the inversion becomes slow on the NMR time

scale.

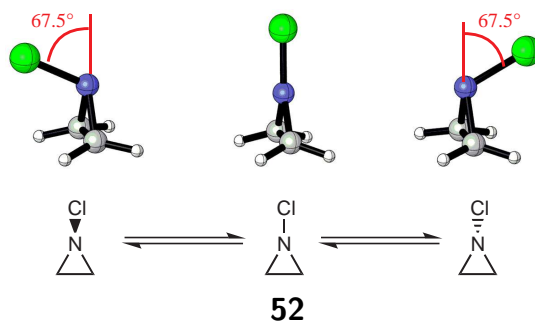


Figure 6: Pyramidal inversion in 1-chloroaziridine **52** (dihedral angle from MP2/6-311+G(2df,2pd) calculations)

2.4 Strained *N*-Spiro and *N*-Bridgehead Aziridinium Ions

A number of highly strained *N*-heterocyclic systems similar to the azoniaspiro[2.2]pentane cation **53** (Figure 7) have been described in the literature. The parent compound has been advocated to account for mass spectrum peaks.^{46,47} A theoretical study on the same compound shows unexpectedly that the ring strain is almost equal to that of protonated aziridine **22**.⁴⁸ In the work of Martinez et al., strain energies and bond paths were calculated for aziridine **20**, protonated aziridine **22** and the azoniaspiro[2.2]pentane ion **53** (Figure 7). In fact, the strain energy of protonated aziridine is about half of the strain energy of compound **53**, which contains two three-membered rings. The claim of equal ring strain should be interpreted per three-membered ring. In Section 4.1 new calculations have been performed on the systems studied by Martinez et al. and on some other relevant compounds using also a broader variety of methods (homodesmotic reactions and other levels of theory).

In another study⁴⁹ the addition of a silver salt to methyl 1-(2-iodo-2-phenylethyl)aziridine-2-carboxylate **54** resulted in an immediate precipitation of alleged 1-methoxycarbonyl-4-phenyl-3-azoniaspiro[2.2]pentane salt **55**⁵⁰ (Scheme 7).

Other *N*-spiro aziridinium ions have been reported.⁵² One interesting example provides mechanistic evidence for an intermediate 6-aza-3-azoniaspiro[2.5]octane cation **57**⁵¹ (Scheme 8). In general, strained *N*-spiranic compounds such as the algal product charamin **60** have been reported.⁵³ Some

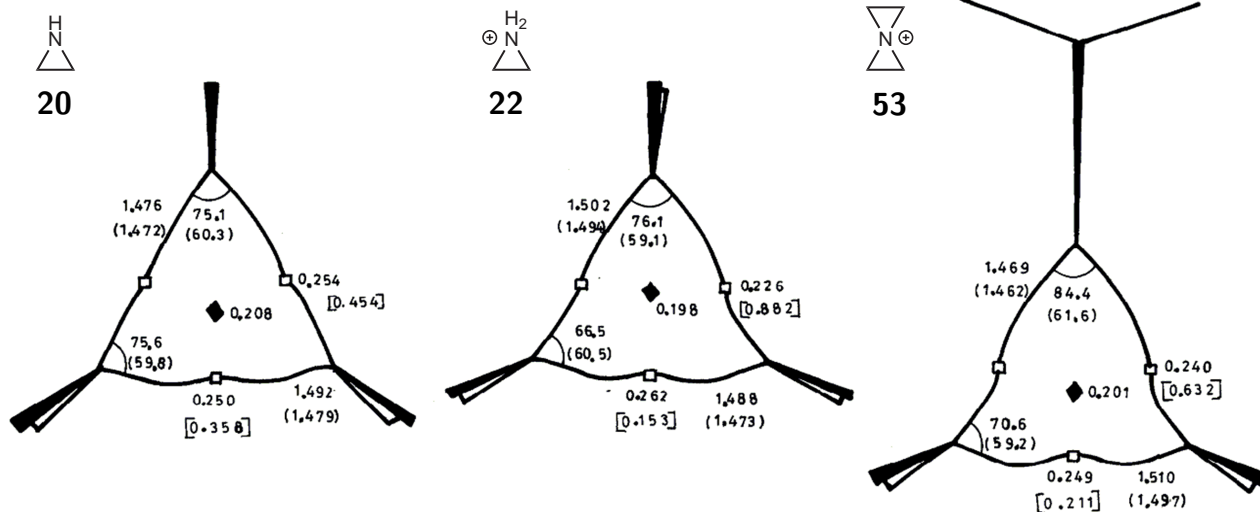
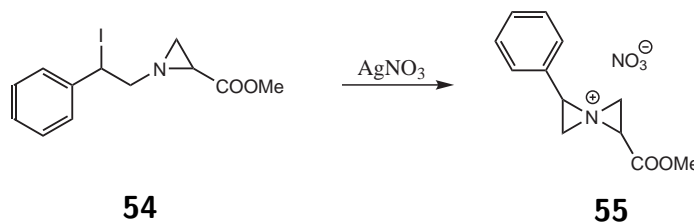
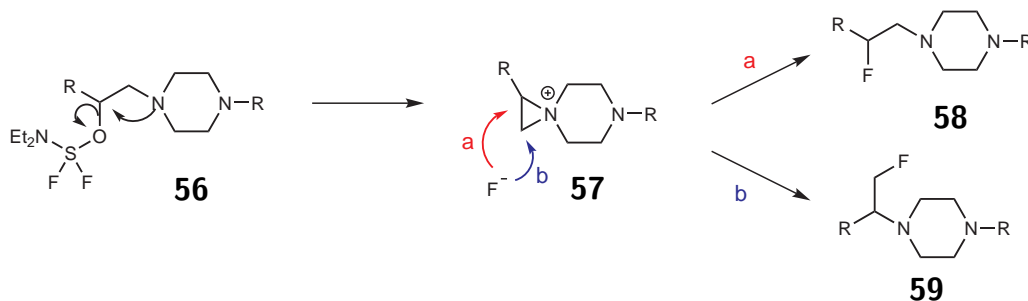


Figure 7: Bond paths (lines), bond lengths and angles determined via bond paths (no parentheses) and via internuclear vectors (round parentheses) of aziridine (**20**), protonated aziridine (**22**) and azoniaspiro[2.2]pentane cation (**53**). Obtained with MP2/6-31G(d)⁴⁸

Scheme 7: Formation of 1-methoxycarbonyl-4-phenyl-3-azoniaspiro[2.2]pentane **55** after addition of silver nitrate to a solution of methyl 1-(2-iodo-2-phenylethyl)aziridine-2-carboxylate **54**⁴⁹



Scheme 8: Mechanistic evidence for the existence of 6-aza-3-azoniaspiro[2.5]octane cation **57**⁵¹



unstrained *N*-spiranic compounds have been marketed as drugs, e.g. the urinary antispasmodic trospium chloride **61**. Furthermore, highly strained *N*-bridgehead bicyclic intermediates can be found in the literature. An example is the aziridine to azetidine conversion found in Scheme 9.⁵⁴ The existence of bicyclic intermediate **62** was postulated on experimental grounds and verified computationally.

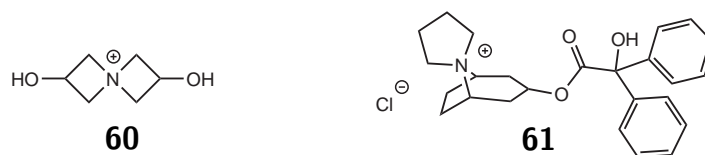
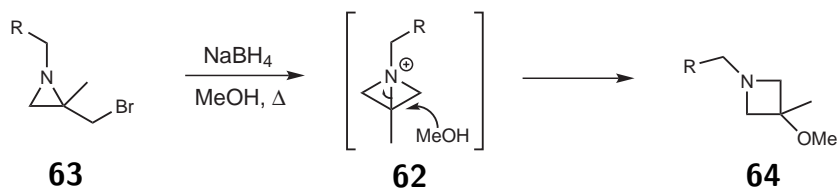


Figure 8: Charamin **60** and trospium chloride **61**

Scheme 9: Aziridine to azetidine conversion via *N*-bridgehead bicyclic intermediate **62**⁵⁴



3 Computational Methods

Theoretical chemistry is the field of chemistry where theoretical models are used to describe the physical and chemical properties of molecules. Several works give an overview of these methods.^{55,56} Molecular modeling techniques can be grouped into three categories: ab initio methods, semi-empirical methods and molecular mechanics. Ab initio methods are based on quantum mechanics and are the most accurate models, but are computationally intensive. They do not use empirical data and can thus be applied to a wide variety of systems. Semi-empirical methods are also based on quantum mechanics, but at various places in the equations empirical data is inserted to decrease the computational cost. Molecular mechanics uses classical physics to describe molecules, i.e. the potential energy is not calculated starting from a quantum mechanical description of the electrons but instead force fields are used that describe the molecules as simple systems consisting out of balls connected via springs.

For each of these methods one can work statically, if only a restricted number of points are calculated on the potential energy surface, or dynamically, if the time evolution of the system is explicitly taken into account. In this work we will restrict ourselves to the first approach for the study of a chemical reaction, of which the reactants, products and transition states will be calculated. In view of the methods used in this thesis, only ab initio methods will be described. Within this class a distinction is made between the Hartree-Fock method, the post-Hartree-Fock methods and Density Functional Theory.

3.1 Ab Initio Methods

All ab initio methods make use of the Born-Oppenheimer approximation, that relies on the fact that nuclei are about a thousand times heavier than electrons. Therefore the electronic and nuclear variables in the Schrödinger equation are solved in a quasi-separable fashion. This results in an electronic wave function and thus energy that depend on the nuclear positions, i.e. the energy of a certain conformer or isomer.

3.1.1 Hartree-Fock (HF) Method

The Hartree-Fock method is a many-body technique in which the electronic wave function is written as a Slater determinant, i.e. as a product of one electron orbitals called molecular orbitals. As such, the total wave function of the N-body system is antisymmetric in accordance with the Pauli exclusion principle. To find the molecular orbitals, an initial guess is taken and the molecular orbitals are varied until a minimal ground state energy is found via the self-consistent field (SCF) method. Every molecular orbital is expressed as a linear combination of basis functions of which the coefficients are varied. In most molecular modeling programs, the basis functions are taken as atomic orbitals which are centered at the positions of the nuclei. The advantage of such basis sets lies in their relatively small dimension. Furthermore each atomic orbital is written as a linear combination of Gaussian type orbitals (GTOs) for reasons of computational efficiency.

After the calculation of the electronic energy of a certain conformer or isomer via SCF, the nuclear positions can be changed. The electronic Hamiltonian will change accordingly and the procedure will be repeated. This iterative procedure can be used to find stationary points of the electronic potential surface and is called a geometry optimization.

HF theory does not describe the correlation part of the electron-electron interaction, but only accounts for the direct Coulomb interaction and the exchange interaction. As such the method was often used in the early days of molecular modeling, but is not reliable enough for the treatment of most chemical problems. Post-HF methods and Density Functional Theory generally give better results as they do incorporate electron-electron correlations.

3.1.2 Post-Hartree-Fock (post-HF) Methods

Post-HF methods start from the HF solution but write the electronic wave function not as a single Slater determinant but as a linear combination of various Slater determinants. As such electron correlation is included, although these methods are computationally expensive. Therefore they are good for benchmarking purposes, but not suited for larger systems like the ones encountered in this thesis. A quite popular method is the Møller-Plesset theory.⁵⁷ In that model, perturbation theory is

used on the HF ground state.

In Section 4.1 MP2 theory with a large basis set (6-311+G(2df,2pd)) will be used to calculate the ring strain and structure of several three-membered rings and spiranic and bicyclic aziridinium ions. This method was chosen to make a comparison with literature results possible. Some of the earlier results reported in the literature were obtained with HF theory and are therefore less reliable than the values obtained in this work.

3.1.3 Density Functional Theory (DFT)

Like post-HF methods, Density Functional Theory (DFT)^{58,59} includes electron correlation, but it does so in a computationally efficient way. DFT is based on the electron density instead of the electronic wave function used in HF theory. The theorems of Hohenberg and Kohn⁶⁰ provide a foundation for this technique. The first theorem gives the relationship between the external potential and the electron density of the ground state. Hence, the ground state electronic energy can be written as a functional of the electron distribution. The second theorem shows that the energy obtained for any electron distribution is always larger than or equal to the true ground state energy for the most optimal density (ground state electronic density). An iterative SCF scheme can be used to obtain the DFT energy of a given isomer or conformer if the functional is known. In practice, this functional is not known and surrogates are used.

DFT is computationally less demanding than post-HF methods, but gives reliable energies and geometries provided that an advanced functional is used. It is not a trivial task to estimate the good functional for a given system and often one has to rely on literature benchmark systems or perform new benchmark calculations. Most calculations in this work are performed with DFT. Almost all geometry optimizations in this thesis are performed with the B3LYP functional and the 6-31+G(d,p) or 6-31++G(d,p) basis set. This functional gives reliable geometries, but unreliable energies. Therefore, a single DFT calculation or energy refinement was done with a different functional. CAM-B3LYP⁶¹ results are given in this work, but M06⁶², BMK⁶³, MPW1B95⁶⁴ and ω B97X-D^{65,66} were also performed. These results are not explicitly taken up in this thesis, but they gave the same qualitative

results. The relatively new functionals CAM-B3LYP and ω B97X-D were used because they are designed to describe long-range effects better. The other functionals are included to compare with previous work.

3.2 Topology of the Electron Density

Molecular modeling typically results in electronic energies and nuclear positions, while organic chemists are accustomed to bonds. It is possible however to extract this information from the wave function that describes the molecular system via the electron density.^{67,68}

The electron density $\rho(\mathbf{r})$ can be obtained from the wave function. Its critical points \mathbf{r}_c ($\nabla\rho(\mathbf{r}_c) = 0$) are associated with atoms, rings, bonds and cages and can be classified by means of the Hessian matrix that contains the second derivatives of $\rho(\mathbf{r})$. The rank ω is the number of nonzero curvatures of $\rho(\mathbf{r})$ and the signature σ is the sum of algebraic signs of the curvatures at a critical point \mathbf{r}_c . \mathbf{r}_c is thus characterized by the tuple (ω, σ) :

(ω, σ)	topology	interpretation
(3,-3)	local maximum	nucleus
(3,-1)	saddle point	middle of a bond
(3,+1)	saddle point	middle of a ring
(3,+3)	local minimum	middle of a cage

Nuclei, bonds, rings and cages are associated with a specific type of critical point: the electron density is the highest around the nuclei (local maximum), a bond critical point (bpc) is associated with every bond. In order to describe bonds, trajectories of $\nabla\rho$ are considered. The trajectory that connects two atoms via a bond critical point is called a bond path and can be identified with a chemical bond. The electron density is accumulated along this path. In Section 4.1 the topology of the electron density is used to apply the bent bond model of three-membered rings to spiranic and bicyclic aziridinium ions.

3.3 Solvation

Accounting for solvation during ab initio calculations has long been a challenging issue. Recently new models became available that allow solvation to be included by means of various models. The oldest method is the implicit solvation model,⁶⁹ in which the molecule is placed in a cavity in a uniform, nondiscrete solvent environment that is described by its dielectric constant (ϵ). The cavity is generally a Van der Waals surface of the molecule. The energy of solvation is a sum of the energy needed to create a cavity in the solvent, the stabilization between the solvent and the molecule by dispersion and the stabilization by electrostatic interaction. The first two terms are proportional to the surface area of the cavity, but the last term can be calculated in different ways. In self-consistent reaction field (SCRF) methods, the molecule induces a polarization of the solvent. This polarization changes the wave function and the electric moments of the molecule. This problem is solved by a self-consistent field and gives the electrostatic stabilization.

Implicit solvation cannot account for specific short-range interactions since the solvent is only described by its dielectric constant. It can be used at every step of a geometry optimization or to calculate the energy of a previously optimized geometry (energy refinement). In this work two version of the Polarizable Continuum Model (PCM) will be used: IEF-PCM⁷⁰ and C-PCM⁷¹ for tetrahydrofuran (THF) and methanol (MeOH) solvation respectively.

Until very recently, implicit solvation was only used for energy refinements of an optimized geometry, but now it has become practically possible to include implicit solvation during the optimization process. There are not much benchmark studies available for this method in the literature. In this thesis a very thorough study using these state-of-the-art methods was performed.

When solvent molecules are able to explicitly interact with the substrate, explicit discrete solvent molecules may be added to the molecular system, i.e. explicit solvation. It is not easy to determine how many solvent molecules need to be added or how they should be oriented with respect to the substrate.^{2-5,72} The number of solvent molecules that need to be added may be guessed by determining the coordination solvation energy. Calculations with explicit solvation may become computationally expensive if a large number of solvent molecules are added, but are necessary to describe short-range

specific interactions such as hydrogen bonding in the first solvation shell. Hence, adding apolar solvent molecules is expected to have little influence. In some cases convergence of energy barriers is obtained if more solvent molecules are added.⁷³

The third solvation method is the explicit/implicit or mixed solvation model in which both discrete solvent molecules (explicit solvation) and embedment in a dielectricum (implicit solvation) are used. The implicit solvation can be applied at every step of a geometry optimization with explicit solvent molecules or only to calculate the energy of a geometry that was previously optimized with explicit solvent molecules. In this work both methods are thoroughly tested for the chemical systems at hand. As such the results obtained in this thesis are interesting from a chemical, as well as a purely theoretical point of view.

3.4 Computational Methodology

All geometry optimizations in this work will be performed with the post-HF method MP2 (Section 4.1) or the DFT method B3LYP (Sections 4.2 and 4.3). The 6-31++G(d,p) basis set was chosen for the geometry optimizations in Sections 4.2 and 4.3 because hydride ions were used and it is mandatory to include sufficient diffuse functions for this application. DFT functionals CAM-B3LYP, M06, BMK, MPW1B95 and ω B97X-D with the 6-311++G(d,p) basis set were chosen for the energy refinements in these sections. Stationary points were characterized as minima or first-order saddle points (transition states) from frequency calculations. The reagent, transition state and product of each reaction were connected via intrinsic reaction coordinate (IRC) calculations followed by full geometry optimizations. For all reactions free energies along the reaction path have been calculated.

All ab initio calculations have been performed with the Gaussian 09⁷⁴ program package. The CYLview⁷⁵ and Multiwfn⁷⁶ freeware packages have been used for visualization and topology calculations.

4 Results and Discussion

4.1 Structure and Stability of Strained Spiranic and Bicyclic Aziridinium Ions

Strained aziridinium ions, which are the topic of this work, can be categorized as the *N*-bridgehead or bicyclic and *N*-spiro or spiranic aziridinium ions. The latter category includes e.g. the 3-azoniaspiro[2.2]pentane cation (**53**), 3-azoniaspiro[2.3]hexane cation (**65**), 3-azoniaspiro[2.4]heptane cation (**66**) and 3-azoniaspiro[2.5]octane cation (**67**), while the former category includes e.g. the 1-methyl-1-azoniabicyclo[1.1.0]butane cation (**68**), 1-methyl-1-azoniabicyclo[2.1.0]pentane cation (**69**) and 1-methyl-1-azoniabicyclo[2.2.0]hexane cation (**70**) (Figure 9). In this section the structure and stability of these ions will be investigated by means of post-HF and DFT calculations, and various properties as introduced in Chapter 2 will be calculated. In order to give a proper interpretation of the various quantitative data, also regular three-membered compounds were included in the dataset. An overview of all structures considered in this section is presented in Figure 9.

4.1.1 Structure

An overview of the structural parameters (defined in Figure 3 of Section 2.1) of some three-membered rings and strained aziridinium ions is given in Table 3 and 4. The methods used in this work are compared with earlier calculations on monocyclic systems (Table 3). Values for bond lengths (C-C, C-X, C-C_{bp}, C-X_{bp}) and bond angles (XCC, CXC, XCC_{bp}, CXC_{bp}) are in good agreement, but larger

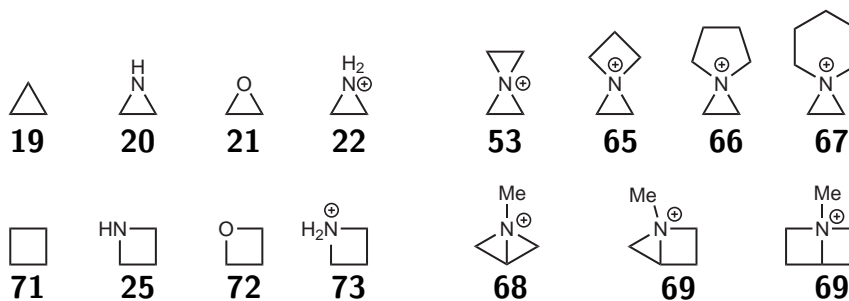


Figure 9: Overview of three-membered rings and spiranic and bicyclic aziridinium ions.

deviations are observed for the other parameters. The calculations in this work were performed at the MP2 level of theory (Chapter 3), which generally gives more reliable results⁷⁷ than the HF level of theory used by Cremer et al.⁹

These methods are now used for the bicyclic and spiranic aziridinium ions **53** and **65-69** (Table 4). The bond length C-C is 1.48-1.50 Å for all compounds and the bond length C-N is 1.46-1.49 Å for monocyclic and spiranic systems and 1.53-1.55 Å for bicyclic systems. Furthermore, there is a small difference (0.01-0.02 Å) between the bond length C-N in the shortest and the longest bridge of the bicyclic systems. This asymmetry can be found in other parameters as well, but is absent in monocyclic and spiranic compounds.

Both bond angles NCC and CNC are 58.2-61.8°: the nuclear positions describe an isosceles, almost equilateral triangle. The bond angle NCC_{bp} increases in the spiranic series **53**, **65**, **66** with the ring size n from 71.4° to 72.1°. This is the result of the bending of both bonds around the carbon atoms. This trend is no longer true for compound **67**, the largest spiranic aziridinium ion. In bicyclic species the bond angle NCC_{bp} depends on whether the central carbon atom is a bridgehead or in the bridge. This difference is 12.3° for compound **68** and 4.6° for compound **69**. The carbon atom with the widest angle can be either a bridgehead atom (for compound **69**) or be in the bridge (for compound **68**).

CNC_{bp} decreases in the spiranic series with increasing ring size n . Although it is tempting to identify $|\text{CNC}_{bp} - 109.5^\circ|$ or $|\text{NCC}_{bp} - 109.5^\circ|$ as a measure for strain, this would result in higher strains for larger ring sizes. This would contradict the results from Section 4.1. CNC_{bp} is smaller for bicyclic aziridinium ions than for spiranic ions with the same number of carbon atoms.

These trends can be explained by means of the one-sided asymmetric deviation Δ as defined in Section 2.1. For spiranic species $|\Delta| < 1^\circ$, while NCC_{bp} and CNC_{bp} are about 10° and 20° larger than NCC and CNC respectively. This indicates that the bending of the C-C bond is greater than that of the C-N bond around a carbon atom. Since bond path angles are defined in terms of tangents, small C-N bending around the carbon atoms does not prevent significant C-N bending around the N atom. Since $\text{CNC}_{bp} \approx \text{CNC} + 20^\circ$, the bending of a C-N bond around the N atom is about 10°.

Table 3: Structural parameters of three-membered rings.^a

\triangle_X	cyclopropane 19 X=CH ₂		oxirane 21 X=O		aziridine 20 X=NH			protonated aziridine 22 X=NH ₂ ⁺		
	this work ^b	Crem. ^c	this work ^b	Crem. ^c	this work ^b	Crem. ^c	Mart. ^d	this work ^b	Crem. ^c	Mart. ^d
C-C	1.50	1.50	1.46	1.45	1.48	1.47	1.48	1.47	1.46	1.47
C-X			1.43	1.40	1.47	1.45	1.47	1.49	1.49	1.49
XCC	60.0	60.0	59.3	58.8	59.9	59.5	59.8	60.4	60.6	60.5
CXC			61.3	62.4	60.2	60.9	60.3	59.1	58.8	59.1
XCC _{bp}	76.9	78.8	74.4	72.8	75.8	77.3	75.6	62.7	60.9	66.5
CXC _{bp}			75.5	75.8	75.7	76.4	75.1	77.1	77.3	76.1
Δ	8.4	9.4	-2.7	0.2	4.4	5.9		-10.1	-11.8	
Q _{CC}	4.78	6.70	14.45	15.80	23.54	10.90	8.79	11.57	11.60	10.18
Q _{CX}			2.45	2.10	2.73	4.10	2.72	19.56	12.80	5.35
η	82.37	82.00	84.84	85.80	82.45	83.10	82.32	84.15	85.00	83.19
$\nabla^2\rho_{CC}$	-19.05	-12.86	-16.89	-16.05	-14.93	-14.69		-17.51	-17.83	
$\nabla^2\rho_{CX}$			-7.62	-1.88	-15.07	-17.79		-8.09	-6.28	

^a Parameters described in Figure 3. If different values are obtained for the same parameter, the average is taken. All distances in Å, angles in degrees, η and Q relative, Laplacians in eÅ⁻⁵.

^b Geometries optimized at the MP2/6-311+G(2df,2pd) level of theory.

^c Geometries optimized at the HF/6-31G(d) level of theory.⁹

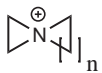
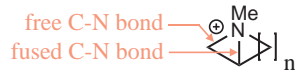
^d Geometries optimized at the HF/6-31G(d) level of theory. Electron density obtained at the MP2/6-31G(p) level of theory.⁴⁸

For bicyclic compounds the C-N bond bending around the carbon atoms is asymmetric (widest angle around bridgehead atom for compound **69**, opposite for compound **68**). In both bicyclic compounds, the C-C bond is considerably bent around the carbon atoms.

The parameter Q as introduced in Section 2.1 describes bond bending globally as a function of the ratio of bond path length and the geometrical bond length. For spiranic systems, C-N bending is smaller than C-C bending. There is no clear trend in C-N bending. C-C bending is relatively large (ca. 20) in spiranic compounds **53**, **65** and **66**, but relatively small (ca. 10) in compound **67**, the largest homologue. For bicyclic compound **68** C-N bending is the smallest for the bond in the shortest bridge. The opposite is true for homologue **69**. For all compounds, the trends in global bending and local bending around the carbon atoms are the same. All these conclusions can be illustrated graphically in contour plots of the electron density (Figure 10).

Variations in η , a parameter which is representative for σ -delocalization, is minimal ($\eta \approx 82$). If the definition of η is extended to larger rings and the same computational methods are used, η values of

Table 4: Structural parameters of spiranic and bicyclic aziridinium ions.^{a,b}

									
	53 (n=1)		65 (n=2)	66 (n=3)	67 (n=4)	68 (n=1)		69 (n=2)	
	this work	Mart. ^c				fused ^d	free ^d	fused ^d	free ^d
C-C	1.50	1.50	1.48	1.48	1.48	1.50		1.50	
C-N	1.46	1.46	1.48	1.48	1.49	1.53	1.54	1.55	1.53
NCC	59.1	59.2	59.9	60.1	60.2	61.2	60.4	60.0	61.8
CNC	61.7	61.6	60.2	59.8	59.7	58.5		58.2	
NCC _{bp}	71.4	70.6	72.0	72.1	71.4	73.3	61.1	65.7	70.3
CNC _{bp}	87.1	84.4	82.0	81.3	74.7	76.5		79.7	
Δ	-0.0		-0.5	-0.6	0.5	-1.2	-9.5	-7.2	-3.2
Q _{CC}	24.88	8.68	18.87	22.80	8.15	11.56		12.57	
Q _{CN}	5.30	4.79	8.87	11.04	3.43	14.60	15.12	21.26	11.11
η	83.14	82.72	83.12	82.91	81.76	81.66		81.11	
$\nabla^2\rho_{CC}$	-15.22		-16.12	-16.42	-13.73	-15.86		-15.93	
$\nabla^2\rho_{CN}$	-8.10		-11.26	-11.80	-10.89	-5.32	-9.57	-8.35	-11.22

^a Parameters described in in Figure 3. If different values are obtained for the same parameter, the average is taken.

^b Geometries optimized at the MP2/6-311+G(2df,2pd) level of theory. All distances in Å, angles in degrees, η and Q relative, Laplacians in eÅ⁻⁵.

^c Geometries optimized at the HF/6-31G(d) level of theory. Electron density obtained at the MP2/6-31G(p) level of theory.⁴⁸

^d fused = values for C-N bond in shortest bridge, free = values for C-N bond in longest bridge.

35.26 and 8.12 are obtained for cyclobutane and the six-membered ring in 3-azoniaspiro[2.5]octane **67** respectively. Three-membered rings have the highest degree of σ -delocalization.

$\nabla^2\rho_{CC}$ and $\nabla^2\rho_{CX}$ indicate that C-X bonds are weaker than C-C bonds. Nucleophilic ring-opening reactions will cleave the C-X bond instead of the C-C bond. In bicyclic systems, the C-X bond in the shortest bridge is the least stable one. Aziridinium ion **69** will preferentially open up to form a five-membered instead of a four-membered ring. This regioselectivity cannot be extrapolated to larger bicyclic compounds. Furthermore, conclusions about reactivity based on topological studies should be tested with geometry optimizations and energy calculations.

4.1.2 Ring Strain

The conventional ring strain of several three-membered rings will be calculated based on the isodesmic and homodesmotic reactions in Scheme 10 as introduced in Section 2.2. For a number of monocyclic

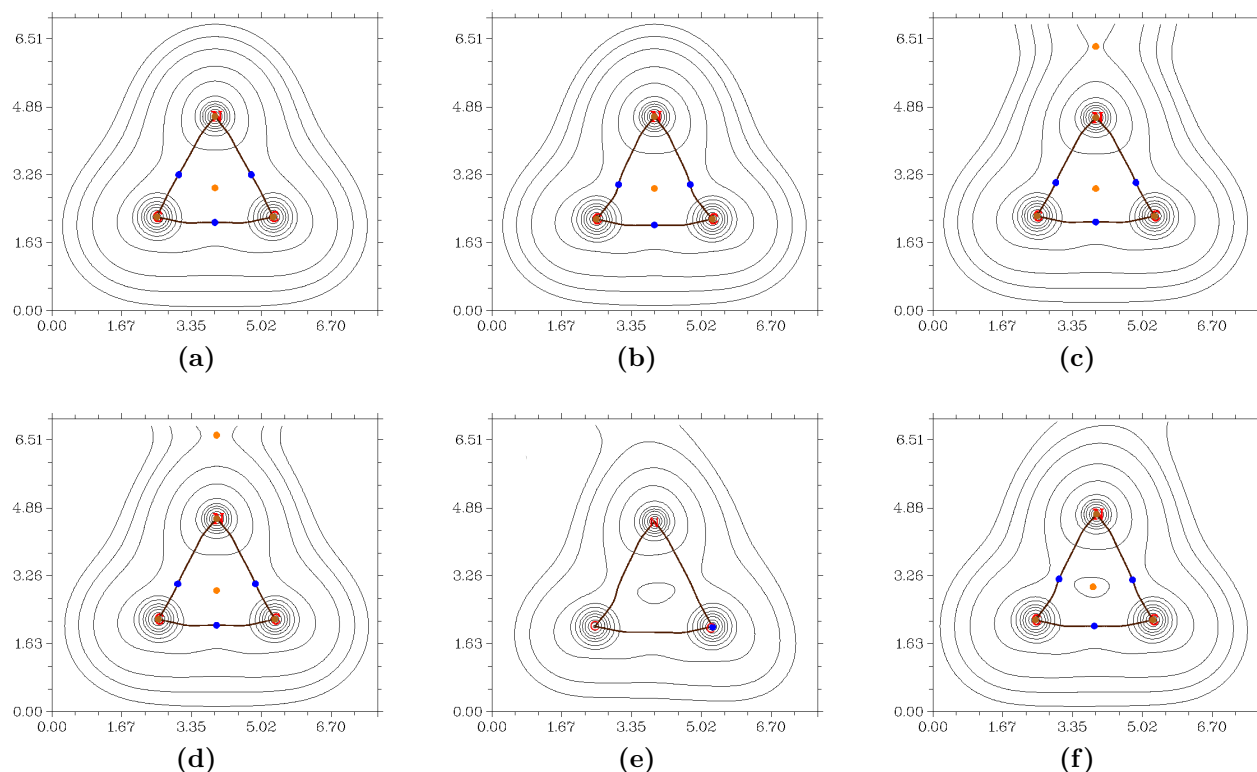
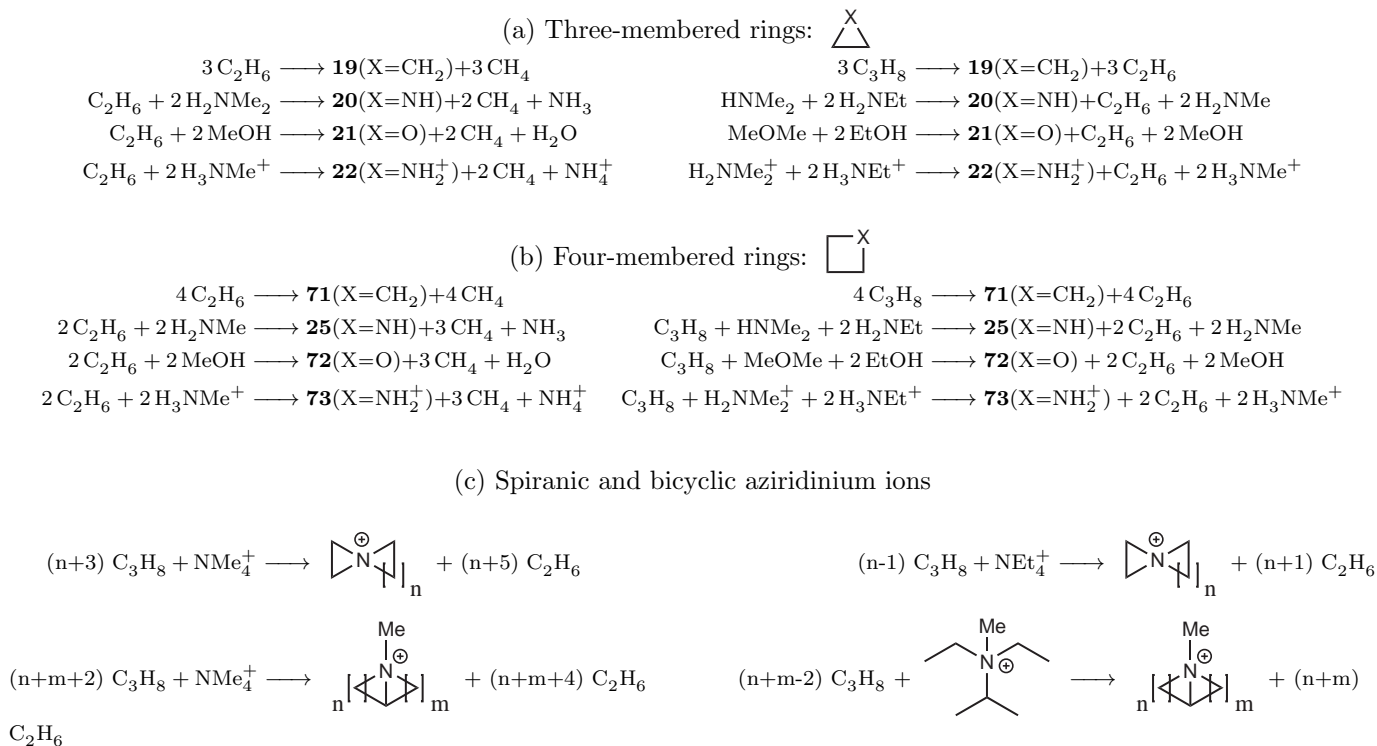


Figure 10: Contour maps of the electron density in the plane of the aziridine ring of (a) aziridine **20**, (b) protonated aziridine **22**, (c) 3-azoniaspiro[2.2]pentane cation **53**, (d) 3-azoniaspiro[2.3]hexane cation **65**, (e) 1-methyl-1-azoniabicyclo[1.1.0]butane cation **68** and (f) 1-methyl-1-azoniabicyclo[2.1.0]pentane cation **69**. Blue point = bond critical point, orange point = ring critical point. Critical points of (e) do not lie in the plane. Distances in Bohr (1 Bohr \approx 0.53 Å).

benchmark compounds previous results are compared with the methods used in this work (Table 5). Calculations were performed at the MP2 level of theory because previous results show good agreement with experiment;^{24,25} the B3LYP level of theory was chosen because it is computationally less expensive. In many cases, chemical accuracy is obtained with homodesmotic reactions at the MP2/6-311+G(2df,2pd) level of theory. Isodesmic values are unreliable and homodesmotic B3LYP/6-31+G(d,p) results are a little less accurate.

Except for protonated aziridine **22** (164.7 kJ/mol), all compounds have a strain energy between 109 and 128 kJ/mol (homodesmotic reactions at the MP2 level of theory). Strain increases in the series oxetane **72** < azetidine **25** < cyclobutane **71** < oxirane **21** < aziridine **20** < cyclopropane **19** < protonated azetidine **73** < protonated aziridine **22**. Three-membered rings are more strained than

Scheme 10: Isodesmic (left) and homodesmotic (right) reactions





four-membered ones. Protonation of azaheterocycles gives highly strained compounds.

The strain energies of some spiranic and bicyclic aziridinium ions are calculated in the same way, although homodesmotic calculations are only performed at the B3LYP level of theory (Table 6). The isodesmic and homodesmotic strains are almost the same for spiranic compounds (difference of 1.1 kJ/mol at the B3LYP level of theory), because the isodesmic reactions are in fact quasi-homodesmotic. These reactions conserve the number of atoms with the same atom number, hybridization state and number of nonhydrogen bonding partners. The last condition is not necessary for isodesmic reactions. For bicyclic aziridinium ions, this condition is not fulfilled and the difference between isodesmic and homodesmotic strains is larger (8.4 kJ/mol at the B3LYP level of theory). This is still smaller than for the three-membered rings in Table 5, because of compensating effects in the isodesmic reactions of the bicyclic aziridinium ions.

The large difference between B3LYP and MP2 isodesmic strain energies (38.3-61.5 kJ/mol) is unexpected, since both methods give similar results for monocyclic compounds. This could be caused by

Table 5: Conventional strain energies of monocyclic compounds.^a

			B3LYP ^b		MP2 ^b		Baric ^c	Dudev ^d	Lewis ^e		experim.	
			iso	homo	iso	homo			iso	homo		
		cyclopropane (19)	X=CH ₂	75.9	100.9	73.9	115.0	121.8	115.9	74.1	115.1	115.1 ⁷⁸
		aziridine (20)	X=NH	57.3	106.0	49.7	114.5	107.9	115.9			111.7 ⁷⁹
		protonated aziridine (22)	X=NH ₂ ⁺	88.9	150.2	90.6	164.7					
		oxirane (21)	X=O	40.3	105.5	32.1	111.1	97.1	111.3			110.0 ⁸⁰
		cyclobutane (71)	Y=CH ₂	63.5	96.8	56.0	110.7	112.1	110.9	56.1	110.9	110.9 ⁷⁸
		azetidine (25)	Y=NH	40.8	97.9	31.8	110.1		106.3			105.4 ⁷⁹
		protonated azetidine (73)	Y=NH ₂ ⁺	41.9	111.5	39.5	127.2					
		oxetane (72)	Y=O	23.4	96.9	17.0	109.7		105.9			103.3 ⁸⁰

^a Energies in kJ/mol.^b Strain energies obtained from electronic energies with ZPE correction based on the reactions in Scheme 10 (iso = isodesmic reactions, homo = homodesmotic reactions). B3LYP = B3LYP/6-31+G(d,p), MP2 = MP2/6-311+G(2df,2pd).^c Homodesmotic reactions for strain calculation at the B3LYP/cc-pVDZ level of theory from literature.²⁴^d Additive scheme for strain calculation at the MP2/6-31+G(d) level of theory from literature.²⁸^e Isodesmic (iso) or homodesmotic (homo) reactions for strain calculation at the MP2/6-311+g(2df,2pd) level of theory from literature.²⁵

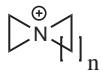
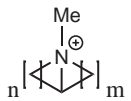
the introduction of tetraalkylammonium ions. Other reactions and levels of theory should be tested to examine this effect.

Every method indicates that strain decreases when methylene units are added to compounds **53** and **68**, the smallest compounds in the spiranic and the bicyclic series. The homodesmotic strain of the largest spiranic compound **67** at the B3LYP level of theory is even smaller than the strain in aziridine **20** at the same level of theory. It is of course unrealistic that a one-ring system is more strained than a two-ring system. This will probably change at the MP2 level of theory, because MP2 strains are higher than B3LYP strains for all the compounds in Table 6.

Bicyclic and spiranic compounds on the same row of Table 6 are structural isomers with the same isodesmic reaction. The difference of the isodesmic strains of both compounds (ΔE in the last column) reveals which isomer is the most stable. Bicyclic compounds are less stable than their spiranic isomers on the B3LYP and MP2 level of theory, although this is not only caused by ring strain.

It can be assumed that the isodesmic strain is almost equal to the homodesmotic strain for MP2 calculations on spiranic and bicyclic aziridinium ions, as is the case at the B3LYP level of theory. Since

Table 6: Conventional strain energies for several spiranic and bicyclic compounds.^a

	B3LYP		MP2		B3LYP		MP2	ΔE^b	
	iso	homo	iso		iso	homo	iso	B3LYP	MP2
53 (n=1)	207.8	208.9	269.3	68 (n=1, m=1)	225.5	217.0	300.0	17.7	30.7
65 (n=2)	149.2	150.3	204.9	69 (n=2, m=1)	150.0	141.6	214.3	0.8	9.4
66 (n=3)	72.9	74.0	111.2	70 (n=2, m=2)	113.4	105.0	169.5	40.5	58.3
67 (n=4)	50.9	52.0							

^a Energies in kJ/mol obtained from electronic energies with ZPE correction according to reactions in Scheme 10 (iso = isodesmic reactions, homo = homodesmotic reactions). B3LYP = B3LYP/6-31+G(d,p), MP2 = MP2/6-311+G(2df,2pd).

^b Difference between isodesmic strains of spiranic (first column) and bicyclic (fifth column) aziridinium ions for a given level of theory (B3LYP = B3LYP/6-31+G(d,p), MP2 = MP2/6-311+G(2df,2pd))

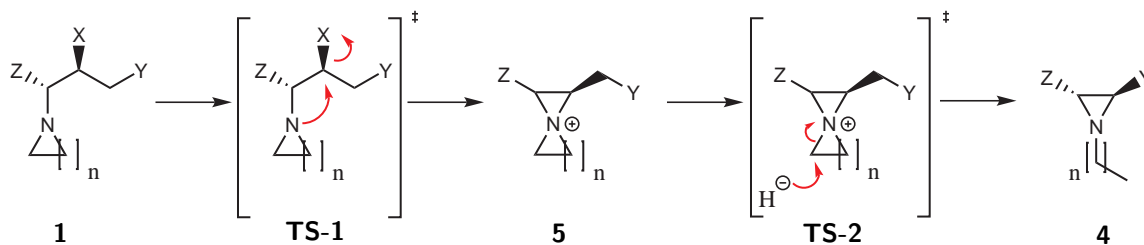
there is good agreement between the homodesmotic strain for MP2 calculations and the experimental strain, the principle of additivity of strain proposed by Martinez et al.⁴⁸ can be tested. According to this principle, the strain of 3-azoniaspiro[2.2]pentane cation **53** is almost equal to the sum of the strains of aziridine **20** and protonated aziridine **22**. This is confirmed by our calculations: the isodesmic strain of compound **53** from MP2 calculations (269.3 kJ/mol) is only 9.9 kJ/mol smaller than the sum of the homodesmotic strains of aziridine **20** (114.5 kJ/mol) and protonated aziridine **22** (164.7 kJ/mol) from MP2 calculations. When the ring size is increased, this difference becomes larger: the isodesmic strain of 3-azoniaspiro[2.3]hexane cation **65** is 69.9 kJ/mol smaller than the sum of the homodesmotic strains of protonated aziridine **22** and azetidine **25**. This is also true for bicyclic compounds. Hence, spiranic and bicyclic aziridinium ions are less strained than would be expected from a comparison with two separate rings, although this difference is small for compound **53**.

4.2 Formation of Spiranic Aziridinium Ions and Their Nucleophile-Induced Ring-Opening Reactions

4.2.1 Introduction

In this section, the formation and subsequent nucleophile-induced ring-opening reactions of spiranic aziridinium ions (Scheme 11) will be investigated by means of DFT calculations. Scheme 11 is a generalization of the reactions dealing with the *N*-spiro bis-aziridinium ion formation taken up in Scheme 4, mentioned in Chapter 1. The *p*-tolyl group of the original compounds introduced in Chapter 1 is replaced by a phenyl group. This was done to reduce the computational cost without altering the reactivity. The formation of spiranic aziridinium ions **5a** and **5b** from aziridines **1a** and **1b** respectively (Scheme 12) and the effect of solvation and substitution on these reactions will be studied thoroughly since it is assumed to be the rate-determining step in the formation of aziridines **4**. The nucleophilic ring opening of compounds **5a**, **5b**, **3** and **74** to form monocyclic aziridines and acyclic amines is exergonic under most conditions^{81,82} and will be studied in less detail. As an example, the opening of aziridinium ion **5a** to form aziridine **4a** is studied.

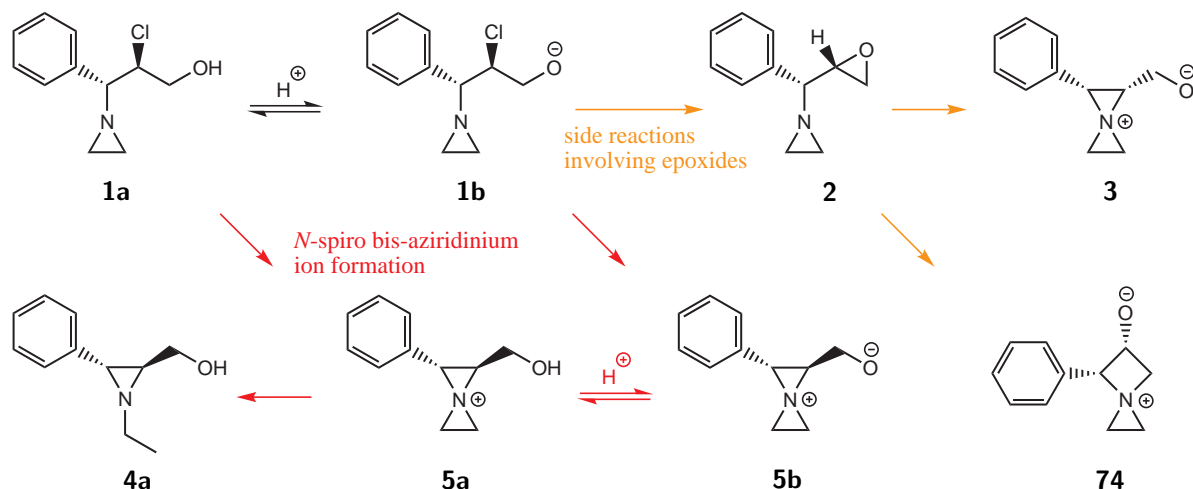
Scheme 11: Formation and ring opening of spiranic aziridinium ion **5**.



The side reactions starting from 1-[oxiran-2-yl(phenyl)methyl]aziridine **2** (Scheme 12, side reactions involving epoxides) will be discussed in Section 4.3. Since the products from these reactions have a different stereochemistry than the products from the former reactions (Scheme 12, *N*-spiro bis-aziridinium ion formation), it is possible to discriminate between these pathways experimentally.

In the previous section it was shown that the strain energy of spiranic aziridinium ions is relatively high. Therefore, high values are expected for the free reaction energy ΔG_{rxn} (Figure 11) of the

Scheme 12: Overview of the reactions of aziridine **1a**.



formation of these compounds. The reaction is thus expected to be endergonic. However, in order to be formed, the free energies of activation ΔG^\ddagger need to be evaluated as these determine the rates of formation. If ΔG^\ddagger and ΔG_{rxn} are moderately high, formation may be expected and afterwards these elusive compounds will rapidly convert into more stable compounds.

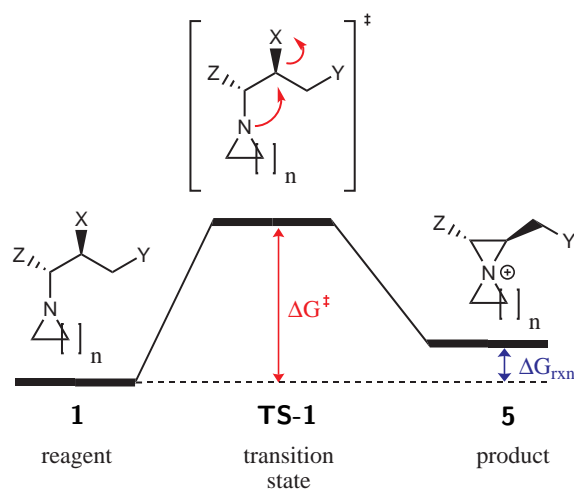


Figure 11: Energetical barriers of a reaction, illustrated for the formation of spiranic aziridinium ion **5**.

4.2.2 Solvation Effects on the Formation of Spiranic Aziridinium Ions

At first instance, the influence of solvation on the formation of intermediates **5a** and **5b** will be investigated. These intermediates were selected because the original experiments took place in a

basic environment. Although the focus of this study will be on MeOH and THF solvation, several other solvents will be tested as well. MeOH and THF were chosen because they were used in previous experiments.¹ In some of these experiments, the hydroxyl side chain is deprotonated because LiAlH₄ is present. It is of particular importance to assess the influence of solvent on the reactivity for both protonation states, as solvation will be different in both cases.

4.2.2.1 Reactivity in Vacuo

The simplest way to assess the reactivity of compounds **1a** and **1b**, is to perform gas-phase or in vacuo calculations, which account for no solvation at all. These results serve as a reference for the more complicated solvation models. Gibbs free energy profiles for the formation of compounds **5a** and **5b** from calculations in vacuo are shown in Figure 12. Two clearly distinct conformers were found for aziridine **1a** and transition state **TS-1a** which are shown in Figure 12. In the most stable conformers the chlorine atom interacts with the hydroxyl group at the β -position via a hydrogen bond. In the less stable conformers, the hydroxyl group is turned away from the chlorine atom. ΔG_{rxn} and ΔG^\ddagger are 73.4 and 147.2 kJ/mol for these conformers, which is lower than the values for the more stable conformers. In the product, the chloride ion interacts with the positively charged nitrogen center and the hydrogen bond donor. This is probably an artefact due to the absence of solvation. With proper solvation, the chloride ion would have the tendency to leave.

Since aziridine **1b** has no hydrogen bond donor, only one clearly distinct conformer was found for aziridine **1b** and transition state **TS-1b**. Furthermore, the distance in transition state **TS-1** between the nitrogen and the carbon atom of the forming bond (C-N_{TS}) is considerably longer in **TS-1b** than in **TS-1a** (1.80 and 1.72 Å respectively). The length of the aziridine C-N bond is 1.47-1.49 Å in all equilibrium geometries, which corresponds to the earlier results (Section 4.1). Since no intramolecular hydrogen bonding is possible in compound **5b**, the chloride ion will leave the product even in absence of surrounding solvent molecules. This effect was not expected, because optimizations in vacuo do not stabilize free ions.⁸³ In most cases an ion will have the tendency to leave the product (displacement of more than 3.5 Å from the initial reaction center) if the following two conditions are fulfilled: (a) there

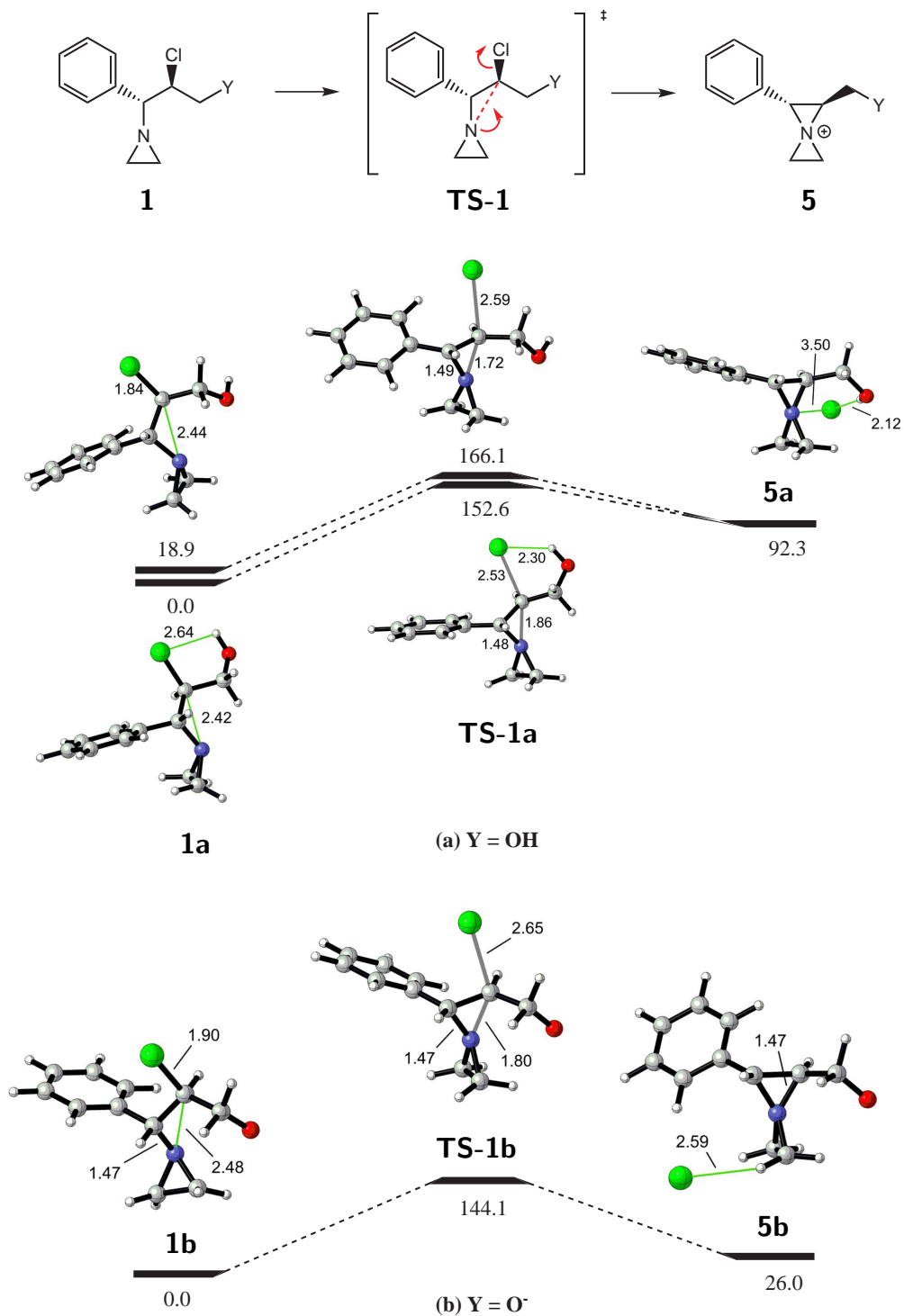


Figure 12: Gibbs free energy profiles (CAM-B3LYP/6-311++G(d,p)//B3LYP/6-31++G(d,p)) for the formation of spiranic aziridinium ions **5a** and **5b** from calculations in vacuo. Free energies in kJ/mol at 298 K and 1 atm. Some critical distances are given in Å.

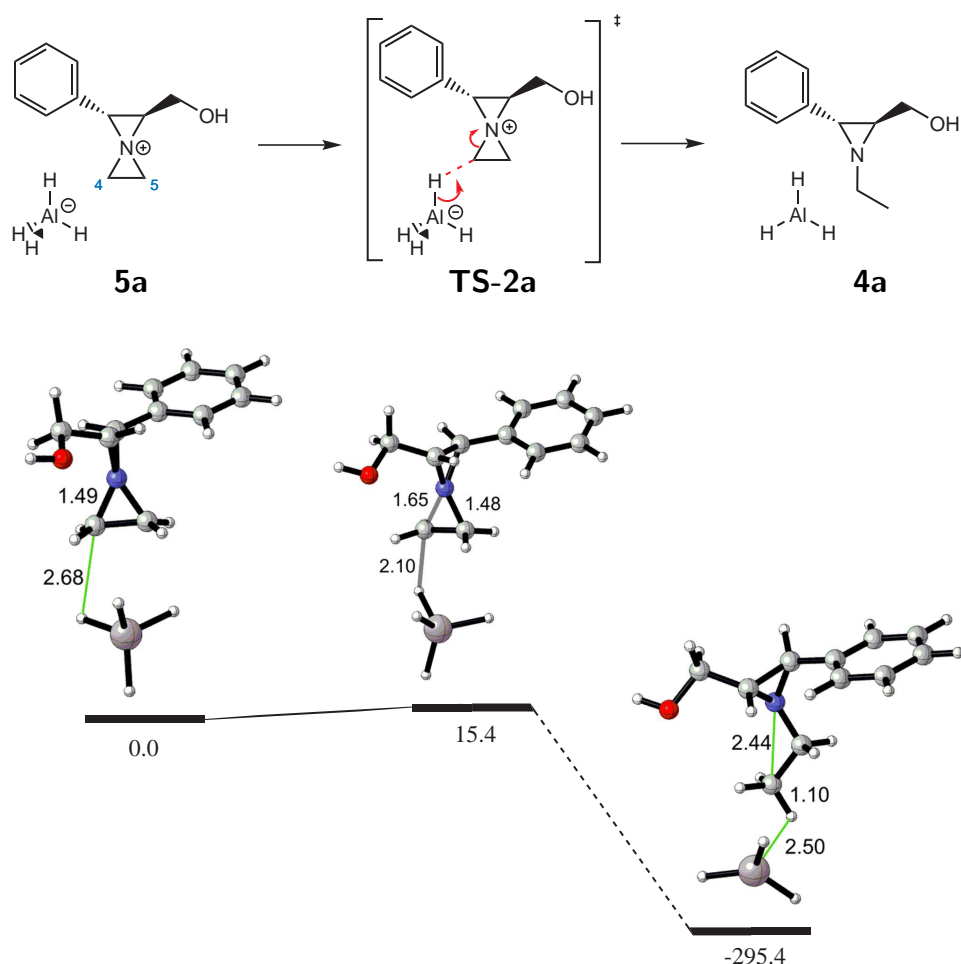


Figure 13: Gibbs free energy profile (CAM-B3LYP/6-311++G(d,p)//B3LYP/6-31++G(d,p)) for the ring opening of spiranic aziridinium ion **5a** from calculations in vacuo. Free energies in kJ/mol at 298 K and 1 atm. Some critical distances are given in Å.

is no strong interaction between the ion and the reaction complex and (b) there must be sufficient solvent stabilization of the ion.

The next step of the reaction scheme concerns the ring opening of the spiranic intermediate (Scheme 12). Gibbs free energy profiles for the ring opening of intermediate **5a** from calculations in vacuo are shown in Figure 13. The hydroxyl group in compound **5a** has its oxygen atom turned towards the positive center. This is another gas-phase artefact: solvent stabilization will probably be stronger than this electrostatic interaction.

CAM-B3LYP energy refinements on the calculations in vacuo on the formation of compounds **5a** and **5b** can be found in Table 7. For both spiranic compounds ΔG^\ddagger is higher than 140 kJ/mol, which

is quite high. Since ΔG^\ddagger is lower for **5b** than for **5a**, the formation of intermediate **5b** seems more favorable than that of **5a**. A possible explanation is the mutual stabilization of negative and positive charges in compound **5b**, i.e. zwitterionic stabilization. This stabilization has a greater impact than the intramolecular hydrogen bonding. In practice, the acidity of the environment determines the equilibrium between compounds **1a** and **1b** and thus the starting product for the formation. The less stable conformers of reagent **1a** and transition state **TS-1a** are respectively 18.9 and 13.5 kJ/mol higher in energy than the most stable conformers (Figure 12).

CAM/B3LYP energy refinements on the calculations in vacuo on the ring opening of compound **5a** to form aziridine **4a** can be found in Table 8. Since ΔG_{rxn} is very negative (-295.4 kJ/mol) and ΔG^\ddagger is small (15.4 kJ/mol), this step is very fast and the formation of intermediates **5a** and **5b** is the rate determining step of the conversion of aziridine **1** to aziridine **4** in Scheme 12 as anticipated. From now on the focus of this study will be on the formation. There is no significant energetical difference between the ring opening at the 4 or the 5 position of compound **5a** (Figure 13): ΔG_{rxn} and ΔG^\ddagger differ about 0.5 kJ/mol at the B3LYP/6-31++G(d,p) level of theory. The phenyl and hydroxymethyl group are too far away from the reaction center to have a significant influence. From these results it follows that spiranic aziridinium ions are unstable and prone to nucleophilic attack.

4.2.2.2 Implicit Solvation

Implicit solvation can be taken into account at two levels, either only for energy refinements or either performing full geometry optimizations using the implicit solvation model. The last procedure has only become available very recently and most literature works discuss only energy refinements. From this point of view the results presented here are not only interesting for the specific chemistry but also to assess state-of-the-art computational methods.

Gibbs free energy profiles for the formation of compounds **5a** and **5b** from optimizations with implicit THF solvation can be found in Figure 14. In contrast to the gas-phase results in Figure 12 the chloride ion does not stay close to the product. Two clearly distinct conformers are not only found for reagent **1a** and transition state **75a**, but also for product **5a**. In the less stable conformers, there is no

hydrogen bond between the chlorine atom and the hydroxyl group and the ion drifts away from the product. In the most stable pathway, this hydrogen bond is never broken. The free energy difference between the reactant conformers is only 0.6 kJ/mol because in the less stable conformer there is a hydrogen bond between the aziridine nitrogen atom and the hydroxyl hydrogen atom. These geometry alterations obtained by optimizing with implicit solvation give a more realistic picture of the chemical system at hand.

The distances between the nitrogen and the carbon atom of the forming bond ($C-N_{TS}$) and the carbon and the chlorine atom of the breaking bond ($C-Cl_{TS}$) in the transition state can be correlated with ΔG^\ddagger (see further). An early transition state with a small $C-Cl_{TS}$ and a large $C-N_{TS}$ is similar to the reagent and has a small ΔG^\ddagger (Hammond postulate).⁸⁴ The opposite is true for late transition states. $C-N_{TS}$ is longer in **TS-1a** geometries from optimizations with implicit THF solvation than from optimizations in vacuo (1.86 and 1.72 Å respectively) and $C-Cl_{TS}$ is shorter than in geometries optimized in vacuo (2.53 and 2.66 Å respectively). $C-N_{TS}$ is longer in **TS-1b** (1.93 Å) than in compound **TS-1a** just like in geometries optimized in vacuo. Optimizations with implicit MeOH solvation result in transition states similar to those with implicit THF solvation and will be discussed later.

The distance in the transition state between the carbon atoms of the breaking bond ($C-C_{TS}$) is longer in **TS-2a** geometries from optimizations with implicit THF solvation than from optimizations in vacuo (1.74 and 1.65 Å respectively) and the distance between the carbon and the hydrogen atom of the forming bond ($C-H_{TS}$) is shorter than for optimizations in vacuo (1.86 and 2.10 Å respectively).

CAM-B3LYP/implicit solvation energy refinements on both the optimizations in vacuo and the optimizations with implicit solvation are listed in Table 7. When using only implicit solvation without additional optimization ΔG^\ddagger is 95.1 and 82.6 kJ/mol for the formation of intermediate **5a** and 97.3 and 87.8 for the formation of compound **5b**, in THF and MeOH respectively. If the geometries are also reoptimized the values are slightly higher giving 112.9 and 107.5 kJ/mol for **5a** and 103.6 and 80.9 kJ/mol for **5b**, in THF and MeOH respectively. The same trends hold for ΔG_{rxn} . ΔG_{rxn} and ΔG^\ddagger are smaller for implicit solvation than for calculations in vacuo (previous section), because

Table 7: Relative Gibbs free energies (kJ/mol, calculations at 298 K and 1 atm) for the formation reaction of spiranic aziridinium ions **5a** and **5b**.^a

optimization	energy refinement	X = OH			X = O ⁻		
		1a	TS-1a (ΔG^\ddagger)	5a (ΔG_{rxn})	1b	TS-1b (ΔG^\ddagger)	5b (ΔG_{rxn})
in vacuo	in vacuo	0.0	152.6	92.3	0.0	144.1	26.0
	implicit (THF) ^b	0.0	95.1	33.7	0.0	97.3	5.4
	implicit (MeOH) ^c	0.0	82.6	22.2	0.0	87.8	2.9
implicit (THF) ^b	implicit (THF) ^b	0.0	112.9	38.4	0.0	103.6	-6.1
	implicit (MeOH) ^c	0.0	107.5	13.6	0.0	80.9	-14.0
explicit (1 THF) ^d	in vacuo	0.0	150.1	87.7	0.0	138.9	79.8
	implicit (THF) ^b	0.0	103.0	40.7	0.0	96.1	8.6
explicit (1 MeOH) ^d	in vacuo	0.0	126.6	70.5	0.0	148.2	97.2
	implicit (MeOH) ^c	0.0	82.1	18.3	0.0	106.2	-3.6
explicit (2 MeOH) ^d	in vacuo	0.0	109.0	69.4			
	implicit (MeOH) ^c	0.0	83.0	6.3			
	implicit (THF) ^b	0.0	115.6	38.1	0.0	103.4	10.7
explicit/implicit (1 THF) ^e	implicit (MeOH) ^c	0.0	101.0	5.1			
explicit/implicit (1 MeOH) ^e	implicit (MeOH) ^c	0.0	91.0	-4.8			
explicit/implicit (2 MeOH) ^e	implicit (MeOH) ^c	0.0					

^a B3LYP/6-31++G(d,p) optimized structures, CAM-B3LYP/6-311++G(d,p) energy refinements. Results for the most favorable pathway shown.

^b Implicit solvation with IEF-PCM ($\epsilon = 7.4$).

^c Implicit solvation with C-PCM ($\epsilon = 32.6$).

^d Optimization with the corresponding number of explicit solvent molecules.

^e Optimization with implicit solvation and the corresponding number of explicit solvent molecules.

charge separation increases along the reaction coordinate. Implicit solvation stabilizes ions more than neutral species.⁸⁵ The decrease of ΔG_{rxn} and ΔG^\ddagger is larger for MeOH than for THF. Remarkable results were found for the formation of compound **5b**: for optimizations with implicit solvation the decrease of ΔG_{rxn} is so large that the reaction becomes exergonic ($\Delta G_{\text{rxn}} < 0$). The aziridinium ion **76** is stabilized by zwitterionic stabilization which is the mutual stabilization of negative and positive charges in the molecule.

CAM-B3LYP/implicit solvation energy refinements for the ring opening of compound **5a** on both the optimizations in vacuo and the optimizations with implicit solvation can be found in Table 8. ΔG_{rxn} and ΔG^\ddagger increase because the ionic character decreases along the reaction coordinate. This effect is the largest for optimizations with implicit solvation.

Table 8: Relative Gibbs free energies (kJ/mol, calculations at 298 K and 1 atm) for the ring opening of spiranic aziridinium ion **5a** (in vacuo and implicit THF optimizations).^a

optimization	energy refinement	5a	TS-2a (ΔG^\ddagger)	4a (ΔG_{rxn})
gas-phase	gas-phase	0.0	15.4	-295.4
	implicit (THF) ^b	0.0	31.6	-215.7
implicit (THF) ^b	implicit (THF) ^b	0.0	52.5	-189.6

^a B3LYP/6-31++G(d,p) optimized structures, CAM-B3LYP/6-311++G(d,p) energy refinements. Results for most favorable pathway shown.

^b Implicit solvation with IEF-PCM ($\epsilon = 7.4$).

4.2.2.3 Explicit Solvation

Unlike optimizations with implicit solvation, optimizations with explicit solvation can account for specific interactions between the solvent and the reaction complex. Gibbs free energy profiles for the formation of compounds **5a** and **5b** from optimizations with explicit optimizations can be found in Figures 15 and 16 respectively.

THF stabilizes the chlorine atom by coordination with two of its hydrogen atoms. The only other possibility for specific interaction between THF and the reaction complex is the electrostatic stabilization of the positively charged nitrogen center by the oxygen atom of THF. Steric hindrance probably disfavors this interaction, although this was not tested. The geometries from optimizations in vacuo (Figure 12) and optimizations with one explicit THF molecule are similar, except for the position of the chloride ion in the product. As could be anticipated explicit solvation will not alter the geometries substantially in case of THF.

It is expected that explicit or explicit/implicit optimizations are necessary for MeOH, since it is a polar protic solvent and a hydrogen bond donor and acceptor. Up to two MeOH molecules were added, though adding more molecules does not always increase accuracy.⁸⁶ MeOH molecules are hydrogen bonded to the chlorine atom throughout the reaction. Just as in optimizations with implicit solvation, the chloride ion drifts away from the reaction complex. This drift is small in product complex **5a** because of the hydrogen bond between the hydroxyl group of the product and the chloride ion.

In product complex **5b** there is no such interaction and the chloride ion drifts away more easily. Optimizations with explicit or explicit/implicit solvation of the ring opening will not be performed as it was already found that this is not the rate-determining step of the overall reaction scheme.

CAM-B3LYP energy refinements on the optimizations with explicit solvation are also given in Table 7 and visually represented in Figures 15 and 16. Calculations in THF give ΔG_{rxn} and ΔG^\ddagger values that are high and similar to calculations in vacuo. The reader should bear in mind that at this point only some explicit solvent molecules were added without embedding the complex in an electrostatic solvent environment. ΔG_{rxn} and ΔG^\ddagger decrease if an extra MeOH molecule is added for the conversion of **1a** to **5a**. The lowest barriers are found for optimizations with two explicit MeOH molecules: $\Delta G_{\text{rxn}} = 69.4$ kJ/mol and $\Delta G^\ddagger = 109.0$ kJ/mol versus 92.3 and 152.6 kJ/mol from calculations in vacuo. These calculations confirm the earlier hypothesis that MeOH and THF have another effect on the formation.

4.2.2.4 Explicit/implicit (Mixed) Solvation

Explicit/implicit or mixed solvation is a combination of the methods used in the previous sections. In this case, explicit solvent molecules are added to the reactive complex and the whole system is further embedded in a dielectricum. The transition state geometries obtained by mixed explicit/implicit solvent optimization of the formation of compounds **5a** and **5b** resemble the transition state geometries from optimization with implicit solvation alone, for both MeOH and THF (Figures 17 and 18). The chloride ion drifts away from the product, but hydrogen bonds remain intact (not shown). MeOH molecules are hydrogen-bonded to the chlorine atom throughout the reaction.

CAM-B3LYP/implicit solvation energy refinements for both the optimizations with explicit solvation and the optimizations with explicit/implicit solvation are listed in Table 7. ΔG_{rxn} values from optimizations with explicit/implicit solvation are lower than those from optimizations with explicit solvation, the opposite is true for ΔG^\ddagger . The formation of intermediate **5a** for example has ΔG^\ddagger values of 82.1 and 101.0 kJ/mol and ΔG_{rxn} values of 18.3 and 5.1 kJ/mol using implicit solvation for the energy refinements for geometries from the explicit and the explicit/implicit model, respectively.

Irrespective of the solvation model used, one can conclude that the values for the barriers decrease when the system is embedded in a solvent environment. The precise magnitude is dependent on the solvent model used and on the precise nature of the solvent molecules. The formation of intermediate **5a** is exergonic for optimizations with explicit/implicit solvation (two MeOH molecules).

One side remark concerns the number of MeOH molecules used in the explicit solvation model. It seems that the energies from implicit solvation energy refinements for optimizations with explicit MeOH solvation converge: ΔG^\ddagger and ΔG_{rxn} change little if two MeOH molecules are used instead of one. If this trend would continue for three MeOH molecules, it could be concluded that one molecule is sufficient to model this reaction.

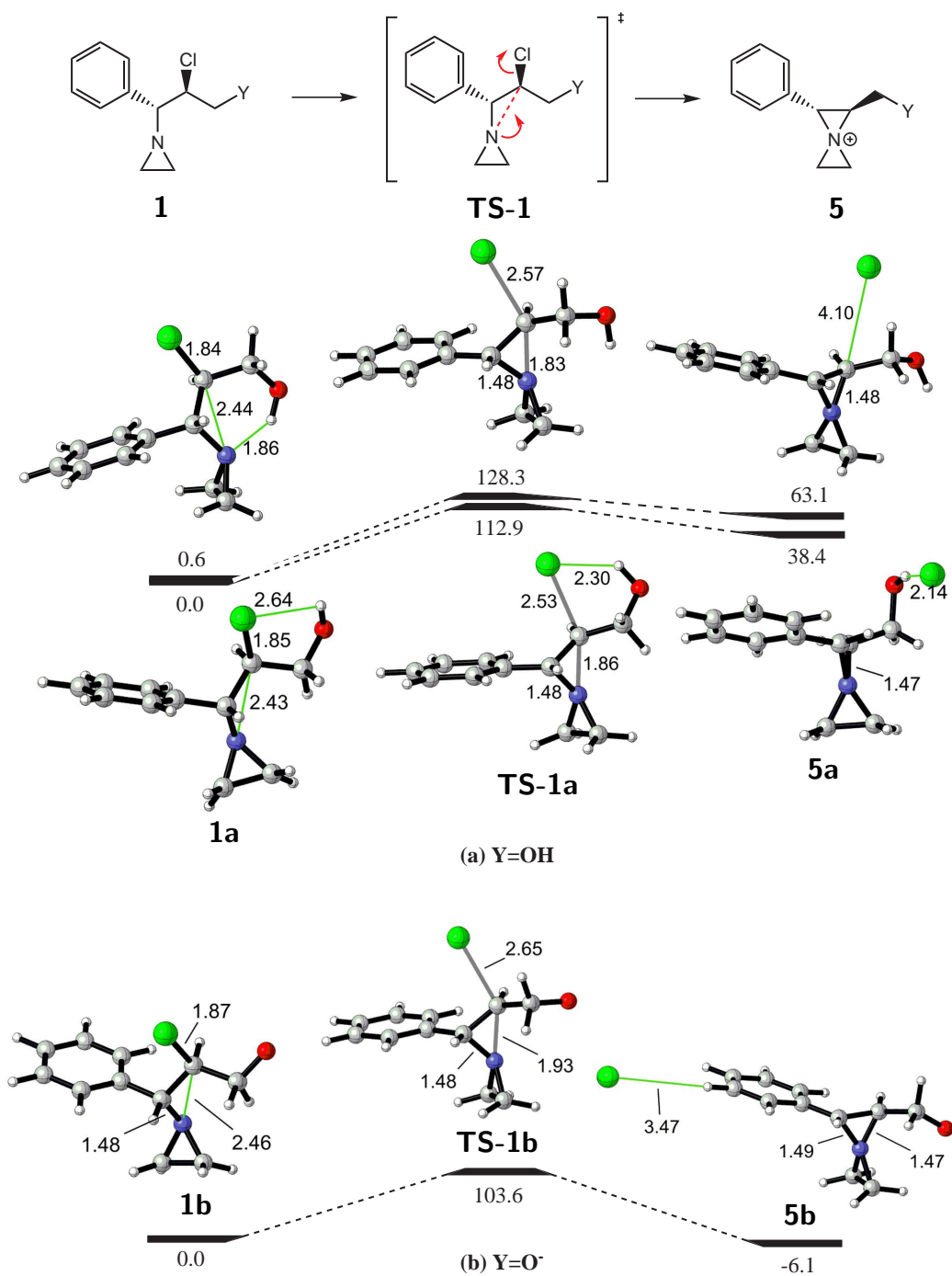


Figure 14: Gibbs free energy profiles (CAM-B3LYP/6-311++G(d,p)//B3LYP/6-31++G(d,p)) for the formation of spiranic aziridinium ions **5a** and **5b** from optimizations with implicit THF solvation (IEF-PCM, $\epsilon = 7.4$). Free energies in kJ/mol at 298 K and 1 atm. Some critical distances are given in Å.

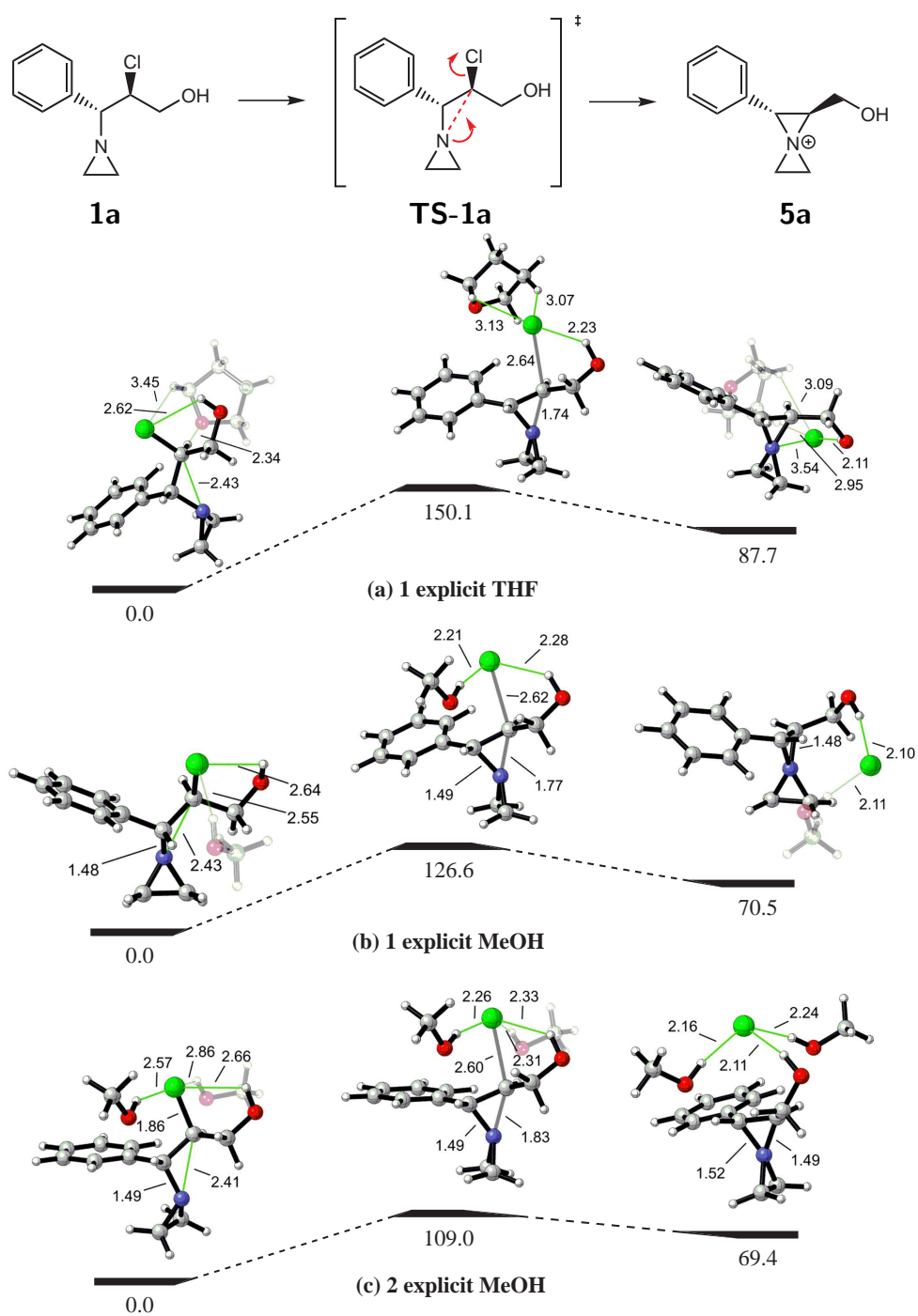


Figure 15: Gibbs free energy profiles (CAM-B3LYP/6-311++G(d,p)//B3LYP/6-31++G(d,p)) for the formation of spiranic aziridinium ion **5a** from optimizations with explicit solvation. Free energies in kJ/mol at 298 K and 1 atm. Some critical distances are given in Å.

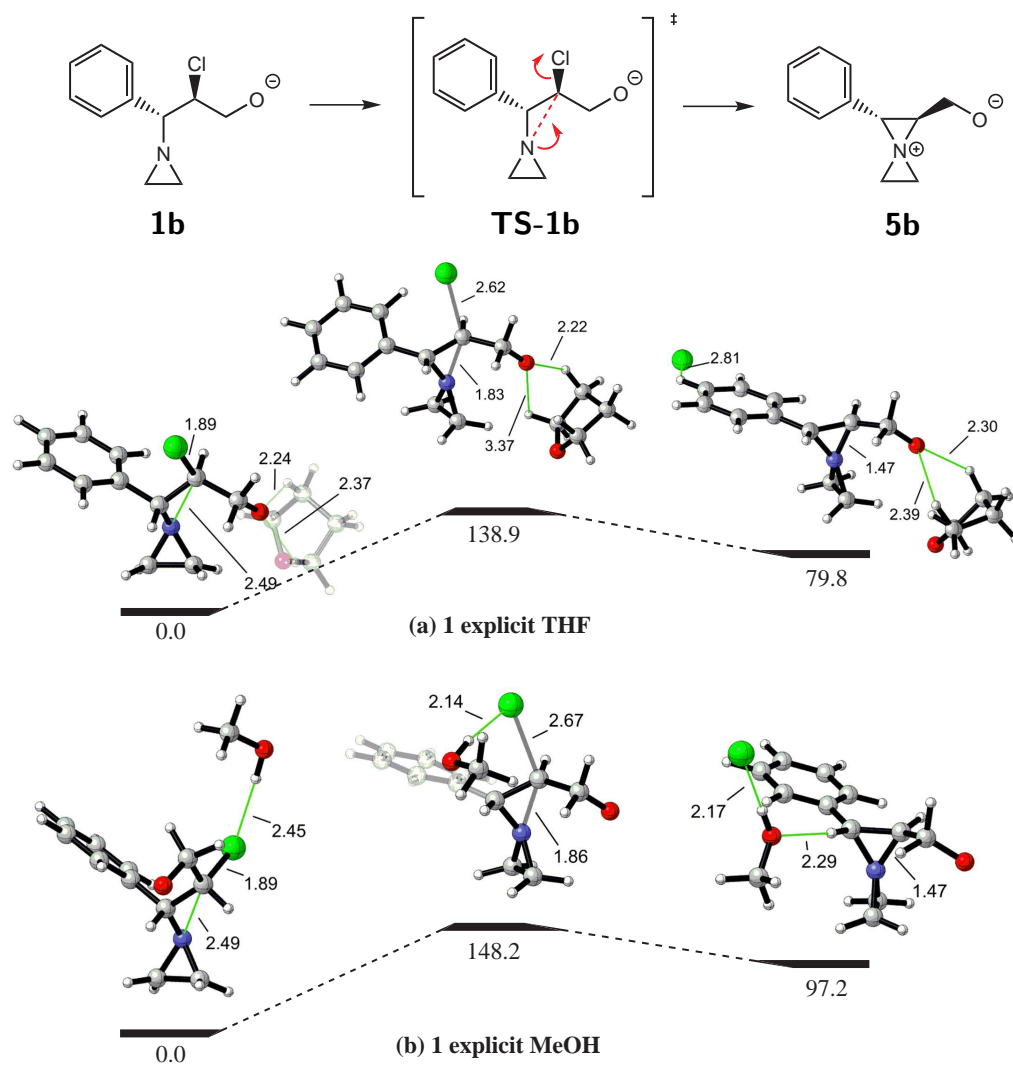


Figure 16: Gibbs free energy profiles (CAM-B3LYP/6-311++G(d,p)//B3LYP/6-31++G(d,p)) for the formation of spiranic aziridinium ion **5b** from optimizations with explicit solvation. Free energies in kJ/mol at 298 K and 1 atm. Some critical distances are given in Å.

4.2.2.5 Comparison of Solvation Methods

An overview of the geometries of transition state **TS-1a** obtained with the various solvation methods is given in Figure 17. These geometries can be divided into two categories (Figure 19a): transition states with or without any implicit solvation. A high impact of solvation gives rise to an earlier transition state with a smaller C-Cl_{TS} and a larger C-N_{TS}, and less impact of solvation gives rise to a later transition state with a larger C-Cl_{TS} and a smaller C-N_{TS}. These two critical distances in transition states **TS-1a** and **TS-1b** are plotted in Figures 19a and 19b. For the conversion of aziridine **1a** to intermediate **5a** the impact of solvation increases in the following series: in vacuo, explicit with one THF, explicit with one MeOH, explicit with two MeOH, implicit THF, implicit MeOH, explicit/implicit with one MeOH and explicit/implicit with two MeOH. To assess the influence of these geometrical changes on ΔG^\ddagger and ΔG_{rxn} , additional scatter plots are made showing ΔG^\ddagger versus ΔG_{rxn} in Figures 19c and 19d for the formation of intermediates **5a** and **5b**. These scatter plots show that early transition states are accompanied by small ΔG_{rxn} and ΔG^\ddagger values which means that the reactions are thermodynamically and kinetically favorable. This is an illustration of the Hammond postulate.⁸⁴

An overview of the geometries of transition state **TS-1b** from various solvation methods is given in Figure 18. The results (Figures 19b and 19d) are less clear than for **TS-1a**: although C-N_{TS} varies in the same way for **TS-1a** and **TS-1b**, this is not the case for C-Cl_{TS}. Calculations with any implicit solvation give rise to similar transition states.

All optimizations above have been performed at the B3LYP/6-31++G(d,p) level of theory. To investigate the influence of dispersion, some transition states were re-optimized with the ω B97X-D functional and the same basis set. This is a well-known functional that is especially designed for optimizations and energy calculations where dispersions are taken into account consistently. C-Cl_{TS} is generally shorter, but good agreement is obtained for C-N_{TS}. Energy refinements have not only been performed with CAM-B3LYP/6-311++G(d,p), but also with ω B97X-D, MPW1B95, M06-2X and BMK using the same basis set. Most data are not explicitly taken up in this thesis but it should be noted that the same trends are found with other functionals.

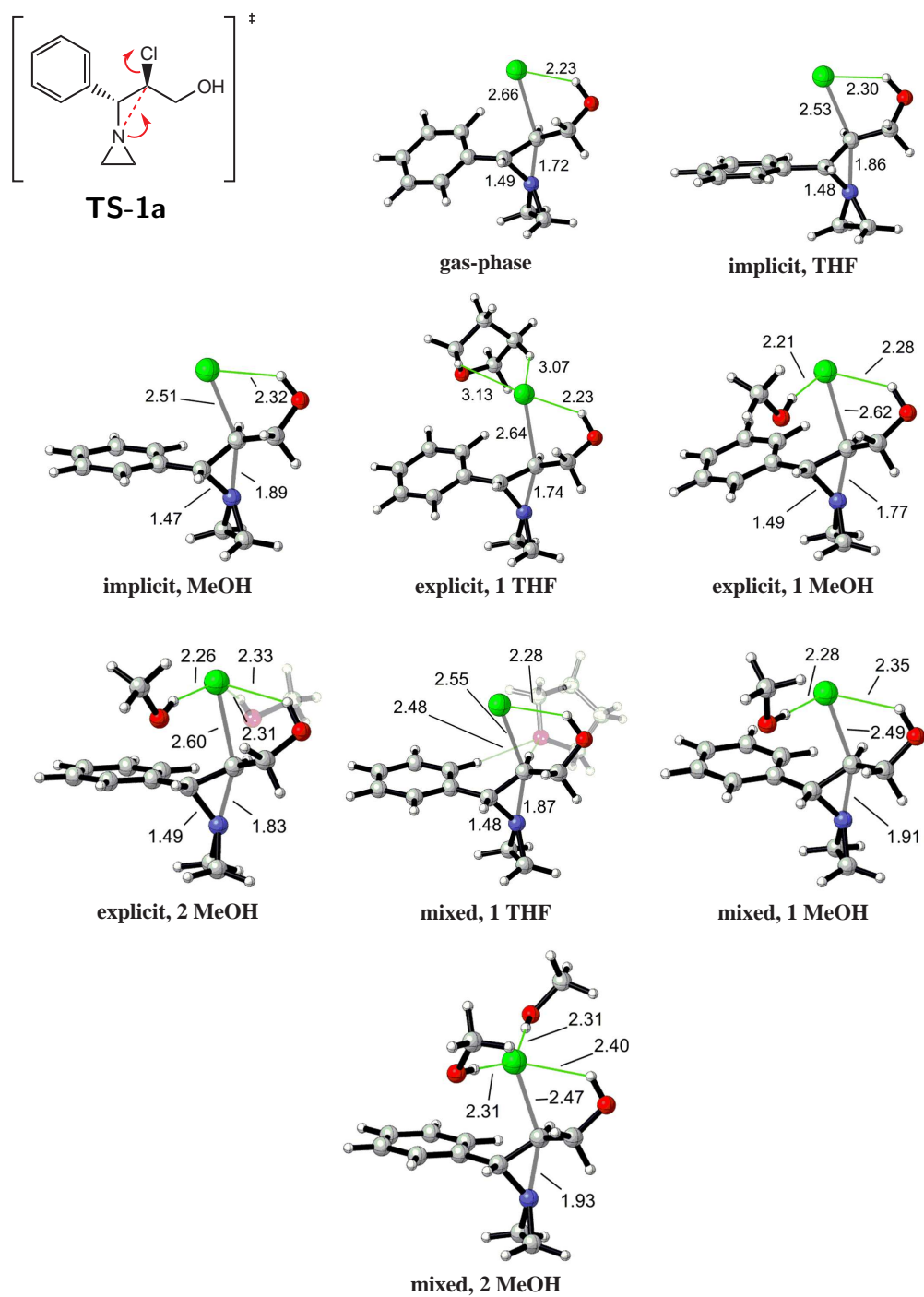


Figure 17: Overview of the transition state geometries of **TS-1a** for several optimization methods at the B3LYP/6-31++G(d,p) level of theory. Implicit and explicit/implicit solvation with IEF-PCM for THF ($\epsilon = 7.4$), C-PCM for MeOH ($\epsilon = 32.6$). Some critical distances are given in Å.

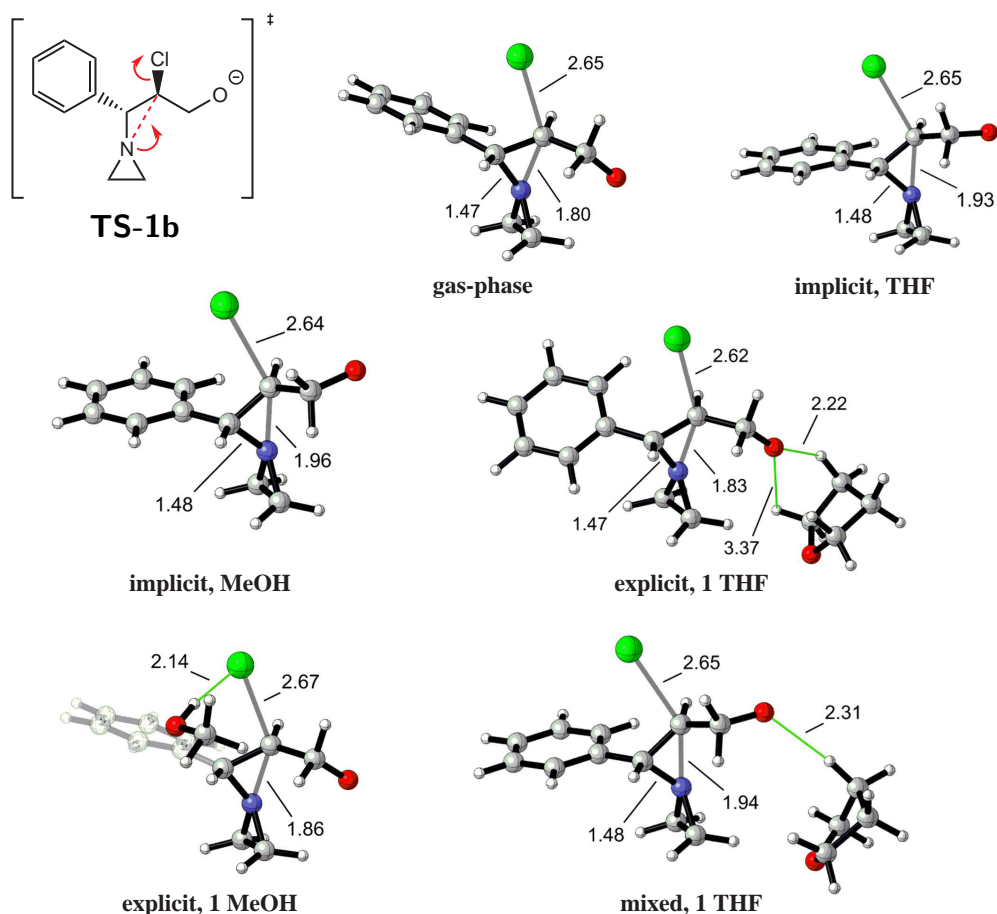


Figure 18: Overview of the transition state geometries of **TS-1b** for several optimization methods at the B3LYP/6-31++G(d,p) level of theory. Implicit and explicit/implicit solvation with IEF-PCM for THF ($\epsilon = 7.4$), C-PCM for MeOH ($\epsilon = 32.6$). Some critical distances are given in Å.

The choice of a solvation method during optimization depends on the solvent and the reaction complex. A few rules of thumb follow from the study of the formation of spiranic aziridinium ions. An optimization with implicit solvation will probably suffice if there is no strong specific interaction between the solvent and the reaction complex. If such an interaction is present, explicit solvent molecules have to be added. The number of explicit solvent molecules, their orientation and the possibility of implicit solvation during optimization can make this approach cumbersome. In the best case, energetic convergence is obtained and the addition of extra solvent molecules becomes obsolete. For example, one explicit MeOH molecule is enough to describe the explicit solvation of the formation of spiranic aziridinium ions. It should however be kept in mind that adding only explicit solvent molecules without embedding the complex in a dielectric medium is not sufficient.

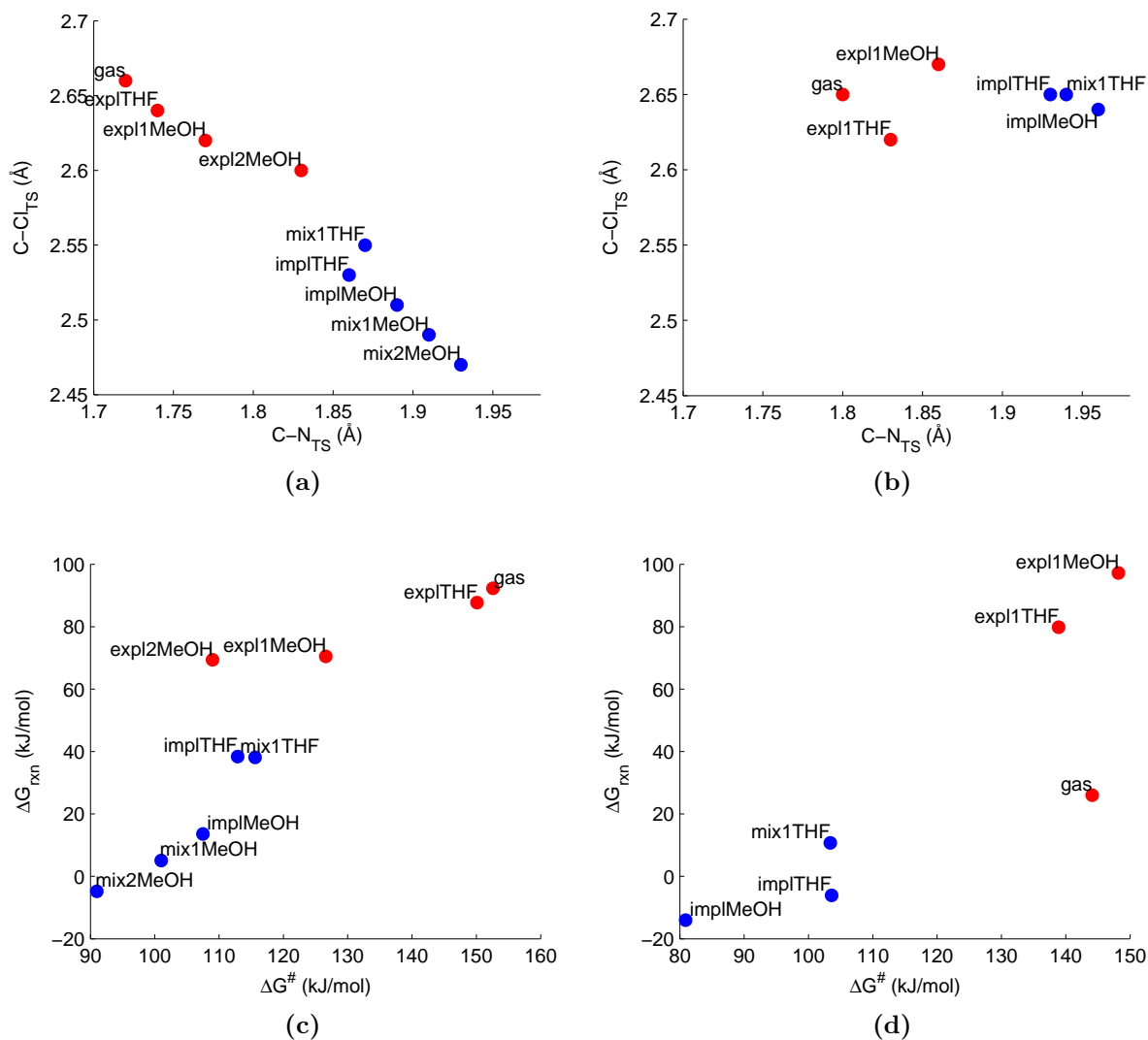


Figure 19: Overview of the critical distances C-N_{TS} and C-Cl_{TS} in transition states **TS-1a** (a) and **TS-1b** (b), and the barriers of the formation of intermediates **5a** (c) and **5b** (d). (Grouping: ● optimization without any implicit solvation, ● optimization with implicit solvation. Solvation during optimization: gas = calculations in vacuo, expl = explicit solvation, impl = implicit solvation, mix = explicit/implicit solvation. Type of solvent and number of explicit solvent molecules are indicated.)

In the remaining part of this work implicit optimizations will be used to model the formation reaction of intermediates **5**. This method has several advantages: it accounts for the influence of the solvent on geometry, it is a general approach (i.e. the number and the orientation of solvent molecules do not need to be determined) and it is computationally feasible. Moreover this detailed assessment study has shown that the correct qualitative trends were found using this methodology.

Table 9: Relative Gibbs free energies (kJ/mol, calculation at 298 K and 1 atm) and critical distances in the transition state for the formation reaction of spiranic aziridinium ion **5a** in various solvents (optimizations with implicit solvation).^a

	1a	TS-1a (ΔG^\ddagger)	5a (ΔG_{rxn})	C-Cl _{TS}	C-N _{TS}
THF ($\epsilon = 7.4$)	0.0	112.9	38.4	2.53414	1.86011
1-butanol ($\epsilon = 17.3$)	0.0	110.6	27.7	2.51531	1.88223
EtOH ($\epsilon = 24.9$)	0.0	109.2	17.2	2.51091	1.88754
MeOH ($\epsilon = 32.6$)	0.0	108.4	15.1	2.50849	1.89050
acetonitrile ($\epsilon = 35.7$)	0.0	108.2	15.0	2.50782	1.89132
DMSO ($\epsilon = 46.8$)	0.0	107.6	14.0	2.50613	1.89341
H ₂ O ($\epsilon = 78.3$)	0.0	106.8	7.4	2.50395	1.89613
formamide ($\epsilon = 108.9$)	0.0	106.4	9.5	2.50304	1.89727

^a CAM-B3LYP/6-311++G(d,p)//B3LYP/6-31++G(d,p) calculations with implicit solvation (IEF-PCM) during optimization and energy refinement. Results for the most favorable pathway are shown.

4.2.2.6 Other Solvents

In order to assess the impact of solvation on the formation of spiranic aziridinium ions the previous computational results were further extended to a broad set of solvents characterized by different dielectric constants. In this section, the influence of the solvent environment on ΔG_{rxn} , ΔG^\ddagger and the transition state geometry for the formation of intermediate **5a** will be studied. Optimizations with implicit solvation (IEF-PCM) are performed for eight different solvents and thus dielectric constants: THF ($\epsilon = 7.4$), 1-butanol ($\epsilon = 17.3$), ethanol (EtOH, $\epsilon = 24.9$), MeOH ($\epsilon = 32.6$), acetonitrile ($\epsilon = 35.7$), dimethylsulfoxide (DMSO, $\epsilon = 46.8$), H₂O ($\epsilon = 78.4$) and formamide ($\epsilon = 108.9$).

C-N_{TS} and C-Cl_{TS} are shown in Table 9 and Figure 20. Solvents with higher dielectric constants give rise to earlier transition states with larger C-N_{TS} and smaller C-Cl_{TS} values, which is confirmed by a decrease of ΔG^\ddagger . Comparison with earlier calculations (Table 7) shows that the difference between C-PCM and IEF-PCM calculations is negligible for MeOH. Differences in C-N_{TS} and C-Cl_{TS} are less than 0.01 Å and differences in ΔG_{rxn} and ΔG^\ddagger are less than 2 kJ/mol, which fits the error margin. Since ΔG_{rxn} and ΔG^\ddagger decrease when the dielectric constant is increased, more polar solvents facilitate the formation of **5a**, both kinetically and thermodynamically. Solvents, especially very polar ones, cannot be described by a small set of parameters of course. Specific interactions, side reactions

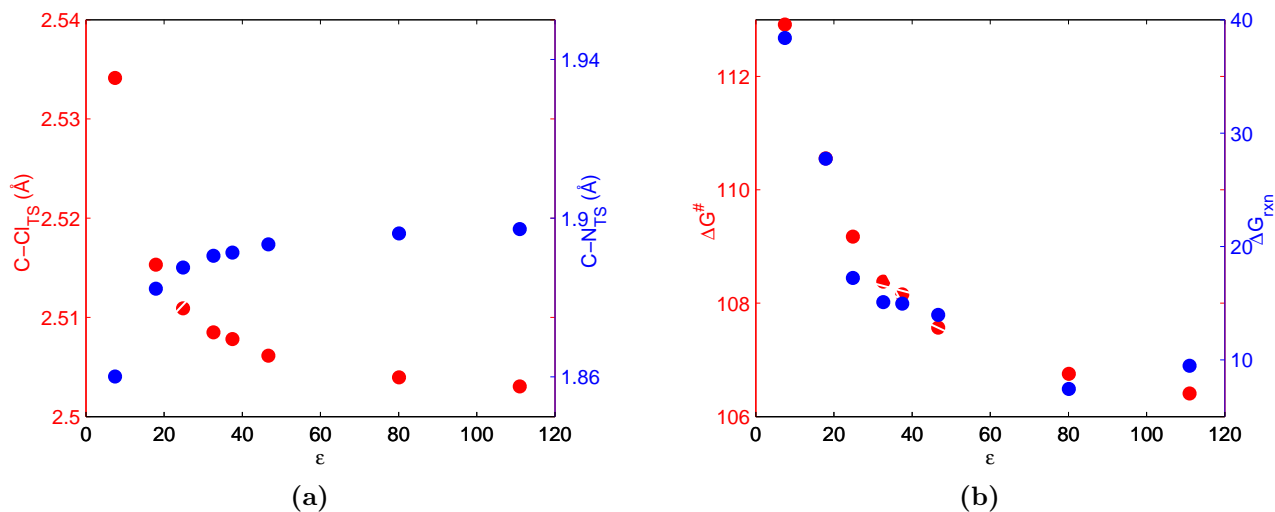


Figure 20: Overview of the influence of different solvents on the formation of spiranic aziridinium ion **5a**: critical distances $C-N_{TS}$ and $C-Cl_{TS}$ in the transition states (a), CAM-B3LYP/6-311++G(d,p) energy refinements. (Optimizations with implicit solvation (IEF-PCM) at the B3LYP/6-31++G(d,p) level of theory.)

and solubility are only a few issues that require extra attention. The present calculations give some qualitative trends on the optimal solvent for this reaction, but of course it needs to be assessed which solvents are possible to implement experimentally.

4.2.3 Substituent Effects on the Formation of Spiranic Aziridinium Ions

In this section the study of the formation of spiranic aziridinium ions is further extended by evaluating the influence of various substituents. Several parameters (X , Y , Z , n) are introduced to describe substituent effects on the formation of spiranic aziridinium ions (Scheme 11). The leaving group (X), β -substituent (Y) and phenyl substituent (Z) of the original compound **1a** will be varied, as well as

Scheme 13: Formation and ring opening of spiranic aziridinium ion **5**.

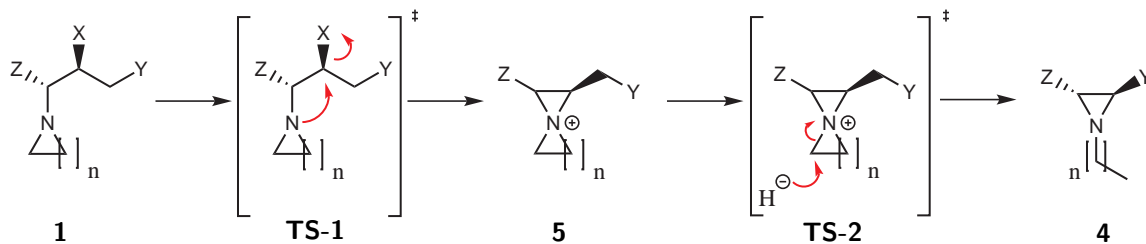


Table 10: Compounds used to study the solvation and substituent effect on the formation of spiranic aziridinium ion **5**.^a

	X	Y	Z	n
a	Cl	OH	Ph	1
b	Cl	O ⁻	Ph	1
c	F	OH	Ph	1
d	Br	OH	Ph	1
e	I	OH	Ph	1
f	OPh	OH	Ph	1
g	OMe	OH	Ph	1
h	Cl	NH ₂	Ph	1
i	Cl	H	Ph	1
j	Cl	SH	Ph	1
k	Cl	SeH	Ph	1
l	Cl	OH	H	1
m	Cl	OH	Cl	1
n	Cl	OH	Ph	2
o	Cl	OH	Ph	3
p	Cl	OH	Ph	4

^a Structural parameters defined in Scheme 13.

the size of the heterocyclic ring (n). The various investigated combinations are given in Table 10.

4.2.3.1 Leaving Groups (X)

The chlorine atom in aziridine **1a** is essential for the formation of intermediate **5a**. It is expected that the ability of the leaving group is correlated with ΔG_{rxn} and ΔG^\ddagger of the formation. This is tested by varying the leaving group: F, Cl, Br and I can reveal periodic trends; OPh and OMe are bad leaving groups. Furthermore OPh was used besides Cl in the experimental studies mentioned in Chapter 1. Optimizations with implicit THF solvation of the ring closure of compounds **1a-1g** show that ΔG_{rxn} and ΔG^\ddagger increase in the series X = I, Br, Cl, F, OPh, OMe (Table 11). It was expected that better leaving groups result in lower ΔG^\ddagger and ΔG_{rxn} values and that high values ($\Delta G_{\text{rxn}} > 90$ kJ/mol, $\Delta G^\ddagger > 160$ kJ/mol) are obtained with bad leaving groups (OMe, OPh, F). Descriptors for leaving group ability are available.⁸⁷ For completeness, transition state geometries are given in Figure 21.

Table 11: Relative Gibbs free energies (kJ/mol, calculation at 298 K and 1 atm) for the formation of spiranic aziridinium ion **5** with various leaving groups.^a

	1	TS-1 (ΔG^\ddagger)	5 (ΔG_{rxn})	$\Delta\Delta G^\ddagger$ ^b	$\Delta\Delta G_{\text{rxn}}$ ^b
a (X = Cl)	0.0	112.9	38.4	0.0	0.0
c (X = F)	0.0	163.6	99.4	50.7	61.0
d (X = Br)	0.0	106.9	24.8	-6.0	-13.6
e (X = I)	0.0	102.8	15.7	-10.1	-22.7
f (X = OPh)	0.0	206.0	141.5	93.1	103.1
g (X = OMe)	0.0	243.2	180.1	130.3	142.7

^a CAM-B3LYP/6-311++G(d,p)//B3LYP/6-31++G(d,p) calculations with implicit solvation (IEF-PCM with $\epsilon = 7.4$) during optimization and energy refinement. Results for the most favorable pathway are shown.

^b $\Delta\Delta G^\ddagger$ and $\Delta\Delta G_{\text{rxn}}$ are ΔG^\ddagger and ΔG_{rxn} values relative to **a**.

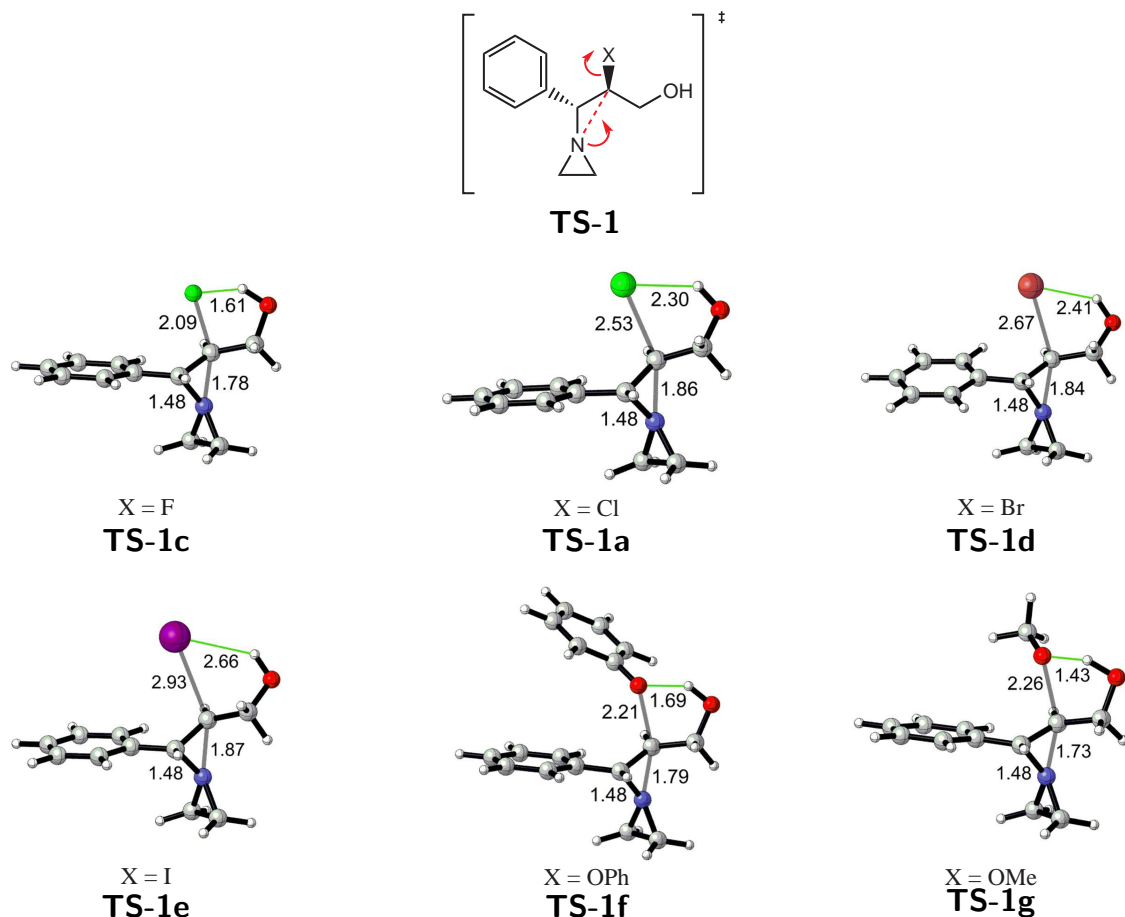


Figure 21: Influence of the leaving group (X = F, Cl, Br, I, OPh, OMe) on the transition state geometry for the formation of spiranic aziridinium ion **5**. Optimizations with implicit THF solvation (IEF-PCM, $\epsilon = 7.4$) at the B3LYP/6-31++G(d,p) level of theory.

Table 12: Relative Gibbs free energies (kJ/mol, calculation at 298 K and 1 atm) for the formation of spiranic aziridinium ion **5** with various β substituents.^a

	1	TS-1 (ΔG^\ddagger)	5 (ΔG_{rxn})	$\Delta\Delta G^{\ddagger b}$	$\Delta\Delta G_{\text{rxn}}^b$
a (Y = OH)	0.0	112.9	38.4	-8.8	-23.3
b (Y = O ⁻)	0.0	103.6	13.2	-18.1	-13.0
h (Y = NH ₂)	0.0	119.5	48.6	-2.2	-43.0
i (Y = H)	0.0	121.7	61.6	0.0	0.0
j (Y = SH)	0.0	122.6	46.6	0.9	-15.0
k (Y = SeH)	0.0	122.2	46.1	0.5	-15.5

^a CAM-B3LYP/6-311++G(d,p)//B3LYP/6-31++G(d,p) calculations with implicit solvation (IEF-PCM with $\epsilon = 7.4$) during optimization and energy refinement. Results for the most favorable pathway are shown.

^b $\Delta\Delta G^\ddagger$ and $\Delta\Delta G_{\text{rxn}}$ are ΔG^\ddagger and ΔG_{rxn} values relative to **i**.

4.2.3.2 β -Substituents (Y)

β -substituents indicated as functional group Y in Scheme 13 are varied to determine the effect of intramolecular hydrogen bonding and zwitterionic stabilization. The former effect is investigated by substituting weak hydrogen bond donors (NH₂, SH, SeH) and a strong hydrogen bond donor (OH) and comparing these results with Y = H. The latter effect is estimated by comparing Y = H with Y = O⁻ and is present under basic conditions as in the original experiments.

An overview of the transition state geometries can be found in Figure 22. Relative Gibbs free energies from CAM-B3LYP/implicit solvation energy refinements are presented in Table 12. ΔG^\ddagger decreases with 8.8 kJ/mol and ΔG_{rxn} with 23.3 kJ/mol for **5a**, with respect to **5i** (Y = H). For weaker hydrogen bonds (Y = NH₂, SH, SeH) ΔG^\ddagger is similar to that of **5i** (Y = H), although ΔG_{rxn} is still smaller. Transition states with weaker hydrogen bonds generally have a larger C-Cl_{TS}. The zwitterionic stabilization is larger than the effect of hydrogen bonding: the formation of compound **5b** shows a 18.1 kJ/mol decrease of ΔG^\ddagger and a 48.4 kJ/mol decrease of ΔG_{rxn} relative to compound **5i**.

4.2.3.3 Z-Substituents

To elucidate the effect of the phenyl group in aziridine **1a** it was replaced by a hydrogen and a chlorine atom (**l** and **m** in Table 13). Furthermore, two new formation reactions were introduced (Scheme

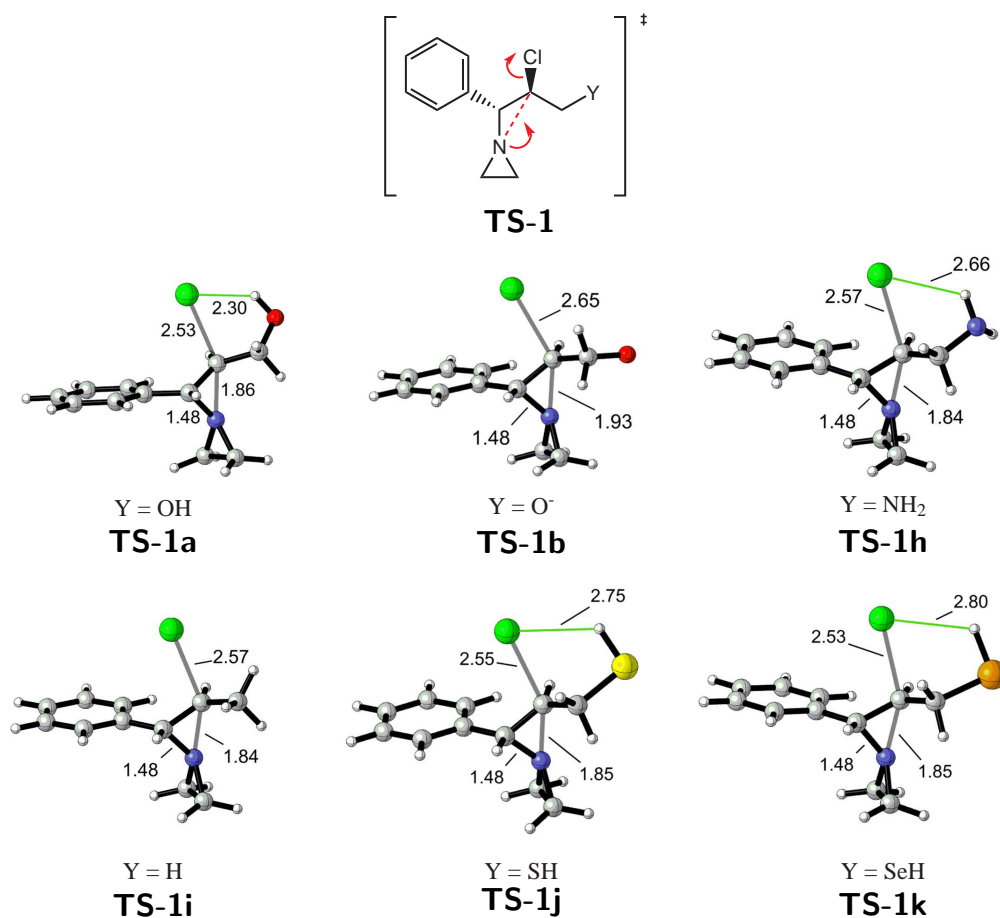
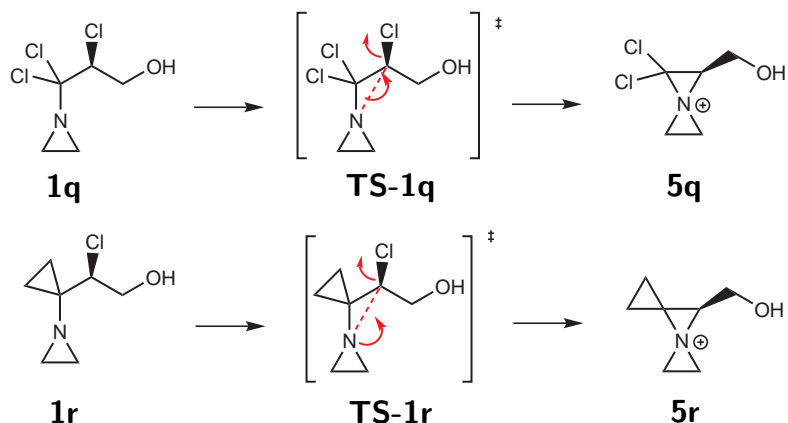


Figure 22: Influence of the β -substituent ($Y = \text{OH}, \text{O}^-, \text{NH}_2, \text{H}, \text{SH}, \text{SeH}$) on the transition state geometry for the formation of spiranic aziridinium ion **5**. Optimizations with implicit THF solvation (IEF-PCM, $\epsilon = 7.4$) at the B3LYP/6-31++G(d,p) level of theory.

14) forming the geminal dichloro spiranic aziridinium ion **5q** and intermediate **5r** with two spiranic centers and three three-membered rings.

Relative Gibbs free energies from CAM-B3LYP/implicit solvation energy refinements are given in Table 13. ΔG^\ddagger and ΔG_{rxn} increase by 8.8 and 17.9 kJ/mol respectively if the phenyl group is replaced by a hydrogen atom and by 45.6 and 48.2 respectively if it is replaced by a chlorine atom. Higher barriers are correlated with later transition states (Figure 23). For in vacuo calculations and explicit THF solvation, these differences are larger (not shown).

The geminal dichloro group increases ΔG_{rxn} and ΔG^\ddagger slightly relative to intermediate **5m** ($Z = \text{Cl}$). The formation of intermediate **5r** is kinetically and thermodynamically more favorable than that of

Scheme 14: Formation of spiranic aziridinium ions **5q** and **5r****Table 13:** Relative Gibbs free energies (kJ/mol, calculation at 298 K and 1 atm) for the formation of spiranic aziridinium ions with various Z substituents.^a

	1	TS-1 (ΔG^\ddagger)	5 (ΔG_{rxn})	$\Delta\Delta G^\ddagger$ ^b	$\Delta\Delta G_{\text{rxn}}$ ^b
a (Z = Ph)	0.0	97.7	34.3	0.0	0.0
l (Z = H)	0.0	106.5	52.2	8.8	17.9
m (Z = Cl)	0.0	143.3	82.5	45.6	48.2
q	0.0	145.0	86.8	47.3	52.2
r	0.0	112.6	64.6	14.9	30.3

^a CAM-B3LYP/6-311++G(d,p)//B3LYP/6-31++G(d,p) calculations with implicit solvation (IEF-PCM with $\epsilon = 7.4$) during optimization and energy refinement. Results for the most favorable pathway are shown.

^b $\Delta\Delta G^\ddagger$ and $\Delta\Delta G_{\text{rxn}}$ are ΔG^\ddagger and ΔG_{rxn} values relative to **a**.

the chloro-substituted spiranic aziridinium ions. It should be noted that ΔG_{rxn} and ΔG^\ddagger give no information about the stability of the reagent and even more three-membered rings could probably be added without a significant effect on these barriers. The conventional strain energy is a better measure for the stability of intermediate **5r**. An intuitive explanation for these results is the inductive effect: electronegative groups such as chlorine atoms destabilize the cationic product. On the other hand, a phenyl group could increase the electron density around the positive center.

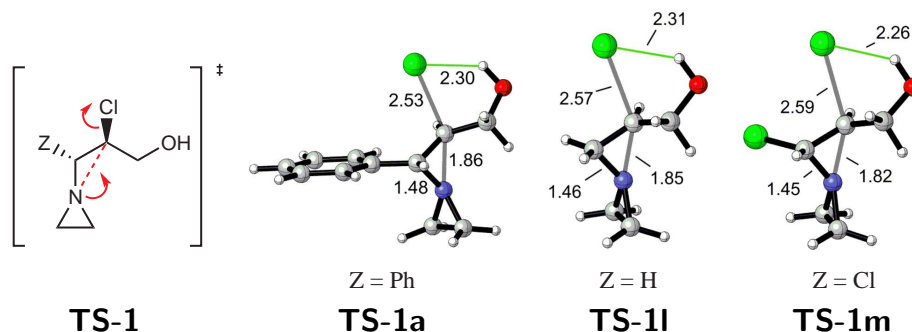


Figure 23: Influence of phenyl group substitution in **1a** ($Z = \text{Ph}, \text{H}$) on the transition state geometry for the formation of spiranic aziridinium ion **5**. Optimizations with implicit THF solvation (IEF-PCM, $\epsilon = 7.4$) at the B3LYP/6-31++G(d,p) level of theory.

Table 14: Relative Gibbs free energies (kJ/mol, calculation at 298 K and 1 atm) for the formation of spiranic aziridinium ion **5** with various heterocyclic ring sizes.^a

	1	TS-1 (ΔG^\ddagger)	5 (ΔG_{rxn})	$\Delta\Delta G^{\ddagger\text{b}}$	$\Delta\Delta G_{\text{rxn}}^{\text{b}}$
a ($n = 1$)	0.0	112.9	38.4	0.0	0.0
n ($n = 2$)	0.0	83.7	-13.4	-29.2	-51.8
o ($n = 3$)	0.0	84.8	-8.5	-28.1	-46.9
p ($n = 4$)	0.0	87.6	-3.9	-25.3	-42.3

^a CAM-B3LYP/6-311++G(d,p)//B3LYP/6-31++G(d,p) calculations with implicit solvation (IEF-PCM with $\epsilon = 7.4$) during optimization and energy refinement. Results for the most favorable pathway are shown.

^b $\Delta\Delta G^\ddagger$ and $\Delta\Delta G_{\text{rxn}}$ are ΔG^\ddagger and ΔG_{rxn} values relative to **a**.

4.2.3.4 Heterocyclic Ring Size

The effect of increasing the ring size (n) of aziridine **1a** ($n = 1$) to form azetidinium **1n** ($n = 2$), pyrrolidinium **1o** ($n = 3$) or piperidinium **1p** ($n = 4$) on the formation of spiranic aziridinium ions was examined next. This was done to generalize the discussion to the spiranic aziridinium ions introduced in Section 4.1. The relative Gibbs free energies from CAM-B3LYP/implicit solvation energy refinements in Table 14 show that the formation is thermodynamically exergonic for $n \geq 2$. However, ΔG_{rxn} and ΔG^\ddagger are minimal for $n = 2$ and increase for $n > 2$, an effect that cannot be explained easily. A possible explanation for the high barriers of **1a** relative to **1n** is angle compression. Since the angle between the exocyclic bonds at the nitrogen atom is larger in an aziridinium ion than in an azetidinium ion (Figure 25), the compression to 60° is harder. The latter argument should be tested.

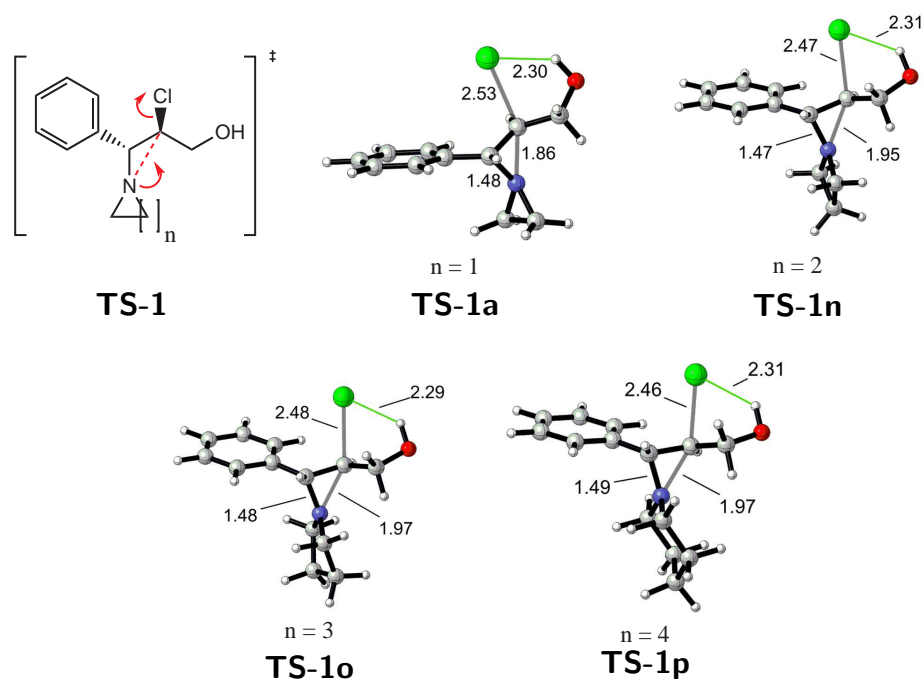


Figure 24: Influence of heterocyclic ring size ($n = 1, 2, 3, 4$) on the transition state geometry for the formation of spiranic aziridinium ion **5**. Optimizations with implicit THF solvation (IEF-PCM, $\epsilon = 7.4$) at the B3LYP/6-31++G(d,p) level of theory.

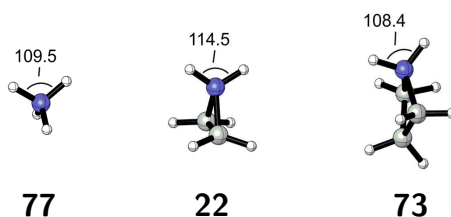


Figure 25: Exocyclic bond angle at the nitrogen atom of the ammonium ion **77**, protonated aziridine **22** and protonated azetidine **73**. Geometries from MP2/6-311+G(2df,2pd) optimizations in vacuo.

4.2.3.5 Overview of Substituent Effects

An overview of the influence of different substituent effects on ΔG_{rxn} and ΔG^\ddagger for the formation can be found in Figure 26. The easiest way to lower ΔG_{rxn} and ΔG^\ddagger is by deprotonation of the β -hydroxyl group. Furthermore a good leaving group is absolutely necessary. Intramolecular hydrogen bonding and the replacement of the Z group give only moderate effects on the barriers. ΔG_{rxn} and ΔG^\ddagger are also lowered by a larger heterocyclic ring.

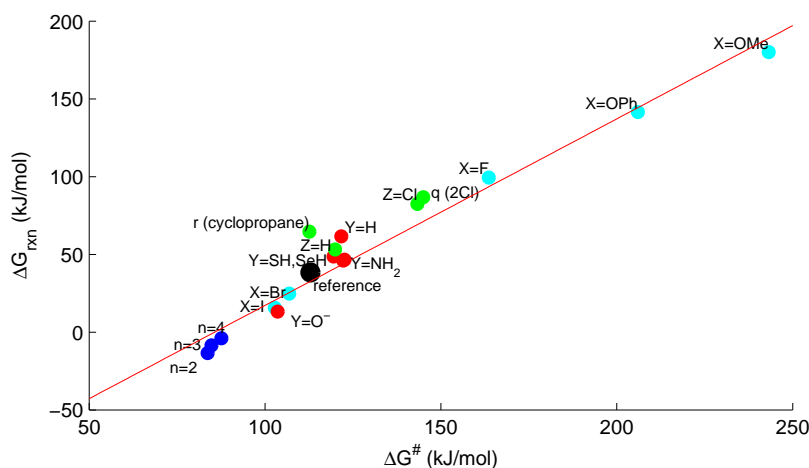


Figure 26: Overview of the influence of substituent effects on the barriers of the formation of spiranic aziridinium ion **5**: reference (X = Cl, Y = OH, Z = Ph, n = 1), • replacement of leaving group, • replacement of the β -substituent, • replacement of Z-substituent, • variation of ring size, r(cyclopropane) = formation of **5r**, q(2Cl) = formation of **5q**, — linear regression. CAM-B3LYP/6-311++G(d,p)//B3LYP/6-31++G(d,p) calculations with implicit solvation (IEF-PCM with $\epsilon = 7.4$) during optimization and energy refinement.

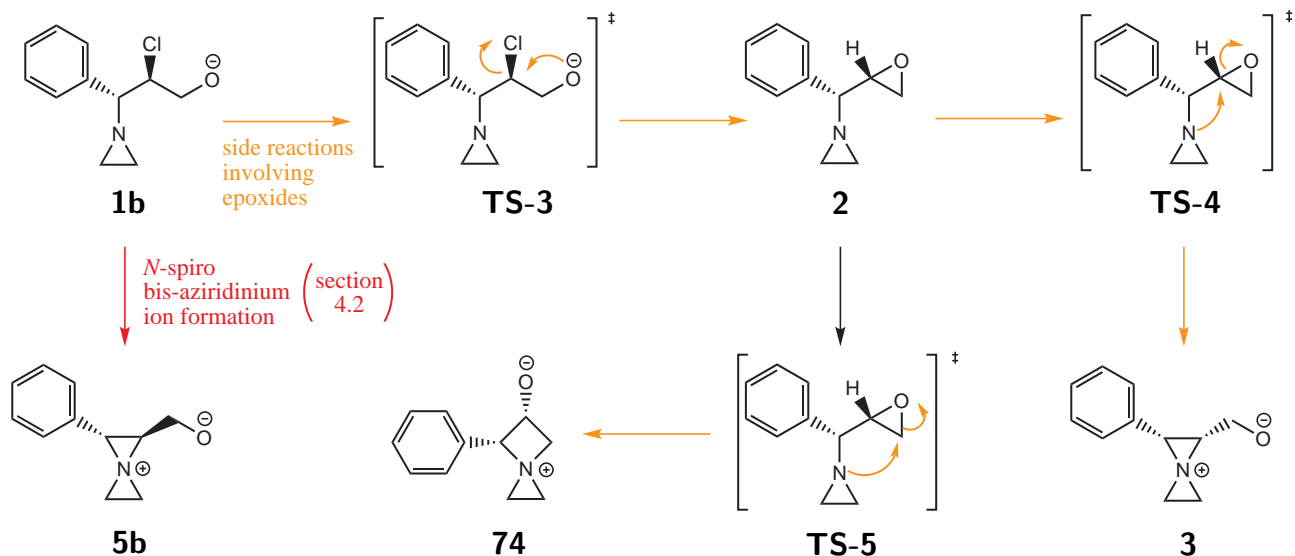
The relation between ΔG_{rxn} and ΔG^\ddagger can be described by a linear regression, $\Delta G_{\text{rxn}} = 1.198 \Delta G^\ddagger - 98.909 \text{ kJ/mol}$ ($R^2 = 0.949$). This is reminiscent of the Bells-Evans-Polanyi principle,^{88,89} although here the free reaction energy is used instead of the reaction enthalpy. This relationship provides an educated guess of ΔG^\ddagger if no transition state can be found for a closely related formation reaction.

One of the most hands-on conclusions of this section is that the formation of spiranic aziridinium ion **5a** should be performed in basic environment. The acid-base equilibrium **1a** \rightleftharpoons **1b** would shift to the right, favoring the formation of intermediate **5b** (Scheme 12). It would be hard to isolate this species in an basic environment however, unless no nucleophiles are present.

4.3 Formation of Spiranic Aziridinium Ions via Side Reactions Involving Epoxides

The formation of spiranic aziridinium ions from **1b** described in the previous section competes with the intramolecular nucleophilic substitution of the chlorine atom by the oxygen anion in aziridine **1b** (Scheme 15). This reaction forms epoxide **2**, which can be opened by a nucleophilic attack of the

Scheme 15: The formation of epoxide **2** and spiranic aziridinium ions **3** and **74** with *cis* configuration.



aziridine nitrogen atom. In this way spiranic aziridinium ions **3** and **74**, which have a *cis* configuration, are formed, in contrast to the aziridines obtained in the previous section, which have a *trans* configuration. Although only the *trans* configuration was established in the original experiments,¹ it is interesting to study these side reactions. Additional experiments have recently been performed in which this reaction takes place.

Gibbs free energy profiles for the formation of epoxide **2** from aziridine **1b** from optimizations with implicit THF and explicit MeOH solvation are shown in Figure 27. Optimizations with implicit

Table 15: Relative Gibbs free energies (kJ/mol, calculations at 298 K and 1 atm) for the formation of epoxide **2** and spiranic aziridinium ions **3** and **74**.^a

	formation of 2			formation of 3			formation of 74		
	1b	TS-3 (ΔG^\ddagger)	2 (ΔG_{rxn})	2	TS-4 (ΔG^\ddagger)	3 (ΔG_{rxn})	2	TS-5 (ΔG^\ddagger)	74 (ΔG_{rxn})
THF ^b	0.0	46.3	- 110.8	0.0	186.2	159.3	0.0	201.6	80.0
MeOH ^c	0.0	63.8	-77.2	0.0	133.5	95.2	0.0	179.4	43.2

^a CAM-B3LYP/6-311++G(d,p)//B3LYP/6-31++G(d,p) calculations. Results for the most favorable pathway shown.

^b Optimization and energy refinement with implicit solvation (IEF-PCM, $\epsilon = 7.4$).

^c Optimization with one explicit MeOH molecule, energy refinements with implicit solvation (C-PCM, $\epsilon = 32.6$).

solvation for THF and one explicit MeOH molecule for solvation in MeOH were chosen to describe the nonspecific and specific interactions of the reaction complex with these solvents. CO_{TS} is 2.02 and 1.90 Å for implicit THF and explicit MeOH solvation respectively and CCl_{TS} is 2.40 and 2.53 Å respectively. Implicit solvation gives rise to an earlier transition state and thus a lower ΔG^\ddagger .

Gibbs free energy profiles for the formation of spiranic aziridinium ions **3** and **74** from epoxide **2** are shown in Figures 28 and 30. Unlike for the epoxide formation, implicit solvation gives later transition states and thus higher ΔG^\ddagger values. Explicit MeOH molecules are hydrogen bonded to the epoxide oxygen atom or the chlorine atom.

CAM-B3LYP energy refinements on the reactions in Scheme 15 are shown in Table 15. ΔG_{rxn} and ΔG^\ddagger for the formation of epoxide **2** cannot be compared with ΔG_{rxn} and ΔG^\ddagger for the formation of spiranic aziridinium ions **3** and **74**, because the chloride ion is not present in these reaction complexes. The effects of the chloride ion on the formation of ion **3** do not cancel out since it would stabilize the zwitterionic product more than the neutral reagent **2**. The formation of compounds **3** and **74** can be compared: the closure of a three-membered ring to form **3** has a lower ΔG^\ddagger , but a higher ΔG_{rxn} than the closure of a four-membered ring to form **74**.

The formation of epoxide **2** is favorable since it has a relatively low ΔG^\ddagger for all methods. This reaction can be compared with the formation of spiranic aziridinium ion **5b** from aziridine **1b** since these reactions have the same reagent. A relative Gibbs free energy profile is shown in Figure 29. These results point out that the epoxide formation has a lower ΔG^\ddagger and ΔG_{rxn} than the formation of spiranic compounds and therefore that the epoxide formation will always occur. Under kinetic control, epoxide **2** will be the only compound formed. If the reactions are under thermodynamic control, the most stable product will be formed, most likely via a ring-opening reaction of a spiranic aziridinium ion. From these data it is not possible to determine the ratios of these products.

It is likely that the long reaction times and thermodynamic conditions in the original experiments made the detection of an epoxide impossible. Instead, it reacted to form spiranic aziridinium ions with a *trans* configuration. This could mean that the ring opening of epoxide **2** with the formation of aziridinium ions **3** and **74** and the subsequent ring-opening reactions are less favorable than the

formation of products with a *trans* configuration.

ΔG^\ddagger and ΔG_{rxn} of the formation of spiranic aziridinium ions **3** and **74** are lower in MeOH than in THF, because zwitterionic character increases along the reaction coordinate. ΔG^\ddagger and ΔG_{rxn} of the formation of epoxide **2** increase in MeOH, probably because a chloride ion is more stable than an oxygen anion.

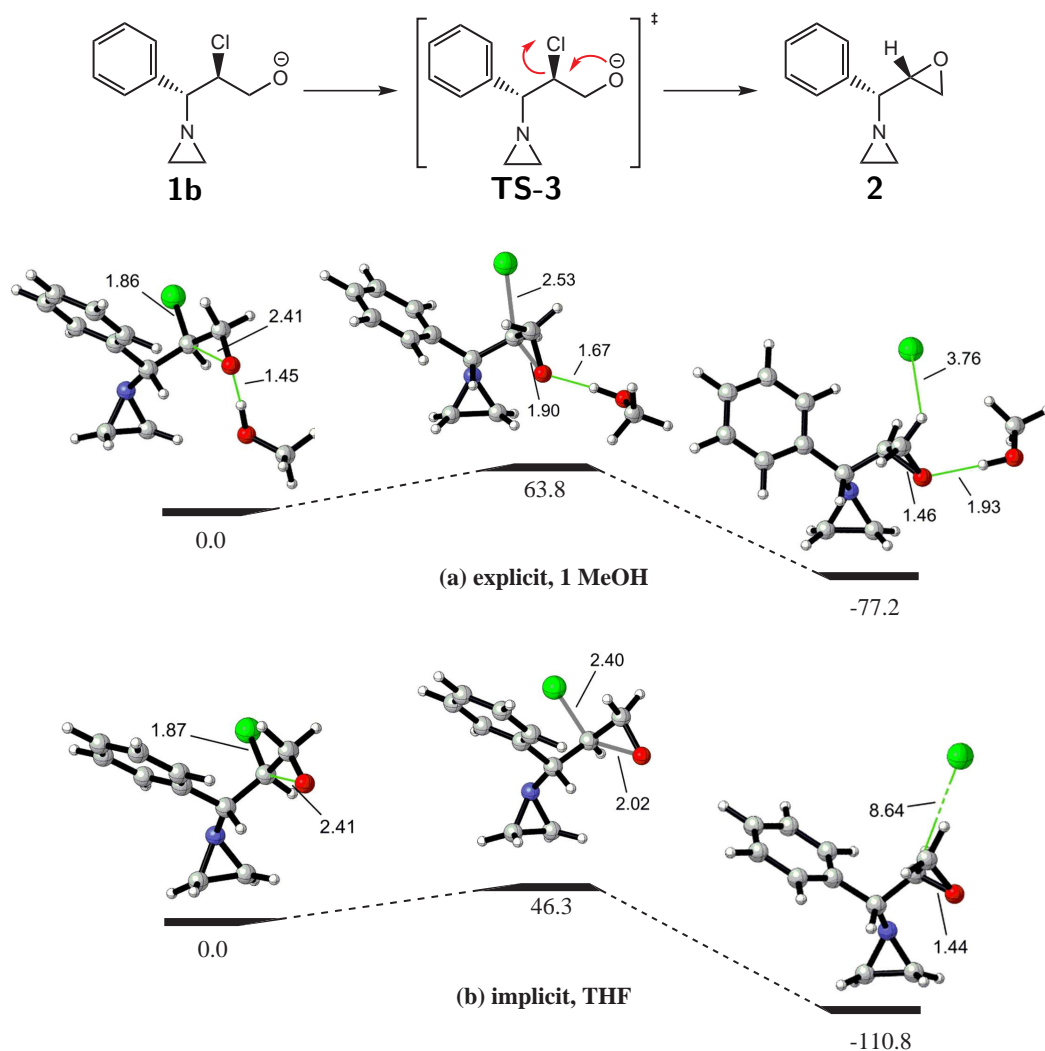


Figure 27: Gibbs free energy profiles (CAM-B3LYP/6-311++G(d,p)//B3LYP/6-31++G(d,p)) for the formation of epoxide **2**. Optimizations with one explicit MeOH molecule and energy refinements with implicit solvation (C-PCM with $\epsilon = 32.6$) (a), Optimizations and energy refinements with implicit solvation (IEF-PCM with $\epsilon = 7.4$) (b). Free energies in kJ/mol calculated at 298 K and 1 atm. Some critical distances are given in Å.

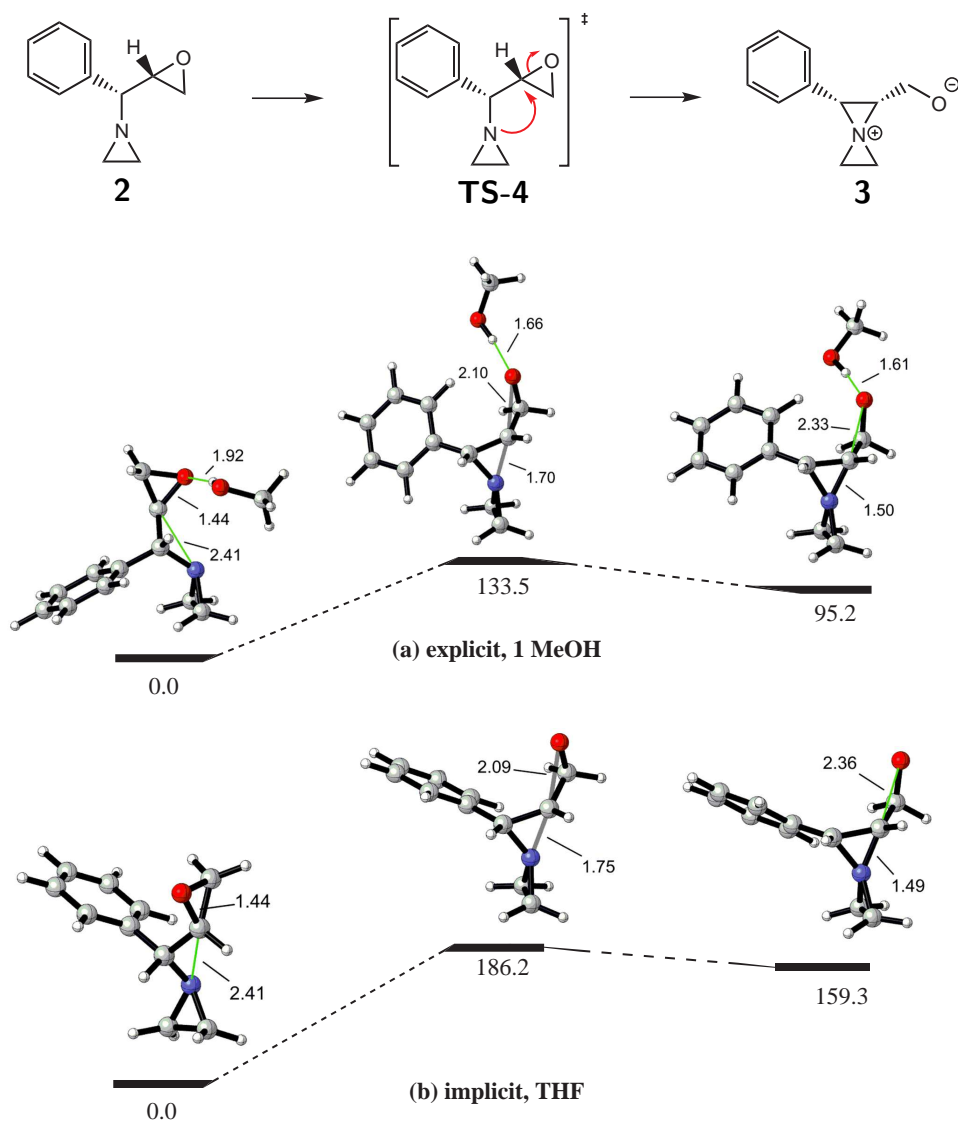


Figure 28: Gibbs free energy profiles (CAM-B3LYP/6-311++G(d,p)//B3LYP/6-31++G(d,p)) for the formation of spiranic aziridinium ion **3**. Optimizations with one explicit MeOH molecule and energy refinements with implicit solvation (C-PCM with $\epsilon = 32.6$) (a), Optimizations and energy refinements with implicit solvation (IEF-PCM with $\epsilon = 7.4$) (b). Free energies in kJ/mol calculated at 298 K and 1 atm. Some critical distances are given in Å.

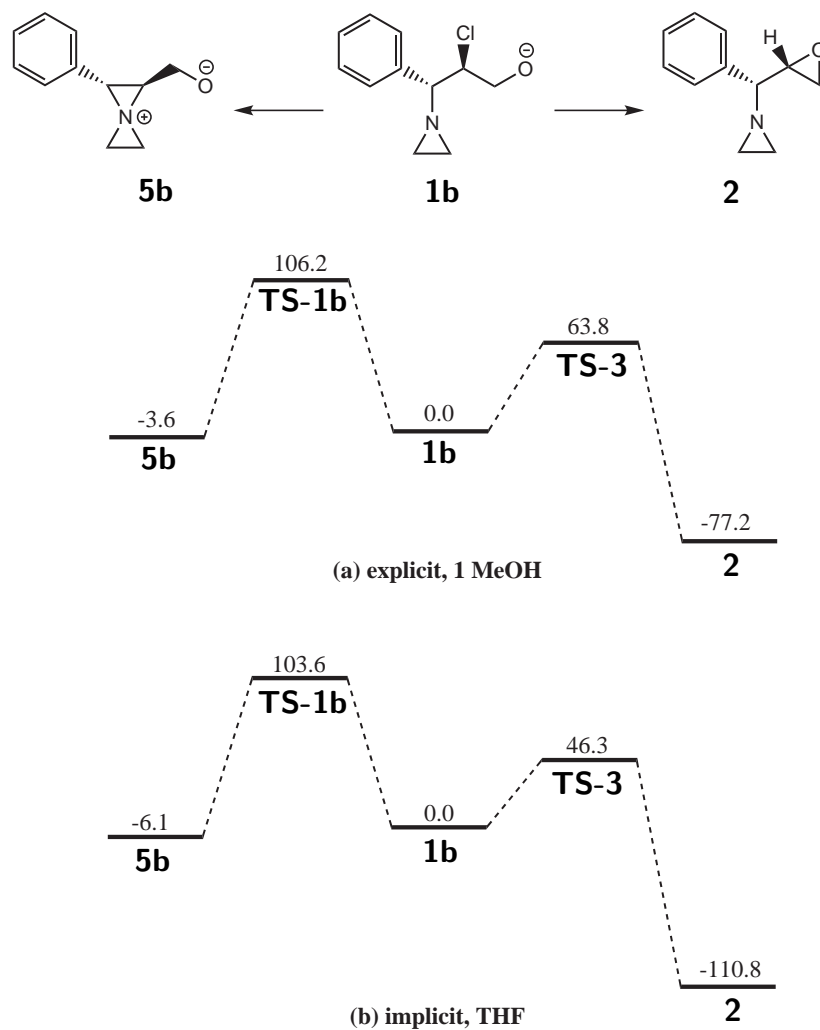


Figure 29: Comparison of the formation of epoxide **2** and spirocyclic aziridinium ion **5b** from aziridine **1b**. CAM-B3LYP/6-311++G(d,p)//B3LYP/6-31++G(d,p) calculations. Optimization with one explicit MeOH molecule, energy refinement with implicit solvation (C-PCM, $\epsilon = 32.6$) (a) and optimization and energy refinement with implicit solvation (IEF-PCM, $\epsilon = 7.4$) (b). Free energies in kJ/mol calculated at 298 K and 1 atm.

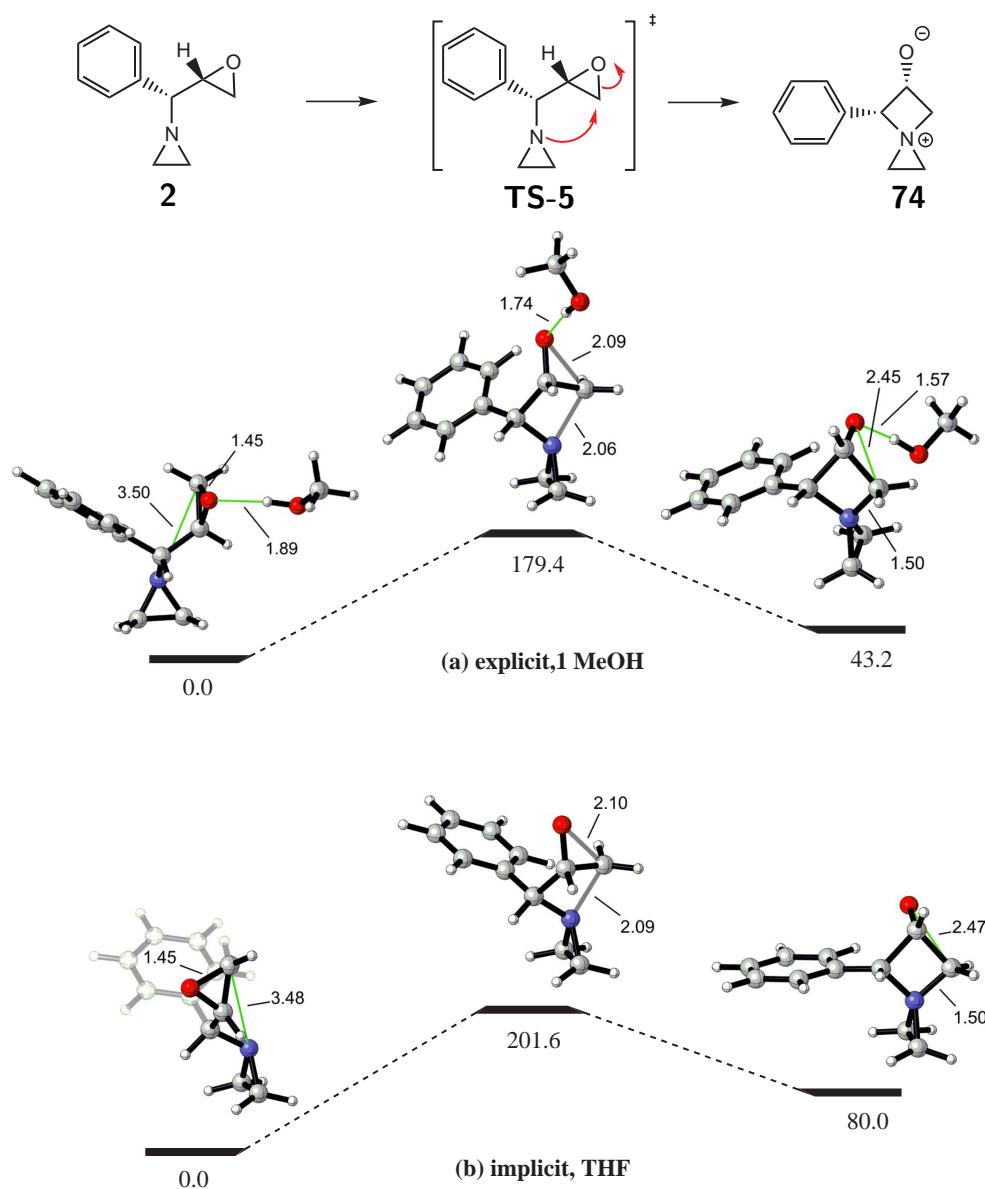
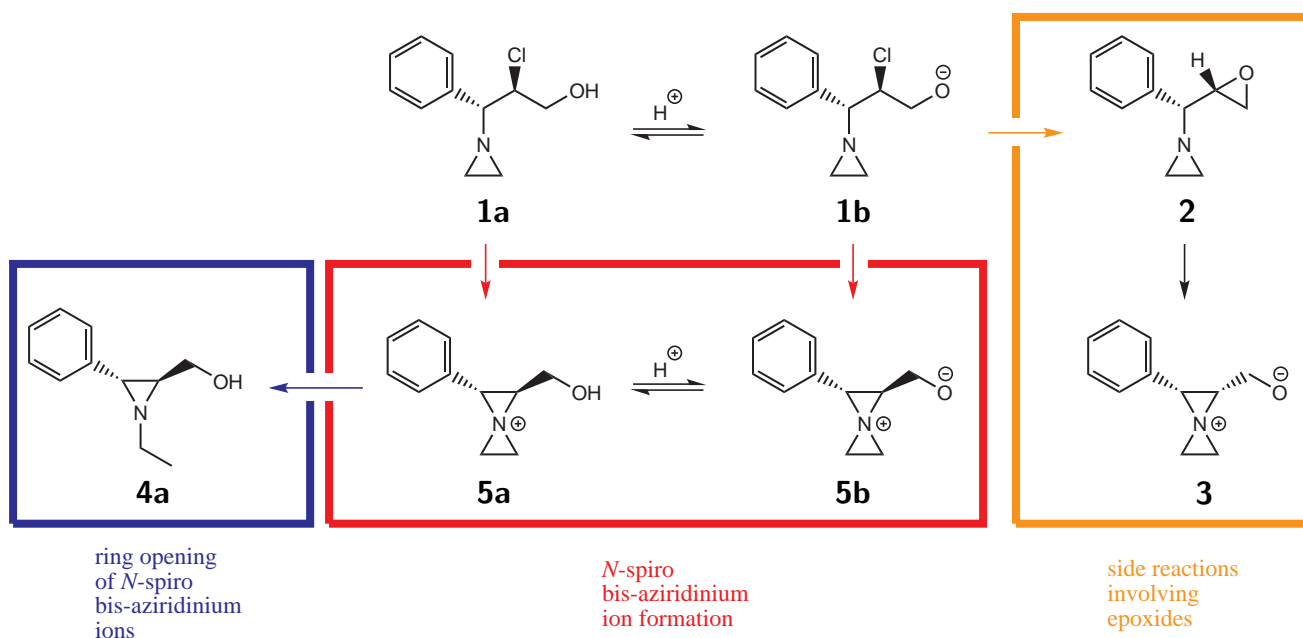


Figure 30: Gibbs free energy profiles (CAM-B3LYP/6-311++G(d,p)//B3LYP/6-31++G(d,p)) for the formation of spiranic aziridinium ion **74**. Optimizations with one explicit MeOH molecule and energy refinements with implicit solvation (C-PCM with $\epsilon = 32.6$) (a), Optimizations and energy refinements with implicit solvation (IEF-PCM with $\epsilon = 7.4$) (b). Free energies in kJ/mol calculated at 298 K and 1 atm. Some critical distances are given in Å.

5 Conclusion

The experiments of Mollet et al. that proposed a *N*-spiro bis-aziridinium ion in the reaction scheme leading to aziridine **4a** (Scheme 16) were the main rationale for the computational study performed in this thesis.¹ As *N*-spiro bis-aziridinium ions were not isolated and are thought to be relatively unstable, it was the aim to investigate by computational methods whether these elusive intermediates could be formed and under which conditions their formation is preferred. This discussion was the starting point for the study of spiranic and bicyclic aziridinium ions in general and was used to investigate the effects of different solvation methods in a systematic way.

Scheme 16: Overview of reactions starting from aziridine **1a**



The discussion of *N*-spiro bis-aziridinium ions was placed in the broader perspective of strained spiranic and bicyclic aziridinium ions. The structure of some representative members of both classes was examined with the bent bond model. Furthermore, the conventional strain energy of all these compounds was determined by means of homodesmotic reactions. The bond bending and α -delocalization in these compounds is considerable and can be compared with other three-membered rings. The strain energies however are very high (> 200 kJ/mol) for spiranic and bicyclic aziridinium ions with two three or four-membered rings. Moreover, bicyclic compounds are less stable than their spiranic

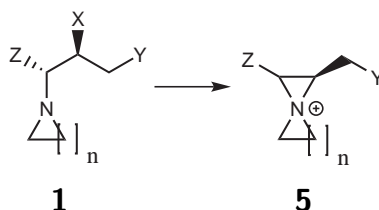
isomers and ring strain decreases when the ring size increases. The strain of spiranic and bicyclic aziridinium ions is less than the sum of the strains of their constituent rings however.

The formation of spiranic aziridinium ions **5a** and **5b** from aziridines **1a** and **1b** (Scheme 16) was modeled with four types of solvation methods: in vacuo, explicit, implicit and explicit/implicit or mixed solvation during optimization. The last two methods are state-of-the-art models that have not been tested systematically. They resulted in different transition state geometries and lower barriers for the formation of spiranic aziridinium ions. Implicit solvation during optimization was selected as the method of choice for reactions in THF.

Using the preferred solvent models the following conclusions were drawn: formation of spiranic intermediates **5a** and **5b** is generally endergonic and has free energy barriers of activation of the order of 100 kJ/mol. The higher the polarity of the solvent, the lower the barrier becomes. As such, reactions in MeOH are preferred compared to reactions in THF.

The effect of substituents on the formation reaction of intermediates **5a** and **5b** was examined in THF with implicit solvation during optimization. Four types of substituents were introduced to describe these effects (Scheme 17). ΔG_{rxn} and ΔG^\ddagger of the formation were correlated with the ability of the leaving group X, as was expected. The β -substituent Y turned out to be very important: zwitterionic stabilization by an anionic substituent or intramolecular hydrogen bonding between the leaving group and the Y substituent lower ΔG_{rxn} and ΔG^\ddagger . The former effect is much larger than the latter. These reactions are thus best performed in a basic environment.

Scheme 17: Structural parameters for the formation reaction of spiranic aziridinium ion **5**



The effect of the Z group can be rationalized by the inductive effect: chlorine atoms destabilize and phenyl groups favour the formation. An interesting result came from varying the heterocyclic ring

size n: aziridines are less likely to undergo this type of ring closure than azetidines, pyrrolidines and piperidines. A possible explanation for this statement is the angle expansion between the exocyclic bonds of aziridinium ions. Finally, a Bell-Evans-Polanyi relationship was established for all these substituent effects.

Aziridine **1b**, in equilibrium with aziridine **1a** in a basic environment, will always react to form epoxide **2**. This will be the end product under kinetic control, but this will react further to amines and aziridines with *cis* or *trans* configurations under thermodynamic control. These thermodynamic products are formed from intermediates **5b** and **3** via a wide variety of fast ring-opening reactions. Moreover in the original experiments no epoxides or aziridines with a *cis* configuration were found. This observation indicates that epoxide **2** was quickly transformed into more stable compounds, though it did not react to form *N*-spiro bis-aziridinium ion **3**.

This thesis confirmed that spiranic aziridinium ions, formed after the intramolecular nucleophilic substitution of a leaving group by the aziridine nitrogen atom, may be formed with free energy barriers of activation of about 100 kJ/mol. The barriers are subject to alteration depending on the specific solvent in which the reaction is conducted. After their formation these aziridinium ions will quickly react further into other more stable compounds (e.g. aziridine **4a**) as the rate determining steps for formation of intermediates **5a** and **5b** are endergonic. They are thus elusive, and computational methods provide an ideal tool to study the properties of these intermediates. Although not found in the experimental results of Mollet et al. other types of spiranic aziridinium ions could be formed with a different stereochemistry if side reactions involving epoxide formation are considered. These results point out that the formation of epoxide **2** is very fast and will always take place in a basic environment, although it cannot be concluded whether *cis* or *trans* products are preferentially formed.

References

- [1] Mollet, K.; D'hooghe, M.; De Kimpe, N. *J. Org. Chem.* **2011**, *76*, 264–269.
- [2] D'hooghe, M.; Van Speybroeck, V.; Waroquier, M.; De Kimpe, N. *Chem. Comm.* **2006**, 1554–1556.
- [3] D'hooghe, M.; Van Speybroeck, V.; Van Nieuwenhove, A.; Waroquier, M.; De Kimpe, N. *J. Org. Chem.* **2007**, *72*, 4733–4740.
- [4] Catak, S.; D'hooghe, M.; De Kimpe, N.; Waroquier, M.; Van Speybroeck, V. *J. Org. Chem.* **2010**, *75*, 885–896.
- [5] Catak, S.; D'hooghe, M.; Verstraelen, T.; Hemelsoet, K.; Van Nieuwenhove, A.; Ha, H.-J.; Waroquier, M.; De Kimpe, N.; Van Speybroeck, V. *J. Org. Chem.* **2010**, *75*, 4530–4541.
- [6] Kaupp, G.; Dengler, O.; Burger, K.; Rottegger, S. *Angew. Chem., Int. Ed.* **1985**, *24*, 341–342.
- [7] Fowler, F. W.; Hassner, A. *J. Am. Chem. Soc.* **1968**, *90*, 2869–2875.
- [8] Karadakov, P.; Gerratt, J.; Cooper, D.; Raimondi, M. *Theochem-J. Mol. Struc.* **1995**, *341*, 13–24.
- [9] Cremer, D.; Kraka, E. *J. Am. Chem. Soc.* **1985**, *107*, 3800–3810.
- [10] de Meijere, A. *Angew. Chem. Int. Ed.* **1979**, *18*, 809–826.
- [11] Vayner, E.; Ball, D. *Theochem-J. Mol. Struc.* **2000**, *496*, 175–183.
- [12] Zhang, J. Z.; Tsai, Y.-T.; Sangkaewwattana, K. L.; Goodwin, J. G. J. *J. Catal.* **2011**, *280*, 89 – 95.
- [13] Walsh, A. D. *Trans. Faraday Soc.* **1949**, *45*, 179–190.
- [14] Coulson, C.; Moffitt, W. *Philos. Mag.* **1949**, *40*, 1–35.

- [15] Novikov, V.; Dakkouri, M.; Golubinskii, A.; Popik, M.; Vilkov, L.; Dormov, P.; Lyssenko, K.; Kostyanovsky, R. *Mendeleev Commun.* **2000**, *10*, 103–105.
- [16] Kostyanovsky, R.; Kostyanovsky, V.; Averkiev, B.; Lyssenko, K.; Dormov, P. *Mendeleev Commun.* **2001**, *11*, 141–143.
- [17] Würthwein, E.; Hergenrother, T.; Quast, H. *Eur. J. Org. Chem.* **2002**, *11*, 1750–1755.
- [18] Lias, S. G.; Liebman, J. F.; Levin, R. D. *J. Phys. Chem. Ref. Data* **1984**, *13*, 695–808.
- [19] Allen, F. *Tetrahedron* **1982**, *38*, 2843–2853.
- [20] Bak, B.; Skaarup, S. *J. Mol. Struct.* **1971**, *10*, 385–391.
- [21] Catalan, J.; Mo, O.; Yanez, M. *J. Mol. Struct.* **1978**, *43*, 251–257.
- [22] Gunther, H.; Schrem, G.; Oberhammer, H. *J. Mol. Spectrosc.* **1984**, *104*, 152–164.
- [23] Eicher, T.; Hauptmann, S.; Speicher, A. *The chemistry of heterocycles: structure, reactions, syntheses, and applications*; Wiley-VCH, 2003.
- [24] Baric, D.; Maksic, Z. *Theor. Chem. Acc.* **2005**, *114*, 222–228.
- [25] Lewis, L.; Turner, L.; Salter, E.; Magers, D. *Theochem-J. Mol. Struc.* **2002**, *592*, 161–171.
- [26] Orchin, M.; Macomber, R. S.; Pinhas, A. R.; Wilson, R. M. *The vocabulary and concepts of organic chemistry*; Wiley-Interscience, 2005.
- [27] Khoury, P.; Goddard, J.; Tam, W. *Tetrahedron* **2004**, *60*, 8103–8112.
- [28] Dudev, T.; Lim, C. *J. Am. Chem. Soc.* **1998**, *120*, 4450–4458.
- [29] Wheeler, S. E.; Houk, K. N.; Schleyer, P. v. R.; Allen, W. D. *J. Am. Chem. Soc.* **2009**, *131*, 2547–2560.
- [30] Hu, X. E. *Tetrahedron* **2004**, *60*, 2701–2743.
- [31] Hu, X.; Kim, N. K.; Ledoussal, B.; Colson, A.-O. *Tetrahedron Lett.* **2002**, *43*, 4289–4293.

- [32] Saha, B.; Nandy, J. P.; Shukla, S.; Siddiqui, I.; Iqbal, J. *J. Org. Chem.* **2002**, *67*, 7858–7860.
- [33] D’hooghe, M.; Van Brabandt, W.; De Kimpe, N. *Tetrahedron* **2003**, *59*, 5383–5386.
- [34] Bucciarelli, M.; Forni, A.; Moretti, I.; Prati, F.; Torre, G. *Tetrahedron: Asymmetry* **1995**, *6*, 2073–2080.
- [35] De Smaele, D.; Bogaert, P.; De Kimpe, N. *Tetrahedron Lett.* **1998**, *39*, 9797–9800.
- [36] De Kimpe, N.; Jolie, R.; De Smaele, D. *J. Chem. Soc. Chem. Comm.* **1994**, 1221–1222.
- [37] De Kimpe, N.; De Smaele, D.; Bogaert, P. *Synlett* **1994**, 287–288.
- [38] Hadjadj-Aoul, R.; Bouyacoub, A.; Krallafa, A.; Volatron, F. *Theochem-J. Mol. Struc.* **2008**, *849*, 8–16.
- [39] Rauk, A.; Allen, L. C.; Mislow, K. *Angew. Chem. Int. Ed. Engl.* **1970**, *9*, 400–414.
- [40] Ebrahimi, A.; Deyhimi, F.; Roohi, H. *Theochem-J. Mol. Struc.* **2001**, *535*, 247–256.
- [41] Brois, S. J. *J. Am. Chem. Soc.* **1968**, *90*, 508–509.
- [42] Padwa, A. *J. Org. Chem.* **1971**, *36*, 230–231.
- [43] Schurig, V.; Bürkle, W.; Zlatkis, A.; Poole, C. F. *Naturwissenschaften* **1979**, *66*, 423–424.
- [44] Kostyanovsky, R. G.; Schurig, V.; Trapp, O.; Lyssenko, K. A.; Averkiev, B. B.; Kadorkina, G. K.; Prosyaniuk, A. V.; Kostyanovsky, V. R. *Mendeleev Commun.* **2002**, *12*, 137 – 140.
- [45] Kostyanovsky, R. G.; Korepin, A. G.; Galkin, P. V.; El’natanov, Y. I.; Kadorkina, G. K.; Chervin, I. I.; Kostyanovsky, V. R. *Mendeleev Commun.* **1995**, *5*, 216 – 217.
- [46] Audier, L.; Azzaro, M.; Cambon, A.; Guedj, R. *B. Soc. Chim. Fr.* **1968**, 1013.
- [47] Guedj, R.; Cambon, A.; Audier, L.; Azzaro, M. *B. Soc. Chim. Fr.* **1968**, 1021.
- [48] Martinez, A.; Elguero, J.; Mo, O.; Yanez, M. *Theochem-J. Mol. Struc.* **1994**, *115*, 45–52.

- [49] Yang, X.; Yudin, A. K. *Synlett* **2007**, 2912–2918.
- [50] Halaska, M.; Ralph, G.; Wiedemann, A.; Primus, G.; Ballering-Bruhl, B.; Hofner, K.; Jonas, U. *World J. Urol.* **2002**, *20*, 392–399.
- [51] Chern, J. W.; Chang, J. Y.; Usifoh, C. O.; Gutsait, A. *Tetrahedron Lett.* **1998**, *39*, 8483–8486.
- [52] Grieco, P. A.; Carroll, W. A. *Tetrahedron Lett.* **1992**, *33*, 4401–4404.
- [53] Anthoni, U.; Nielsen, P. H.; Smith-Hansen, L.; Wium-Andersen, S.; Christophersen, C. *J. Org. Chem.* **1987**, *52*, 694–695.
- [54] Stankovic, S.; Catak, S.; D’hooghe, M.; Goossens, H.; Abbaspour Tehrani, K.; Bogaert, P.; Waroquier, M.; Van Speybroeck, V.; De Kimpe, N. *J. Org. Chem.* **2011**, *76*, 2157–2167.
- [55] Cramer, C. *Essentials of computational chemistry: theories and models*; Wiley, 2004.
- [56] Jensen, F. *Introduction to Computational Chemistry*; Wiley, 2006.
- [57] Møller, C.; Plesset, M. S. *Phys. Rev.* **1934**, *46*, 618–622.
- [58] Lee, C.; Yang, W.; Parr, R. *Phys. Rev. B* **1988**, *37*, 785–789.
- [59] Becke, A. *J. Chem. Phys.* **1993**, *98*, 5648–5652.
- [60] Hohenberg, P.; Kohn, W. *Phys. Rev. B* **1964**, *136*, 864–871.
- [61] Yanai, T.; Tew, D. P.; Handy, N. C. *Chem. Phys. Lett.* **2004**, *393*, 51–57.
- [62] Zhao, Y.; Truhlar, D. G. *Theor. Chem. Acc.* **2008**, *120*, 215–241.
- [63] Boese, A.; Martin, J. *J. Chem. Phys.* **2004**, *121*, 3405–3416.
- [64] Zhao, Y.; Truhlar, D. *J. Phys. Chem. A* **2004**, *108*, 6908–6918.
- [65] Chai, J.-D.; Head-Gordon, M. *Phys. Chem. Chem. Phys.* **2008**, *10*, 6615–6620.
- [66] Van der Mynsbrugge, J.; Hemelsoet, K.; Vandichel, M.; Waroquier, M.; Van Speybroeck, V. *J. Phys. Chem. C* **2012**, *116*, 5499–5508.

- [67] Bader, R. *Chem. Rev.* **1991**, *91*, 893–928.
- [68] Bader, R. F. W. *Atoms in Molecules: A Quantum Theory (International Series of Monographs on Chemistry)*; Oxford University Press, USA, 1994.
- [69] Cramer, C.; Truhlar, D. *Chem. Rev.* **1999**, *99*, 2161–2200.
- [70] Cancès, E.; Mennucci, B.; Tomasi, J. *J. Chem. Phys.* **1997**, *107*, 3032–3041.
- [71] Barone, V.; Cossi, M. *J. Phys. Chem. A* **1998**, *102*, 1995–2001.
- [72] Van Speybroeck, V.; Moonen, K.; Hemelsoet, K.; Stevens, C. V.; Waroquier, M. *J. Am. Chem. Soc.* **2006**, *128*, 8468–8478.
- [73] Goossens, H.; Vervisch, K.; Catak, S.; Stankovic, S.; D’hooghe, M.; De Proft, F.; Geerlings, P.; De Kimpe, N.; Waroquier, M.; Van Speybroeck, V. *J. Org. Chem.* **2011**, *76*, 8698–8709.
- [74] Frisch, M. J. et al. Gaussian 09 Revision A.02. Gaussian Inc. Wallingford CT 2009.
- [75] Legault, C. Y. CYLview, 1.0b. Université de Sherbrooke, 2009.
- [76] Lu, T.; Chen, F. *J. Comput. Chem.* **2012**, *33*, 580–592.
- [77] Lynch, B.; Truhlar, D. *J. Phys. Chem. A* **2003**, *107*, 8996–8999.
- [78] Wiberg, K.; Bader, R.; Lau, C. *J. Am. Chem. Soc.* **1987**, *109*, 1001–1012.
- [79] Benson, S.; Cruicksh, F.; Golden, D.; Haugen, G.; Oneal, H.; Rodgers, A.; Shaw, R.; Walsh, R. *Chem. Rev.* **1969**, *69*, 279–324.
- [80] HK, E.; Golden, D.; Benson, S. *J. Phys. Chem.* **1973**, *77*, 1687–1691.
- [81] Ha, H. J.; D’hooghe, M.; Catak, S.; Stankovic, S.; Waroquier, M.; Kim, Y.; Van Speybroeck, V.; De Kimpe, N. *Eur. J. Org. Chem.* **2010**, 4920–4931.
- [82] Catak, S.; D’hooghe, M.; Verstraelen, T.; Hemelsoet, K.; Van Nieuwenhove, A.; Ha, H. J.; Waroquier, M.; De Kimpe, N.; Van Speybroeck, V. *J. Org. Chem.* **2010**, *75*, 4530–4541.

- [83] da Silva, E. F.; Svendsen, H. F.; Merz, K. M. *The J. Phys. Chem. A* **2009**, *113*, 6404–6409.
- [84] Hammond, G. *J. Am. Chem. Soc.* **1955**, *77*, 334–338.
- [85] Marenich, A. V.; Cramer, C. J.; Truhlar, D. G. *J. Phys. Chem. B* **2009**, *113*, 6378–6396.
- [86] Kelly, C. P.; Cramer, C. J.; Truhlar, D. G. *J. Chem. Theory Comput.* **2005**, *1*, 1133–1152.
- [87] Bento, A. P.; Bickelhaupt, F. M. *J. Org. Chem.* **2008**, *73*, 7290–7299.
- [88] Evans, M. G.; Polanyi, M. *Trans. Faraday Soc.* **1938**, *34*, 11–24.
- [89] Fischer, H.; Radom, L. *Angew. Chem. Int. Ed.* **2001**, *40*, 1340–1371.